



A COMPARATIVE STUDY ON THE PERFORMANCE OF BIODIESEL IN A MODERN 1.9 LITRE TURBO DIESEL ENGINE

by

Johan Kotzé

March 2010

FAKULTEIT INGENIEURSWESE
FACULTY OF ENGINEERING



UNIVERSITEIT
STELLENBOSCH
UNIVERSITY

A COMPARATIVE STUDY ON THE PERFORMANCE OF BIODIESEL IN A MODERN 1.9 LITRE TURBO DIESEL ENGINE

By

Johan Kotzé

Thesis submitted in the fulfilment of the requirements for the Degree of:

Master of Science in Engineering

(Mechatronic Engineering)

In the Department of Mechanical and Mechatronic Engineering

At the University of Stellenbosch

Supervised by

Mr. J. van der Spuy (Mechanical and Mechatronic Engineering)

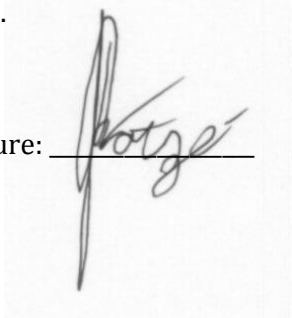
Prof. L. Lorenzen (Process Engineering)

March 2010

DECLARATION

I, Johan Kotzé, hereby declare that the work contained in this thesis is my own original work and that I have not previously in its entirety or in part submitted it at any university for a degree.

Signature: _____

A handwritten signature in black ink, appearing to read 'Kotzé', is written over a horizontal line. The signature is stylized with a large, looped 'K' and a trailing flourish.

ABSTRACT

This thesis comprises of the testing and evaluation of a modern diesel engine running on both biodiesel and mineral diesel on the upgraded Bio-fuels Testing Facility (BTF) at Stellenbosch University. The project was motivated by the need to install a modern diesel engine onto the existing BTF test rig for biodiesel testing. In this project, the BTF was re-designed to support a new Volkswagen 1.9L TDI engine. The capabilities of the BTF were then expanded further by the implementation of a low-cost pressure indicating system, utilising an optical pressure transducer.

During the testing of biodiesel, it was found that the calorific value of the biodiesel was 14% lower than that of the tested mineral diesel. The ignition quality (cetane index) of the biodiesel was also lower than that of the mineral diesel. Even so, the engine only experienced a maximum power loss of 4.2%. During heat-release analysis, it was determined that there was no significant difference in the combustion process of biodiesel and that of mineral diesel. The conclusion could be made that biodiesel is suitable for use in modern TDI engines.

Testing validated the operation of the upgraded test cell, and in trials it was determined that the test results are highly repeatable. The pressure indicating set proved to have some limitations. Only simplified heat-release analyses and reasonable indicated power calculations could be performed with the indicating set. Recommendations were made for improvement in future research.

TO GOD, FOR HIS STRENGTH IS IN MY WEAKNESS.

AND

TO MY FAMILY AND FRIENDS, YOU MEAN THE WORLD TO ME.

ACKNOWLEDGEMENTS

I want to thank:

- My two supervisors, Mr S.J. van der Spuy and Prof L. Lorenzen, for their leadership and support during this project
- Mr R. Haines for all his advice
- Volkswagen of South Africa for their support
- The staff at the Mechanical and Mechatronic Engineering Department's workshop

Table of Contents

1	Introduction	1
2	Literature review.....	3
2.1	Diesel engine.....	3
2.1.1	Turbocharged Direct Injection (TDI) Diesel engine.....	3
2.1.2	Supercharging.....	4
2.1.3	Fuel injection	5
2.1.4	Engine control unit.....	9
2.1.5	Diesel engine summary.....	10
2.2	Diesel fuel.....	10
2.2.1	Mineral Diesel production.....	10
2.2.2	Diesel fuel properties that influence combustion	11
2.2.3	Other diesel fuel properties.....	12
2.2.4	Fuel standards.....	13
2.2.5	Diesel fuel summary	13
2.3	Biodiesel.....	13
2.3.1	Biodiesel production	13
2.3.2	Properties, standards and composition of biodiesel	14
2.3.3	Biodiesel compatibility with mineral diesel engines.....	15
2.3.4	Biodiesel summary.....	16
2.4	Engine testing.....	16
2.5	Combustion in a diesel engine.....	18
2.5.1	Ignition delay period.....	18
2.5.2	Premixed burning period.....	18
2.5.3	Diffusion burning period.....	19
2.5.4	After burning period.....	19
2.5.5	Combustion summary.....	19
2.6	Pressure indicating.....	20
2.6.1	Shaft encoder.....	22
2.6.2	Pressure transducer.....	23
2.6.3	Pressure trace phasing.....	24
2.6.4	Indicating summary	25
2.7	Literature review summary	25
3	Redesign of experimental test cell.....	26

3.1	Previous setup (Palmer, 2008).....	26
3.2	New engine and peripheral components	28
3.3	Engine mounting.....	28
3.4	Drive shaft and coupling.....	29
3.5	Cooling and water supply.....	31
3.5.1	Primary engine cooling	31
3.5.2	Fuel cooling	33
3.5.3	Charge air cooling	34
3.5.4	Forced convection of the engine block.....	34
3.5.5	Dynamometer water supply	34
3.5.6	Cooling and water supply summary.....	35
3.6	Ventilation and exhaust gas extraction.....	37
3.7	Fuel supply.....	38
3.8	Vacuum system.....	39
3.9	Engine electric and electronic system	40
3.9.1	Loom and ECU.....	40
3.9.2	Electric system.....	42
3.9.3	Engine electrical and electronic summary	42
3.10	Test cell electronics.....	44
3.10.1	Test cell and engine control systems	44
3.10.2	Engine and test cell monitoring.....	47
3.10.3	Test cell electronics summary	51
3.11	Control and monitoring software	51
3.11.1	Engine Test Automation (ETA).....	52
3.11.2	PLC program.....	53
3.11.3	VAG-COM	53
3.11.4	Software summary	54
3.12	Indicating setup.....	54
3.13	Experimental test cell setup summary.....	56
4	System commissioning and repeatability analysis	58
4.1	Sensor calibration	58
4.2	Engine and test rig control calibration, tuning in and ECU diagnostics.....	60
4.3	Trial runs and repeatability tests.....	60
4.4	Indicating, data filtering and analysis.....	62
4.4.1	Accuracy of the indicating sensors.....	63

4.4.2	Data filtering.....	63
4.4.3	Repeatability.....	65
4.5	System commissioning and repeatability analysis summary	67
5	Fuels testing	68
5.1	Tested fuel samples.....	68
5.2	Test program	69
5.3	Test results	70
5.4	Fuel consumption measurement.....	72
5.5	Pressure indicating.....	73
5.5.1	Phasing.....	73
5.5.2	Indicated work calculation.....	74
5.5.3	Heat release analysis	76
5.6	Summary	78
6	Conclusions and recommendations.....	79
7	Bibliography.....	1
	Appendix A: Biodiesel composition	I
	Appendix B: US and EU biodiesel specifications.....	III
	Appendix C: Biodiesel compatibility with elastomer materials	IV
	Appendix D: Potential problems in fuel injection systems using biodiesel.....	V
	Appendix E: Geometrical properties of a reciprocating engine.....	VI
	Appendix F: Derivation of the simplified heat release model	VIII
	Appendix G: Pictures of experimental setup	IX
	Appendix H: Drive shaft	XIII
	Appendix I: ECU Pin assignments.....	XIV
	Appendix J: Test software.....	XV
	Appendix K: Pressure indicating equipment.....	XVIII
	Appendix L: Default fault codes for the modified Bosch EDC.....	XIX
	Appendix M: Indicating power spectrums and filter.....	XX

LIST OF TABLES

Table 1 - Comparison between pressure transducers.....	23
Table 2 - Calibration state of re-used sensors	59
Table 3 - Biodiesel test results.....	68
Table 4 - ULSD Test results.....	69
Table 5 - Indicated power.....	76
Table 6 - Composition of common fatty oils	I
Table 7 - Properties of Common Methyl Esters.....	II
Table 9 - US and EU biodiesel specifications	III
Table 9 - Biodiesel compatibility with elastomer materials.....	IV
Table 10 - Potential problems with Biodiesel - Fuel Injection Equipment.....	V
Table 11 - Potential Biodiesel concern by Bosch	V
Table 12 – Optrand AutoPSI-S pressure transducer properties	XVIII
Table 13 - Shaft encoder specifications.....	XVIII
Table 14 - NI USB 9201 Specifications.....	XVIII

LIST OF FIGURES

Figure 1 - Turbocharger cutaway (Courtesy NASA/JPL-Caltech)	4
Figure 2 - Pump unit injector (VWAG, 1998)	6
Figure 3 - Pump unit injector fitted into engine (VWAG, 1998).....	6
Figure 4 - Schematic of a pump unit injector with roller cam connection (VWAG, 1998)	7
Figure 5 - Overhead cam in an engine fitted with pump unit injectors (VWAG, 1998)	8
Figure 6 - Injection cycle (VWAG, 1998)	8
Figure 7 - Injector recoil, taking in more fuel from the low pressure line (VWAG, 1998)	8
Figure 8 - Connection to the low pressure fuel line and low pressure fuel pump (VWAG, 1998) .	9
Figure 9 - Reaction to create biodiesel (Van Gerpen, 2005)	14
Figure 10 - Dynamometer	17
Figure 11 - Dynamic phasing through the use of a Log P-Log V graph (Callahan, et al., 1985).....	24
Figure 12 - Test cell layout (Palmer, 2008).....	26
Figure 13 - Completed test bed at the end of Palmer's project (Palmer, 2008).....	27
Figure 14 - Stripped down test bed before engine installation	28
Figure 15 - CAD model for accurate mounting of the engine.....	29
Figure 16 - Power transmission unit.....	30
Figure 17 - Front end mounting and power transmission.....	31
Figure 18 - Engine cooling pipe flow diagram.....	33
Figure 19 - Intercooler with cooling fan (ducting removed for detail)	34
Figure 20 - Water supply diagram.....	36
Figure 21 - Ventilation system.....	37
Figure 22 - Exhaust system.....	38
Figure 23 - Fuel delivery diagram.....	39
Figure 24 - Vacuum system	39
Figure 25 - Bosch EDC.....	41
Figure 26 - Loom spread out on the floor.....	41
Figure 27 - Engine electric and electronic system.....	43
Figure 28 - Dynamometer connection to PLC.....	44
Figure 29 - Wiring of the pedal actuator	45
Figure 30 - Throttle actuator controller	46
Figure 31 - Throttle actuator	46
Figure 32 - Actuator wiring (Honeywell, 2008)	47
Figure 33 - Valve actuator wiring diagram.....	47
Figure 34 - Thermocouple wiring.....	48
Figure 35 - 4 Channel analogue inputs.....	50
Figure 36 - Control software.....	52
Figure 37 - PSIGlow-A pressure transducers.....	54
Figure 38 - Kübler type 3671 shaft encoder (Kubler, 2009).....	55
Figure 39 - Shaft encoder setup	55
Figure 40 - Indicating set wiring.....	56
Figure 41 - Completed test setup.....	57
Figure 42 - Initial repeatability tests.....	61
Figure 43 - % Difference between the first two power curves.....	61
Figure 44 - Repeatability after modified ECE correction factor	62
Figure 45 - % Difference between runs after ECE correction factor modification.....	62

Figure 46 - Unfiltered data series.....	64
Figure 47 - Filtered data set.....	65
Figure 48 - Repeatability demonstration.....	66
Figure 49 - Power /Torque curves of the engine running on ULSD, Biodiesel and Blends	71
Figure 50 - Percentage difference in corrected power between Biodiesel and blends compared to ULSD.....	71
Figure 51 - Power /Torque curves of the engine running on ULSD and Biodiesel.....	72
Figure 52 - "Motoring" pressure vs. crank angle.....	74
Figure 53 - LogP-LogV for phasing.....	74
Figure 54 - Pressure vs. volume graphs (100% throttle / 1750 rpm).....	75
Figure 55 - Pressure vs. volume graphs (100% throttle / 3250 rpm).....	75
Figure 56 - Heat release (100% throttle / 1750 rpm – maximum torque).....	77
Figure 57 - Heat release (100% throttle / 3250 rpm – maximum power).....	77
Figure 58 - Geometry of a single cylinder and crank connection.....	VI
Figure 62 - Bell housing adaptor plate	IX
Figure 63 - Exhaust thermocouple installation.....	IX
Figure 64 - Oil temperature thermocouple	X
Figure 66 - Electronics backboard.....	X
Figure 67 - Engine coolant temperature control system	XI
Figure 68 - Shell and tube heat exchanger.....	XI
Figure 69 - Clean air system.....	XII
Figure 71 - Complete test setup	XII
Figure 72 – Splined shaft from a Polo gearbox supplied by VWSA.....	XIII
Figure 73 - Shaft with gears ground off and with bearing locators machined.....	XIII
Figure 74 - Complete power transmission	XIII
Figure 75 - Depiction of the ECU 121 Pin plug to the loom	XIV
Figure 76 - ETA user interface.....	XV
Figure 77 - PLC ladder logic program (Palmer, 2008).....	XVI
Figure 80 - Power spectrum of noisy indicating signals (SignalExpress).....	XX
Figure 82 - Power spectrum of indicating signals after filtering (SignalExpress).....	XX

NOMENCLATURE

Abbreviation	Meaning
BDC	Bottom Dead Centre
BTF	Bio fuels Testing Facility
CAE	Cape Advanced Engineering
CCW	Counter Clock Wise
DI	Direct Injection
ECU	Engine Control Unit
EP	End point
FAME	Fatty Acid Methyl Esters
FSI	Fuel stratified injection
IBP	Initial Boiling Point
IC	Internal combustion
IDI	Indirect Injection
OEM	Original Equipment Manufacturer
PD	Pumpe Düse
ROM	Read Only Memory
sfc	Specific Fuel Consumption
TDC	Top Dead Centre
TDI	Turbo Direct Injection
VGT	Variable Geometry Turbocharger
VW	Volkswagen
VWSA	Volkswagen of South Africa

Symbol	Represented property
a	Crank radius
B	Bore
C_p	Specific heat under constant pressure
C_v	Specific heat under constant volume
F	Force
L	Stroke
l	Connecting rod length
m	Mass
N	Rotational speed
P	Power
p	Pressure
Q	Energy
Tr	Torque
T	Temperature
V	Volume
θ	Crank angle
α	ECE Correction factor
h	Enthalpy
η	Efficiency
γ	Ratio of specific heats

1 INTRODUCTION

Sustainability issues are prominent stumbling blocks in modern automotive engineering. The current challenge is to curb carbon dioxide emissions. Switching to bio-fuels seems to be a simple solution to the problem. Two examples of bio-fuels are biodiesel and bio-ethanol. Manufacturers of bio-fuels claim that unmodified engines can run on biodiesel and bio-ethanol. Automotive manufacturers and authorities have concerns about the quality and the long term effects that these fuels have on current engines. Further research is required on quality control, engine compatibility and mass manufacturing of bio-fuels (Dieselnet, 2009) (Jääskeläinen, 2009).

The internal combustion testing facilities at Stellenbosch University closed down in 2004. This project is a joint effort between the Department of Process Engineering and the Department of Mechanical & Mechatronic Engineering to restore the internal combustion engine test facilities. The long term objective is to develop an engine testing facility for bio-fuels research. In 2007/8, Palmer (2008) built an engine test facility as part of his MSc thesis, establishing the Bio-fuels Test Facility (BTF). The first test rig was built to support an old Toyota engine, which was not representative of the engines used in modern cars.

In 2007, Volkswagen donated two new 1.9L TDI engines with pump unit injection systems. The new engine expands the research capabilities of the BTF to a new level, where the research is more applicable to the current state of diesel technology in passenger cars. The pump unit injection system also makes the engine less susceptible to problems normally associated with biodiesel, making it a more stable platform for biodiesel testing.

In this project the test rig built by Palmer for his MScEng thesis was modified to accommodate a Volkswagen 1.9L TDI engine of the ATD variant. The engine was instrumented to allow autonomous control of the engine from the test cell's control computers. Even though the test cell is heavily modified, most of the original hardware from the previous phase of the project was employed to create a cost effective test setup.

To advance the capabilities of the BTF further, research was done on in-cylinder pressure indicating (or indicating for short). It proved to be a good tool to measure fuel performance in an engine. Off the shelf indicating sets from Kistler and AVL proved to be very expensive and the decision was made to start indicating work in the test cell by implementing a cost effective system with the intent to upgrade the indicating equipment further at a later stage.

For the reasons above, the objectives for the project was set out to be:

- To commission and run a modern diesel engine on the test rig built by Palmer (2008).
- To be able to read and log as many engine sensors and operating parameters as possible.
- To compare the effects of biodiesel to ultra low sulphur diesel in the engine by the measured output performance of the engine.
- To implement cost effective pressure indicating instrumentation (measuring in-cylinder pressure).
- To use the pressure indicating set to calculate heat release data and indicated power.
- To evaluate the engine test setup.
- Propose design changes and future work on the test cell.

This thesis consists of:

- A literature study. (Chapter 2)
- A section on experimental setup and the redesign of the test rig. (Chapter 3)
- A section on calibration of instrumentation and repeatability analysis. (Chapter 4)
- Experimental procedures and measured results. (Chapter 5)
- Conclusions and recommendations. (Chapter 6)

2 LITERATURE REVIEW

Before test cell alterations and testing could be done, a proper literature study had to be done to acquire the appropriate background knowledge needed for the project. This chapter highlights basic knowledge needed to understand the rest of this report and is by no means a representation of all the literature that was surveyed.

2.1 DIESEL ENGINE

The invention of the first compression ignition engine can be attributed to two men in the late 1800's, Dr. Rudolf Diesel and Akroyd-Stuart. The idea of a compression ignition engine was the brainchild of Dr. Rudolf Diesel, and in 1892, he filed a patent on an engine initiating combustion by injecting liquid fuel into air heated by compression. With the resources of the Ausburg based company, M.A.N, Diesel took five years to build the first practical engine. Through over a century of development, diesel engines have become the workhorse of the modern world, and can be considered the heart of commercial transportation since the Second World War. (Heywood, 1988)

Diesel engines have much more torque at low speed and better thermal efficiencies than spark ignition engines. The efficiencies of diesel engines may approach 40% where that of spark ignition engines are between 25 and 30%. Diesel engines have a reputation of being noisy and smoky. This made diesel engines an unpopular choice for use in passenger cars. Legislative pressure from first world governments such as the members of the European Union, public environmental awareness and a rise in fuel prices pressured automotive manufacturers to utilize the efficiencies of diesel engines to comply with standards (Heywood, 1988) (Dieselnet, 2007). Recent developments in diesel technology made diesel engines more suitable for passenger vehicles and efficiency of diesel engines made these engines popular for the general public. In the light of sustainable development, this is a step towards better utilization of resources.

It is assumed that the reader is familiar with the basic workings of a four stroke diesel engine, and it will not be discussed in this chapter. This chapter will discuss diesel technologies that are relevant to the research done and the specific engine that is used in this project.

2.1.1 *TURBOCHARGED DIRECT INJECTION (TDI) DIESEL ENGINE*

Some of the more common diesel engines available for public use today is turbocharged direct injection engines. Specifically the TDI trademark is a registered trademark of the Volkswagen Group (includes the passenger car brands VW, Audi, SEAT, Skoda, Lamborghini, Bentley and Bugatti). As the name suggests, the main features of these engines are direct fuel injection and that the air intake is turbocharged.

The specific engine that is used in this project is a VW TDI engine of the ATD variant. Volkswagen of South Africa (VWSA) donated the engine along with all its auxiliary parts that are needed to run the engine. The specifications of the engine are as follows:

- Engine Code: ATD
- Type: 4-cylinder, in-line engine
- Number of valves per cylinder : 2
- Displacement: 1896 ml

- Stroke: 95.5 mm
- Bore: 79.5 mm
- Connecting rod length: 144mm
- Compression ratio: 19:1
- Max. Output: 74kW at 4000 rpm
- Max torque: 240 Nm at 1900 rpm
- Idling speed: 800 rpm
- Cut out speed: 5000 rpm
- Engine management: Bosch EDC 15 P
- Exhaust gas after treatment: EGR and two-way catalytic converter.
- Exhaust emission standard: EU3

2.1.2 SUPERCHARGING

The power output of a four-stroke engine is primarily determined by the amount of fuel burned in the cylinder during the combustion stroke. The amount of fuel that can be injected is limited by the mass of air (oxygen) that is present in the cylinder after the inlet valve closes. One way to increase the mass of air in the cylinder is to pressurise the induced air, known as supercharging. Either one of two (in some cases both) devices are commonly in use to pressurise the air induced into the cylinders. These are:

- Mechanically driven compressor, pump or blower
- Turbocharger

The mechanically driven superchargers are driven from the crankshaft by a belt or gear. There are numerous designs for compressors of which the Roots blower, Sprintex (screw) and sliding vane designs are the most common. A turbocharger is a type of supercharger that is driven by the engine's exhaust gasses. It consists of a turbine and a compressor. The exhaust gasses drive the turbine, while the compressor is used to compress the air that goes into the cylinders (Heywood, 1988). A cutaway of a turbocharger is shown in Figure 1 with the compressor side marked in blue and the turbine marked in red. The turbocharger used in this project is a Variable Geometry Turbocharger (VGT). In a VGT the boost pressure, the rotating speed of the turbine and the backpressure are regulated by changing the pitch of the guide vanes in the housing of the turbine.

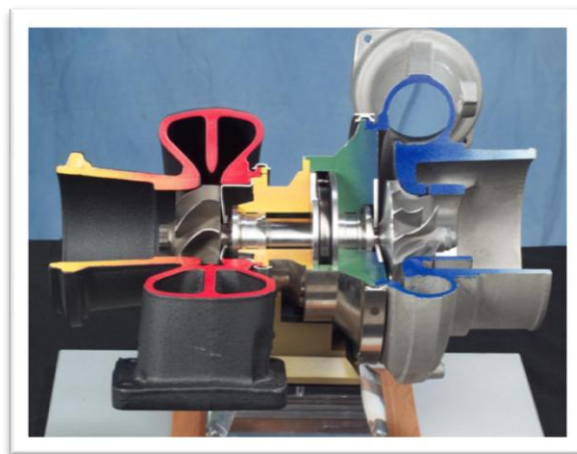


FIGURE 1 - TURBOCHARGER CUTAWAY (COURTESY NASA/JPL-CALTECH)

Due to the compression process, the supercharged air is heated which reduces its density. In some supercharger configurations, to increase the density of the air before it enters the cylinders, the air is passed through an intercooler. An intercooler is a heat exchanger that cools the air in order to approximate isothermal compression of the charge air to increase the volumetric efficiency of the process.

2.1.3 FUEL INJECTION

As mentioned earlier, in a diesel engine, the fuel is injected into the combustion chamber during the combustion stroke of the piston, instead of with the intake stroke as in normal spark ignition engines (exception is with Fuel Stratified Injection (FSI) engines). There are two ways in which diesel can be injected into an engine cylinder. These can be classified as either Direct Injection (DI) or Indirect Injection (IDI).

IDI systems utilize a combustion pre-chamber that is connected to the main combustion chamber through a narrow passage. Air flows through this passage during the compression stroke, causing a fast spinning “whirl” in the pre-chamber. As the piston reaches Top Dead Centre (TDC), the fuel is injected into the pre-chamber via a pinhole. The fuel ignites and the hot burning gasses are forced through the passageway into the main cylinder where it pushes down the piston (Heisler, 1995).

On the other hand, in a DI system, the fuel is injected directly into the combustion chamber at high pressure. Diesel is atomized into very fine droplets as it is injected into the cylinder right above the piston crown as the engine reaches TDC. A number of parameters, of which the sizes of the atomized fuel droplets are one of the most important, influence the emissions of a DI diesel engine. Higher injection pressures ensure finer atomisation of the droplets and reduce emissions (and improve performance). The crown of the piston is machined to induce a flow pattern in the air to improve air-fuel mixing (Heywood, 1988) (Owen, et al., 1990).

Because diesel has to be injected into the cylinder when it is under pressure, the injectors and pumps have to operate at extreme pressures. Regular distributor type injector pumps in IDI engines operate in the range of 300 bar where traditional DI systems operate at up to 1000 bar (Owen, et al., 1990). However, higher injection pressures are favourable and new generation injection technologies have been developed to increase efficiency and reduce emissions.

Two common DI systems are:

- Common rail injection system, and
- Pump unit injection system.

The common rail system uses a central diesel pump that supplies a high pressure fuel line that supplies the solenoid valves on the diesel injectors. Currently third generation common rail injection systems are common, featuring piezo-electric valves for increased accuracy. Common rail systems can inject diesel at pressures of up to 1800 bars. Most car manufacturers such as BMW, Daimler, Fiat, Ford, Honda and Toyota use common rail injectors in their production vehicles (Heisler, 1995).

Pump-unit injection technology is a new diesel injection technology (where unit pump is the older related technology). A small number of car manufacturers like VW, Audi and Volvo embrace it. The pump-unit fuel injector system is marketed under the brand Pumpe Düse (PD)

in VW engines. The injection pressure of pump-unit injection systems is as high as 2050 bar (VWAG, 1998). Since the engine that is used in this project is of the pump-unit injection type the rest of this chapter will discuss the working of pump-unit injectors.

The high injection pressure associated with the PD system has a few significant advantages above older distributor type engines. These are (VWAG, 1998):

- Lower combustion noise (in comparison to the distributor pump system used in older VW engines)
- Better fuel economy (compared to common rail and distributor pump systems)
- Lower emissions
- Better efficiency
- 21% more torque compared to engines fitted with distributor pump systems
- Increased power density

A pump unit injector is a single unit that combines the function of the high-pressure pump, solenoid valve and the injector all in one. Each cylinder is fitted with a pump unit injector that injects fuel directly into the cylinder. Figure 2 shows a pump unit injector and Figure 3 shows the how the unit injector is fitted into the cylinder head.



FIGURE 2 - PUMP UNIT INJECTOR (VWAG, 1998)

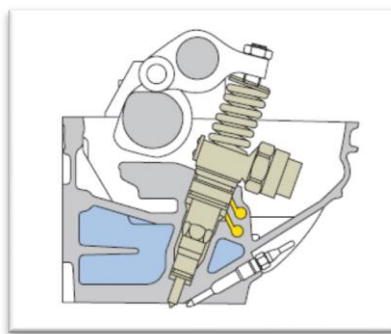


FIGURE 3 - PUMP UNIT INJECTOR FITTED INTO ENGINE (VWAG, 1998)

In the layout in Figure 4 it can be seen that the unit injectors operate like a big syringe. The pump consists of a tube with a plunger fitted in it. The plunger is kept back into the “full” position by a spring. During injection, under action of the rocker arm and cam assembly, the plunger rams the diesel down to the injector. The solenoid controls the flow of the fuel during injection. By opening and closing at the right moment during the injection cycle, the pressurized diesel can be diverted either to the injection needle, or to the fuel return line in the side of the motor head.

When the solenoid valve is energized, flow of the fuel is directed to the needle (otherwise, fuel is returned back to the fuel return channel). As pressure builds up in the needle barrel, the needle is lifted up, and the fuel is ejected out of the holes on the end of the injector. The event of the needle departing from its seat is known as needle lift. This marks the start of the first combustion phase.

The Engine Control Unit (ECU) controls the amount of diesel that is delivered to the combustion chamber and the injection timing electronically. The ECU uses a number of input signals to determine exactly how much and when diesel needs to be injected into the cylinder.

The injector needle is similar to those used in common rail systems and is designed to atomize the diesel as it enters the cylinder during combustion.

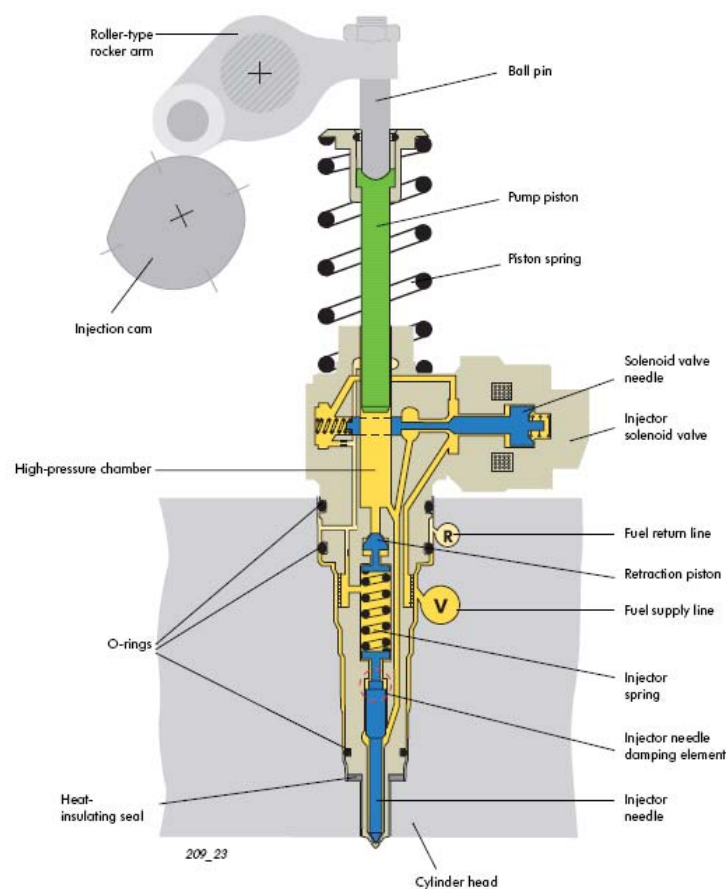


FIGURE 4 - SCHEMATIC OF A PUMP UNIT INJECTOR WITH ROLLER CAM CONNECTION (VWAG, 1998)

The cam system of the PD fitted engines is similar to that of other comparable diesel engines except for the fact that injection cams are also machined onto the same camshaft with the cams that open the valves. Thus, the camshaft has a third more cams on the camshaft as compared to a normal four-cylinder diesel engine. As can be seen in Figure 5, the pump injection cams are connected to the injectors via a rocker arm, and the valves are opened directly by the overhead cam.

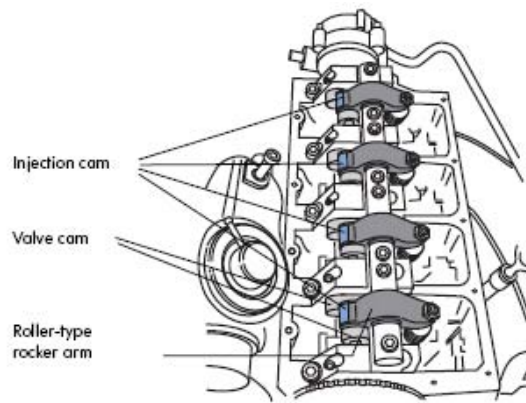


FIGURE 5 - OVERHEAD CAM IN AN ENGINE FITTED WITH PUMP UNIT INJECTORS (VWAG, 1998)

Figure 6 and Figure 7 show how the cam operates to actuate the piston of the pump unit injector.

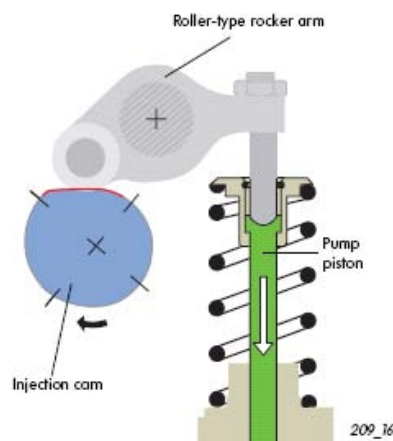


FIGURE 6 - INJECTION CYCLE (VWAG, 1998)

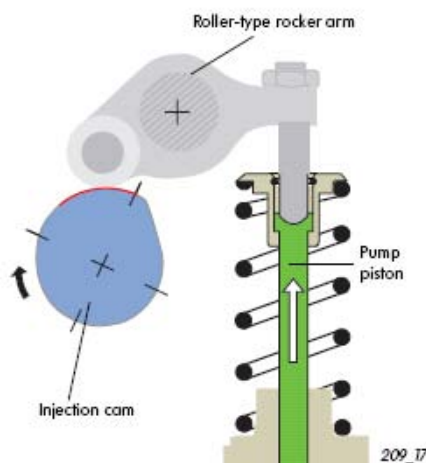


FIGURE 7 - INJECTOR RECOIL, TAKING IN MORE FUEL FROM THE LOW PRESSURE LINE (VWAG, 1998)

Each of the pump unit injectors are connected to a low-pressure supply line and a fuel return line. A fuel pump feeds the supply line, which supply the pump injectors with fuel. In Figure 8 the layout of one of the pump injectors and the low-pressure fuel pump is shown in along with the supply line.

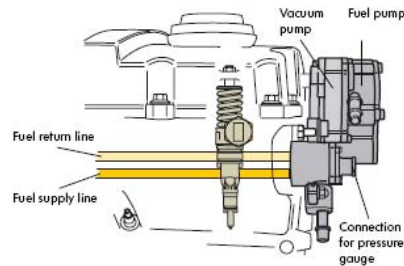


FIGURE 8 - CONNECTION TO THE LOW PRESSURE FUEL LINE AND LOW PRESSURE FUEL PUMP (VWAG, 1998)

The low-pressure fuel pump is a positive displacement, blocking vane type pump. The camshaft drives the fuel pump.

The fuel injection is controlled electronically by the ECU. The ECU measures the engine speed, crank angle and accelerator pedal position. It uses these inputs to determine when and how long to fire each injector.

Injection takes place in two phases, the pre-injection cycle and the main injection cycle. The pre-injection cycle ensures that the combustion process is as smooth and quiet as possible; a tiny amount of fuel is injected into the combustion chamber just before the piston reaches TDC. This causes the temperature and pressure in the cylinder to rise to levels higher than normally obtained and the fuel during the main injection cycle ignites faster and burns more completely. During the main injection cycle, all the fuel required for a single stroke is injected at high pressure. (VWAG, 1998)

2.1.4 ENGINE CONTROL UNIT

As can be deduced from the nature of the fuel injection system, the modern pump unit injector system needs to be under the control of a computer to operate effectively. The engine is controlled by an ECU. Modern ECUs are considerably more advanced than when they were first introduced into the first vehicles in the mid-80's.

The first ECUs were simple, hybrid digital designs, using analogue electronics to process input signals and then using a digital look-up table stored in a ROM chip to determine the output of the ECU. This technique of engine management is relatively simple and robust but lacks flexibility and is only optimal on new engines. As soon as the engine wears out, the fixed control system cannot compensate for the changing parameters anymore and the engine will lose some performance.

Modern ECUs use microprocessors that process the input parameters from the engine in real time and provide calculated output values. The program that controls the ECU is stored on EPROM's (electronically programmable read only memory) or flash memory chips. This means that the ECU's program can be altered electronically via the ECU's communication port using proper software and the appropriate interfacing hardware. The modern ECU does more than only control the engine.

The ECU that is used with the ATD engine is a Bosch EDC 15 P. It is an ECU specially designed for diesel engines. It communicates via a CAN-bus (Controller Area Network), which is a standard developed for vehicles and it allows microcontrollers from various devices in a car to communicate with each other without the need of a host computer. The ECU communicate with

a variety of sensors and actuators directly and has a number of safety and security features included in it (Bauer, 1999).

The ECU used in this project is a modified version of the one used in a production car. Only the basic sensors were monitored that will allow the engine to run. The programming of the ECU is changed to stop the engine from going into limp mode due to the missing input and output signals. The CAN bus will be utilized to communicate with the ECU via a USB connection.

2.1.5 DIESEL ENGINE SUMMARY

In this section, the diesel engine used in this project was discussed. A few features relevant to the 1.9L TDI engine of the ATD variant were discussed. These features include:

- Turbocharger and intercooler,
- Fuel injection and Pump Unit Injectors,
- Engine Control Unit.

Aspects such as Exhaust Gas Recirculation, engine design, CAN communication protocol and automobile electronics have been excluded, as it is not relevant to this project.

2.2 DIESEL FUEL

The first compression ignition engine, conceived by Diesel (1892), was powered by pulverized coal, injected by air blast into the combustion chamber. The idea of injecting liquid fuel into the combustion chamber was a patent filed by Akroyd-Stuart in 1892, predating that of Diesel by two years (Owen, et al., 1990). Around the turn of the century, the development of the diesel engine (spearheaded by Dr. Diesel), its injection system (by Robert Bosch) and diesel fuel were being developed in parallel with spark ignition engines (Owen, et al., 1990). By the time of the First World War, the shortage of gasoline in Germany spurred the development of compression ignition technology, of which the most notable contributors were the companies: Daimler-Benz and M.A.N, who had commercial road vehicles in mind. By the time the Second World War broke out in 1939, diesel was well established in Europe.(Owen, et al., 1990).

Diesel fuel started off as vegetable oil, and in Rudolf Diesel's mind, the future of compression ignition engines was to run on vegetable oils, such as peanut and sunflower oil (Owen, et al., 1990). The abundance of crude oil caused industry to investigate and develop ways to utilize this abundant resource.

In early years, the most valuable fraction of crude oil was kerosene lamp oil. The excess gasoline was burned, the heavy residues were dumped into pits and the "middle distillate" was used to enrich town gas, hence gas oil. With the invention of diesel engines, a better use was found for the middle distillate fraction (Owen, et al., 1990).

2.2.1 MINERAL DIESEL PRODUCTION

Crude oil is a complex mixture of hydrocarbons which can be separated from each other by distillation. In modern refineries, crude oil is typically distilled into three fractions in an atmospheric distillation tower. In each fraction there are some heavier and some lighter hydrocarbons present (Owen, et al., 1990). The heavier fractions can also be broken down to form lighter fractions and streams that can be mixed with the lighter side streams (Owen, et al., 1990).

Modern diesel is a mixture of hydrocarbons, and it is mixed from a number of streams derived from the middle distillate to achieve appropriate fuel properties to meet specifications. There are a number of fuel properties that influence combustion; these will be discussed in the next sub sections.

2.2.2 DIESEL FUEL PROPERTIES THAT INFLUENCE COMBUSTION¹

The composition of diesel fuel is a mixture of hydrocarbons and the exact composition of the diesel is never the same. In order for a diesel fuel to perform properly in an engine, the diesel should have certain properties. The main properties that influence combustion are:

- cetane number,
- volatility,
- density, and
- fuel viscosity

The readiness of diesel fuel to combust under high temperatures and pressures (similar to those in a combustion chamber of a diesel engine) is measured by its Cetane number. A higher Cetane number indicates a fuel that is easier to autoignite, in other words a higher ignition quality. The cetane scale is deduced by taking the combustibility of cetane (n-hexadecane) as 100 and 15 for heptamethyl nonane. A fuel's ignition quality is measured by comparing its combustibility with that of a mixture of cetane and heptamethyl nonane in a test engine. For more information on the testing procedures, refer to ASTM D 613.

Naturally, the Cetane number indicates an ignition delay in the engine after injection; the higher the Cetane value, the shorter the delay. In practice, a lower Cetane number can be linked to heavier fuels, which is preferable due to higher heating values of the longer hydrocarbon chains. However, lower Cetane values give longer ignition delays, causing inefficiencies in the engine and excessive emissions due to unburned fuel that leaves the engine. Modern diesel fuels have Cetane numbers in the range of 45 to 52.

To measure a fuel's cetane number is a complicated process, and therefore a cetane index can be calculated from other fuel properties. This is also a estimate of ignition quality.

The volatility of diesel fuel is expressed in terms of the temperature at which fractions of the fuel are distilled from the fuel under controlled heating. This is done in standardized apparatus and the most widely used test is published as ASTM D 86 in the ASTM book of standards.

Information recorded during the distillation is:

- Initial boiling point (IBP),
- End point (EP),
- Percentage of condensate removed, and
- Percentage residue of non-volatile matter.

The volatility of the fuel is closely linked to the flashpoint and the cloud point of the fuel. Flashpoint is the lowest temperature at which volatile fractions of the diesel come off to form a combustible vapour. Cloud point is the highest temperature at which wax particles are visible.

¹ (Owen, et al., 1990)

By lowering the front-end boiling point, the vapour pressure of the diesel increases and might result in a vapour lock of the engine's fuel injection system, causing the engine to misfire or to fail to restart in hot conditions.

Fuel density is typically measured in kg/m^3 . Higher density fuels mean heavier hydrocarbons that are present in the fuel and more chemical energy in a given volume of fuel. Thus, for a given fuel injection system, the volume of the injected fuel must correspond the energy needed in each cylinder to let the engine run optimally. Another factor is that higher density fuel is linked to more particulate matter in the exhaust gasses.

Fuel viscosity is the fuel's resistance to flow. It is measured in poise (P) and is the force required to move an area of 1cm^2 at a speed of 1cm/s past a parallel surface 1cm away and separated from it by the fluid in question.

The fuel's viscosity alters the way the fuel is injected and it has been shown that an increase in viscosity decreases a fuel injector's penetration rate, cone angle and droplet size. This dependence of the injection system on the viscosity of the fuel makes viscosity a very important factor in diesel quality. A too high viscosity will increase the droplet size of the atomized fuel, while low viscosity will cause starting problems for the engine in cold weather. On the other hand, lower viscosity diesel will leak out of the barrel of the high-pressure diesel pump and cause severe pressure loss, and cause the engine to lose power.

2.2.3 OTHER DIESEL FUEL PROPERTIES

To ensure that the fuel is suitable for use in engines and is suitable throughout its lifecycle, there are a number of different properties that need to be considered. They are listed below along with a brief description of the reason why it is important or a description of the property itself:

- Low temperature characteristics:
 - Cloud point: The highest temperature at which the diesel clouds up with wax particles.
 - Wax appearance point: Similar to cloud point, just a different testing procedure.
 - Pour point: The temperature at which the amount of wax out of solution in the fuel is sufficient to gel the fuel together.
 - Cold filter-plugging point: The highest temperature when wax precipitation in the fuel is sufficient to clog a fuel filter.
- Other diesel specifications:
 - Fuel stability: A measure of how long a fuel can be stored.
 - Flash point: The lowest temperature that will cause volatile fractions of the diesel to vaporise and be ignited by an ignition source.
 - Electrical conductivity: Storage.
 - Water and sediment content: Fuel quality and storage.
 - Sulphur content: Emissions.
 - Ash content: Fuel quality.
 - Carbon residue: Fuel quality.
 - Corrosivity: Fuel quality, storage and engine lifetime.
 - Appearance and colour: Consumer
 - Lubricity: Engine performance and fuel injection equipment life.
 - Heating value (calorific value): Energy contained in the fuel.

- Aromatics content: Emissions.

Most of the low temperature characteristics are of importance in areas where low temperatures prevail for long periods of the year such as in the northern parts of America and Europe.

2.2.4 FUEL STANDARDS

Because diesel fuel is a mixture of chemicals that are determined by the refining process, the chemical composition of diesel fuels vary from one batch to another. To ensure that engine performance is consistent and to ensure the integrity of the supply lines, fuels must adhere to certain standards. Some of these standards are listed below:

- Europe:
 - Automotive diesel fuel: EN 590:1993/1999 (Dieselnet, 2009)
 - Reference diesel fuel: EU 2002/80/EC (Dieselnet, 2009)
 - Biodiesel fuel: EN 14214 (for B100) and EN 590 (blending up to B5) (Dieselnet, 2007)
- North America:
 - Automotive diesel fuel: ASTM D975 (Dieselnet, 2009)
 - Biodiesel fuel: ASTM D6751 (Dieselnet, 2009)

2.2.5 DIESEL FUEL SUMMARY

This section briefly overviews various aspects of mineral diesel fuel such as production and fuel properties. It is established that diesel fuel has to have certain properties to be an effective fuel in a compression ignition engine. These properties can be classified as:

- Properties that influence combustion.
- Low temperature properties.
- Properties that is applicable to the fuel's lifecycle and fuel injection system.

It is clear that stringent control of these properties ensure consistent performance and reliability for diesel engines and therefore the properties of diesel fuels are governed by standards set up by government.

2.3 BIODIESEL

From section 2.2 it is apparent that any fuel that has appropriate properties can be used to fuel a diesel engine and it is not limited to traditional oil or coal-derived diesel. More importantly, if the properties of the alternative fuel closely match that of the fuel that the engine is designed to run on, it can be used in the engine without modification. Biodiesel is the most widely accepted alternative fuel for diesel engines currently available because it can be used on an unmodified engine and due to the fact that it is considered a sustainable fuel source.

Biodiesel is the term coined for vegetable oil or animal fat derived diesel fuel that have been refined so as to obtain the necessary properties. This section is intended to discuss the production of biodiesel and the properties of biodiesel.

2.3.1 BIODIESEL PRODUCTION

Biodiesel consists out of long-chain alkyl esters that are produced by reacting lipids with an alcohol with the help of a catalyst. Biodiesel can be derived from any oil or fat (lipids of various chain lengths); however, feasibility of a feedstock is determined by factors such as water supply,

yield of the feedstock and shortage of available agricultural space. The most popular current feedstocks are sunflower, soybean, cottonseed, rapeseed, peanut oil, oil palm and jatropha curcas, to name a few (Swanepoel, 2008). New developments in algae based oils make algae a very good potential feedstock as it has very high yields per hectare, and do not take up agricultural soil (Swanepoel, 2008).

The biodiesel that is most commonly available is a Fatty Acid Methyl Ester (FAME), and is the result of a process called transesterification. Vegetable oils are made of triglycerides. Alcohol esters and glycerol are formed by creating a reaction between triglycerides and an alcohol utilizing a catalyst (Demirbas, 2006). The reaction is shown in Figure 9.

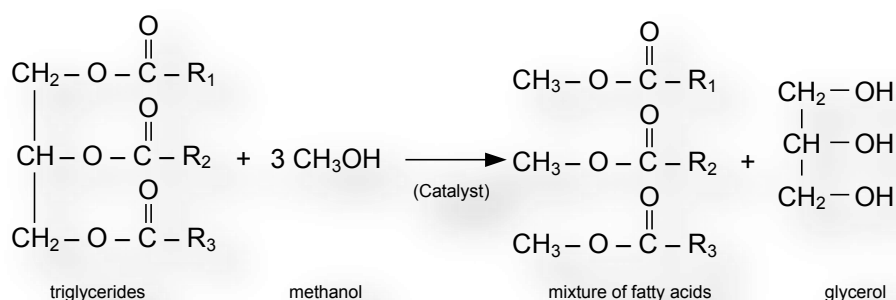


FIGURE 9 - REACTION TO CREATE BIODIESEL (VAN GERPEN, 2005)

The alcohol of choice is methanol along with either sodium or potassium hydroxide as the catalyst (Demirbas, 2006).

The reaction can be performed in a batch reactor, inline reactor, ultra-shear/high-shear reactors or ultrasonic reactors. In the case of a batch reactor, it is important that the molar ratio is correctly calculated and mixed into the reactor along with catalyst. The reactor is heated to speed up the reactions, and the mixture is stirred continuously to ensure mixing.

After the reaction is complete, the glycerol (which has a higher density than biodiesel) is separated from the biodiesel through settling and centrifugation. The catalyst is also removed since it is more soluble in the glycerol (Van Gerpen, 2005). After the excess glycerol is removed the remaining suspended glycerol, methanol, catalyst and other impurities are washed out with water or a 0.5% HCL solution.

2.3.2 PROPERTIES, STANDARDS AND COMPOSITION OF BIODIESEL

Due to variation in feedstock for the production of biodiesel, the properties and composition of biodiesel vary, but similar oils produce similar biodiesels. The composition of some biodiesels from the most common vegetable oils is shown in Appendix A. The properties of each of the components are also listed in Appendix A. (Dieselnet, 2009) (Jääskeläinen, 2009)

Because biodiesel must be able to run in petro-diesel engines, its physical properties need to be regulated stringently. Generally, biodiesel have physical properties that are more or less the same as in mineral diesel. Some of the more important observations that can be made when biodiesel is compared to petrochemical diesel are (Jääskeläinen, 2009):

- Low temperature properties: Biodiesel performs poorer than regular mineral diesel.

- Lubricity: Biodiesel is an excellent lubricant and may even be used as an additive for ULSD to improve its lubricity.
- Cetane number: Biodiesel generally has higher cetane numbers than mineral diesel.
- Fuel stability: There are some thermal and oxidative instability issues with biodiesel, but if fuel is up to standard and kept in a cool place this is no problem.

To ensure that biodiesel can be used in unmodified diesel engines, there are standards set out by standards organisations. Two of the most prominent diesel standards are the European EU14214 and the North American ASTM D6751. These properties are listed in Appendix B.

2.3.3 BIODIESEL COMPATIBILITY WITH MINERAL DIESEL ENGINES

Even with standards in place and the fact that engines run well on biodiesel in the short term, manufacturers limit the use of biodiesel and blends of biodiesel in some engine models and will void warranties on engines running on biodiesel. The reason for this is due to various issues inherent to biodiesel and regular mineral diesel engines. Potential issues can be classified as follows (Jääskeläinen, 2009):

- Material compatibility
- Oil dilution
- Fuel injection equipment

Depending on the model and year of an engine, the engine may consist of materials that are adversely affected by biodiesel. A table that shows the compatibility of some of the common elastomer materials used in piping and sealing in engines are given in Appendix C. Changes in sealing materials may cause leaks, which will cause engine malfunction or loss of performance (Jääskeläinen, 2009).

A study that was done on the effect of biodiesel on metals included copper, steel, brass, aluminium and bronze. The metals were placed in biodiesel at 51.6°C for six months. Copper alloys showed severe corrosion. Steel and aluminium showed no corrosion, but the biodiesel obtained high acid numbers, which could affect elastomers. Zinc was also corroded. Thus, special materials should be used in engines intended to run on biodiesel (Jääskeläinen, 2009).

During engine operation, the biodiesel may leak from the fuel pump or bypass the piston rings into the oil reservoir in the crankcase. The extent to which this happens depends on the condition of the engine. This happens with both Ultra Low Sulphur Diesel (ULSD) and biodiesel, but in the case of ULSD, the heat of the engine oil will cause the diesel's volatile fractions to evaporate and join the blow-by stream. In the case of biodiesel, a significant amount of methyl esters will remain in solution with the oil. This adversely affects the oil's lubricating ability, and causes wear on the engine (Jääskeläinen, 2009).

The fuel system of an engine may be negatively impacted by biodiesel. The adverse low temperature characteristics of biodiesel may cause fuel filters to clog. Biodiesel and its blends also cause finer water droplets to form, which is more difficult to separate from the fuel. Biodiesel does not affect the injection system if appropriate detergent additives are used. The detergent additives prevent deposit formation in the injector. This is especially important in IDI engines as the pintle type injectors tend to form deposits. The high viscosity of pure biodiesel may cause the injector to inject less fuel into the cylinder than normally achieved with ULSD (Jääskeläinen, 2009).

There is a list of problems that automotive manufacturers are concerned with included in Appendix D. Currently, European automotive companies are settling on a maximum biodiesel blend of B7 (7% biodiesel, 93% mineral diesel) on account of problems encountered with biodiesel in engines (Jääskeläinen, 2009). However, specially designed engines and retrofit kits are available for customers who want to use biodiesel in high concentrations. It must be noted that biodiesel only increased the maintenance cost for some of the engines of fleets running on biodiesel blends. The difference lies in the specific engine's design and materials used. It is recommended that the biodiesel compatibility of an engine be checked with the Original Equipment Manufacturer (OEM) before it is run on biodiesel for extended periods.

2.3.4 BIODIESEL SUMMARY

This section discussed:

- Biodiesel production
- Biodiesel properties
- The compatibility of biodiesel with regular petro-diesel engines.

From the discussion, it is clear that it is possible to use biodiesel blends in most diesel engines, but problems may be expected with material degradation. A slight loss in performance due to lower injector performance and lower heating value of biodiesel can also be expected.

2.4 ENGINE TESTING

In this project the performance of an engine running on normal ULSD will be compared to its performance when running on biodiesel. To evaluate the engine's performance, there are a number of engine parameters that can be monitored. Only those parameters applicable to this project will be elaborated on.

In Appendix E the geometrical properties of an IC engine is discussed along with some equations for calculating the volume of the cylinder (as a function of crank angle), the average velocity of the piston and the instantaneous piston velocity.

Whenever a test is conducted on an engine, one has to decide what needs to be measured to answer the research question at hand. In this project, the question is to see to what extent biodiesel affects the performance of a modern diesel engine with a high-pressure injection system. The secondary question is to find out what causes the performance (if observed) difference using combustion analysis. Thus, the engine's maximum output needs to be measured and analysis on the combustion process of biodiesel is needed. The combustion analysis of an engine is a very complicated process, and merits further discussion on section 2.6.

To evaluate the engines output performance, the maximum power and torque need to be determined; this is called a power curve. A dynamometer is used to load the engine during a power curve. The engine is run at 100% throttle at maximum speed. The engine is then loaded in increments to "step" its speed down to idle speed. Throughout this process the engine torque and speed is measured and plotted onto a graph with engine speed as an independent variable. The power is calculated as a product of engine torque and engine speed:

$$P = \frac{2\pi NT}{60} \quad [2.1]$$

With N as the engine speed in rpm and T is the engine torque in Nm. Torque is a measure of the engines ability to do work, while engine power is a measure of the rate at which an engine can do work (Heywood, 1988).

The engine torque is measured using a load cell on the side of the dynamometer and the engine speed is measured using a hall sensor in proximity to a toothed wheel. The load cell measures the force needed to stop the dynamometer from rotating, which can be reworked into torque using the dynamometer geometry. The hall sensor generates a series of pulses as the toothed wheel passes it. The frequency of the hall sensor signal can be used to calculate engine speed by dividing the frequency of the signal by the number of teeth on the toothed wheel. Figure 10 shows a diagram of a dynamometer.

The BTF is equipped with a Schenk D360 waterbrake dynamometer. A waterbrake dynamometer dissipates the engine's energy into water by using viscous shear. Control of the load applied to the engine is achieved by varying the water level in the stator. The water level control is done using a butterfly valve actuated by a servomotor. A PID controller controls the servomotor. A waterbrake dynamometer can only load the engine, and cannot be used to motor the engine (to drive the engine like a piston compressor) as in the case of a DC dynamometer.

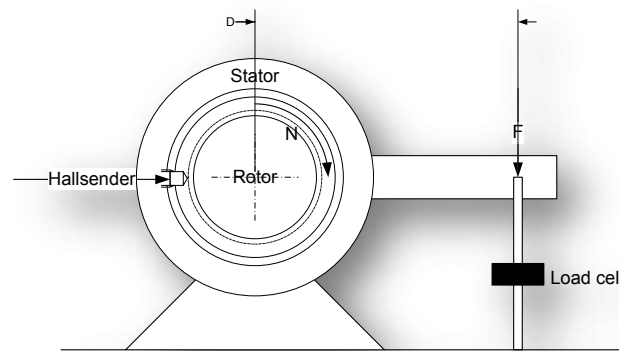


FIGURE 10 - DYNAMOMETER

Another measure of performance is the engine's specific fuel consumption and efficiency. Fuel consumption can be measured using a fuel consumption meter. Specific fuel consumption (sfc) is a measure of how efficient an engine is using its fuel to do the work (Heywood, 1988):

$$sfc = \frac{\dot{m}_f}{P} \quad [2.2]$$

Where \dot{m}_f is the mass flow rate and P is the corrected brake power of the engine.

The thermal efficiency of the engine can be measured if the energy content of the fuel is known and engine power output can be compared to the rate of fuel energy consumption.

$$\eta = \frac{P_{Engine \text{ out}}}{P_{Fuel \text{ consumption}}} \quad [2.3]$$

The BTF is fitted with an AVL 7030 mass fuel balance. A mass fuel balance measures the rate at which the engine consumes fuel by monitoring the mass of fuel in a vessel. The fuel is supplied to the engine from this vessel, and the engines fuel return is added to the vessel. The vessel is refilled if the vessel's fuel level falls below a minimum.

Humidity, air pressure and temperature affect the performance of an engine, which means that power curves of an engine performed on different days and locations will not be comparable. Therefore, a correction factor is used to adapt the torque readings read off by ETA. The correction factor recommended by VWSA is from the 80/1269/EEC European Union agreement on automotive testing (Palmer, 2008). The following equation is the correction factor used for turbo-charged engines:

$$\alpha = \left(\frac{990}{P_s - P_d} \right)^{0.7} \times \left(\frac{T}{298} \right)^{1.5} \quad [2.4]$$

Where:

P_s = Air pressure at the engine inlet in mbar,

P_d = Vapour partial pressure in mbar (Calculated by taking the product of the relative humidity and the saturation vapour pressure at ambient temperature), and

T = Ambient temperature at the inlet of the engine.

All of these properties are continually measured by ETA during testing, correcting the torque output from the engine. As mentioned in this chapter, the ECE correction factor is effective in ensuring that the test results are repeatable regardless of the atmospheric conditions of the day.

2.5 COMBUSTION IN A DIESEL ENGINE

The combustion process of diesel fuel in a DI diesel engine can be divided into four phases:

- ignition delay period,
- premixed burning period,
- diffusion burning period, and
- after burning period.

These phases will be discussed in more detail the next four paragraphs.

2.5.1 IGNITION DELAY PERIOD

The ignition delay period starts with the beginning of needle lift, when fuel injection starts. The injected diesel atomises into a spray of fine droplets. As the droplets mix with the hot air, the diesel heats up and evaporates from the droplet. The vapour mixes with the air and forms a flammable mixture, which initiates combustion. An auto-accelerating reaction takes place, where the heating of the combusted diesel vapour causes the temperature to rise. This causes more diesel to evaporate rapidly and combust. This reaction accelerates until it reaches auto-ignition, which marks the end of the ignition delay. The end of this phase is marked by a notable rise in the pressure of the cylinder. (Hsu, 2002)

2.5.2 PREMIXED BURNING PERIOD

The explosive stage marks the start of the premixed burning period, where flames start to spread rapidly through the flammable, air-vapour mixture. Consequently, the heat release rate

of the burning diesel vapour causes a rapid increase in cylinder pressure, which is characteristic of this phase. In this phase chemical kinetics control the reaction rate, and therefore this phase is also called the kinetic phase. In this phase, the fuel that is burned is the part of the fuel that is in vapour form and already mixed with air, fully prepared for combustion. The premixed burning period finishes as soon as all the evaporated fuel is burned. The amount of fuel that is burned in this phase is dependent on the length of the ignition delay period. The longer the ignition delay, the more fuel can premix with the air and more fuel is burned in this way. The heat release rate will be higher if the ignition delay is longer. (Hsu, 2002)

2.5.3 DIFFUSION BURNING PERIOD

After all the vaporized fuel is burned, the diffusion-burning phase starts (Hsu, 2002). The aerodynamic drag of the moving piston causes the jet of fuel to break up into more droplets. The droplets evaporate and mix with the air forming a more flammable fuel-air mixture. The mixture combusts and causes the temperature of the cylinder to become very high. The high temperature causes the pressure of the cylinder to rise accordingly, pressing the piston down. The high temperature causes more fuel to rapidly evaporate, where the air-fuel mixture is lean further away from the droplet, and very rich closer to the droplet. Due to the high temperature of this process and the lack of oxygen near the droplet surface, not all the fuel can undergo oxidation and falls into pyrolysis. This causes soot generation. The soot is burned as it is exposed to the available oxygen in the cylinder. (Hsu, 2002)

2.5.4 AFTER BURNING PERIOD

After the end of fuel injection, the remaining fuel and soot will continue to combust. There still is excess oxygen left for combustion because diesel engines always run lean. Piston motion is now in the expansion phase, and the temperature of the cylinder will start to decrease. The lower temperature will cause the soot burn-up to accelerate and the formation of NO_x to cease. Unburned soot, hydrocarbons, NO_x 's and carbon monoxide will remain until the exhaust valve opens. It will be released into the atmosphere as unwanted emissions. (Hsu, 2002)

2.5.5 COMBUSTION SUMMARY

The combustion of diesel fuel in the cylinder of a diesel engine was discussed in this section. From this discussion it is clear that finer droplets (or finer atomisation) of diesel as it is injected into the combustion chamber lower soot formation, shorten ignition delay, lower emissions and ensures complete combustion of the fuel. Finer atomisation can be achieved by using higher injection pressures.

By knowing the combustion phases, it is possible to pass informed judgement on the combustion process using heat release analysis or cylinder pressure curve analysis.

2.6 PRESSURE INDICATING

Pressure indicating, or indicating, as it is referred to in industry, is the measurement of pressures inside different components of the engine. These pressure measurements indicate the operating conditions in various parts of an engine such as:

- Intake and exhaust manifold pressures.
- In-cylinder pressure
- Fuel injection pressure

As internal combustion engine are heat engines, thermodynamic analysis can provide significant information on the engine's performance and efficiency. In this project, the focus is on the comparison of the performance of biodiesel and mineral diesel in an internal combustion engine. One way of comparing the performance of the diesel engine running on the different blends of fuel is to compare the output of the engine. This will give the difference of net power output of the engine, but still does not give an intuitive understanding of what is causing the difference in performance.

In thermodynamic analysis the work done on the piston head per cycle is calculated by the equation (Heywood, 1988):

$$W_{c,i} = \oint p dV \quad [2.5]$$

Where p is pressure in Pa and V is the piston volume in m^3 , subscript c is for cycle and i is for indicated.

And the power per cylinder is related to the indicated work per cycle by (Heywood, 1988):

$$P_i = \frac{W_{c,i} N}{n_R} \quad [2.6]$$

Where n_R is the number of crank revolutions per power stroke per cylinder (2 for four-stroke engines) and N is the crankshaft rotational speed. Using this information one can calculate the mechanical efficiency of the engine.

$$\eta_m = \frac{P_b}{P_i} \quad [2.7]$$

Where P_b is brake power. Naturally, the indicated power per cylinder must be multiplied by the number of cylinders.

If the calorific value of the fuel and the injected quantity of fuel per cycle is known, the chemical energy conversion efficiency can also be calculated, but due to some limitations with the fuel consumption measurement hardware, such measurements could not be made.

Further analysis of cylinder pressure versus crank angle data can be used to obtain quantitative information on the progress of the combustion of fuel in the cylinder. Methods exist to calculate the rate at which the fuel's chemical energy is released (known as heat release) and the mass of fuel that is burned (Heywood, 1988). Applying the first law of thermodynamics on a model representing a diesel engine's combustion chamber (the work volume), results in the following equation:

$$\frac{dQ}{dt} - p \frac{dV}{dt} + \sum_i \dot{m}_i h_i = \frac{dU}{dt} \quad [2.8]$$

Where $\frac{dQ}{dt}$ is the heat transfer rate across the system boundary into the system and $p \frac{dV}{dt}$ represents the rate of work transfer done by the system due to system boundary displacement. \dot{m}_i is the mass flow rate across the system boundary at location i (if the flow is out of the system, it would be negative), h_i is the enthalpy of flux i crossing the system boundary, and U is the energy of the material contained inside the boundaries of the system (Heywood, 1988).

This model is however very difficult to apply to a real world diesel engine due to the following (Heywood, 1988):

- Due to the injection into the cylinder and the non uniform mixture of fuel to the air in the cylinder, the process is not quasi static.
- The composition of the burning gasses are not uniform and can be considered to be unknown
- The heat transfer correlations for diesel engines are not defined well and are inaccurate.
- Crevice regions, like the volumes between the piston rings and the cylinder wall, constitute a few percent of the clearance volume. The gas in these regions is cooled to close to the wall temperature, which increases the density of the gasses in these crevices, making these volumes relatively important. Thus, these crevices add to the heat transfer across the walls of the work volume, and make it a non-negligible fraction of the combustion gases.

The situation is further worsened by other factors such as measurement errors, filter behaviour and signal noise. However, it is possible to use simplified indicating methods to give approximate answers and is able to serve as a comparative basis in fuels analysis (Heywood, 1988).

In this project, a direct injection engine is used. The combustion chamber model for this type of engine describes the cylinder contents as a single open system with the only mass flow (while valves are closed) being the fuel injection and crevice flow. The model then yields the equation:

$$\frac{dQ}{dt} - p \frac{dV}{dt} + \dot{m}_f h_f = \frac{dU}{dt} \quad [2.9]$$

There are two popular ways to obtain combustion information using this equation, in which the assumption is made that the temperature of the combustion gasses at any instant of time is uniform. Only the heat release analysis method will be used in this project to compare the performance of the fuels. In Appendix F, the derivation of the simplified heat release model is presented.

$$\frac{dQ_n}{dt} = \frac{\gamma}{\gamma - 1} p \frac{dV}{dt} + \frac{1}{\gamma - 1} V \frac{dp}{dt} \quad [2.10]$$

Where: $\gamma = \frac{c_p}{c_v}$ [2.11]

The value of γ , or the ratio of specific heats that will give the most accurate heat release data is not very well defined but a value of γ between 1.3 and 1.35 is recommended (Heywood, 1988). Using numerical methods, an estimation of the heat released can be calculated using pressure and crank angle values. The volume of the combustion chamber can be calculated using equation E.1 (in Appendix E). The heat release can also be calculated as a function of crank angle instead of time.

Another and more direct aspect of fuel performance that can be measured using cylinder indicating is the ignition quality of the fuel. As discussed in section 2.2.2, the fuel's Cetane number is an indicator of the ignition quality of the fuel, but it is hard to measure and Stellenbosch University does not have the necessary equipment to perform such tests. The most common test method is the ASTM D 613 test. This test involves the fuel to be compared to premixed blends of n-cetane and heptamethyl nonane in a test engine (Owen, et al., 1990). Another option to estimate the ignition quality is to calculate the cetane index. The cetane index is an estimation of the cetane number.

A third way is to compare ignition delay of a fuel by comparing the pressure curves inside the engine. A later rise of pressure relative to crank angle indicates that the fuel is of a lower ignition quality than the fuel to which it is compared, vice versa.

To perform indicating a shaft encoder is needed to read off the angle of the crankshaft, a pressure transducer is needed to measure the cylinder pressure and appropriate hardware is needed for high-speed data acquisition.

2.6.1 SHAFT ENCODER²

To measure the crank angle of the engine, a device called a shaft encoder or a rotary encoder is needed. Two main types can be used for angular encoding: absolute and incremental. Both of these have advantages and disadvantages, but the most important selection criteria for this project were cost, since a limited budget was available.

The most common type of angle encoder is of the incremental type. Incremental type shaft encoders use a rotating disk with incremental slots cut into it. The incremental slots can be picked up either by a photo diode or a hall sensor. Using one rotating disk with slots cut at regular intervals only the speed of the shaft can be calculated by relating the output frequency of the hall sensor or the photo diode with the number of teeth or slots on the rotating wheel. Angle encoding can be done by using a second wheel (or another slot on the same wheel) indicating the 0° mark. Therefore, by counting the number of pulses that passed by on the first wheel, after the pulse made by the second wheel or slot, and taking it as a fraction of the total number of slots in the wheel, the angle can be calculated in real time. An electronic signal condition unit can be used to convert the raw signals from the hall sensor or the photoelectric diode, to a more user-friendly signal such as 0 to 10V. The advantage of this type of encoder is that it is robust, but the problem is that the resolution of the measurements taken is limited to the number of slots cut into the wheel.

The second and more attractive type of shaft encoder is a multi turn, absolute encoder that is designed to give a 0 to 10V output depending on shaft position. There are a number of designs available (Kübler being one more well known supplier), but the most appealing feature of these

² (Figliola, et al., 2006)

encoders is the fact that the encoder itself delivers a signal where 0V correlates with 0° and 10V correlating with 360° and with perfect linearity between 0° and 360°. These shaft encoders are robust, compact and they are much cheaper than the incremental type encoders are. There is also no need for signal post processing since the signal is already in a 0 to 10V format.

2.6.2 PRESSURE TRANSDUCER

Traditionally pressure transducers used in automotive testing are of the piezo-electric type. Two of the most popular brands are Kistler and AVL, where Kistler is synonymous with piezo-electric pressure transducers itself and AVL being the leading name in engine testing equipment.

Piezo-electric crystals are crystals that generate electric potential when stressed. Generally, an electric potential is generated across the faces of the crystal, which can be picked up as a signal using a charge amplifier. Two of the most popular piezo-electric crystal materials used today is quartz (SiO₂) and Gallium Orthophosphate (GaPO₄) due to their long term stability (AVL, 2002).

Even though piezo-electric pressure transducers are the industry standard, the great cost associated with these sensors made alternative and more cost effective sensors a viable option. A company called Optrand created a fibre optic based pressure transducer that is favourably priced within budget. The prices of the sensors (all excl VAT) were:

- AVL – R 50700 (AVL, 2008)
- Kistler – R 37470 (INHER S.A, 2008)
- Optrand – R 8327.82 (Optrand, 2008)

The Optrand sensor uses two optical fibres, one carrying light from an LED light source, and the other returns reflected light off the diaphragm to the measuring electronics. The light carried by the one optic fibre is directed onto an Inconel diaphragm. The second (return) optic fibre picks up the light that is reflected by the diaphragm. As pressure increases, the diaphragm deflects. This deflection causes the reflected beam of light to shift relative to the inlet of the return optic fibre, hence altering the light intensity in the return optic fibre. The design had been proven to give excellent linearity and the sensor performs well against piezo-electric sensors (see Table 1). (Włodarczyk, et al., 1998)

	Kistler	AVL	Optrand
Measuring range:	0 to 200 bar	0 to 250 bar	0 to 200 bar
Lifetime:	1.00E+09	1.00E+09	1.00E+09
Overload:	250.0 bar	300.0 bar	400 bar
Sensitivity:	15 pC/bar	15 pC/bar	1.42mV/psi
Natural frequency:	130 kHz	130 kHz	>120 kHz
Nonlinearity:	<±0.6 %FSO	Not quoted	±1% FSO
Operating temperature:	-50 to 350 °C	up to 400°C	-40 to 300°C

TABLE 1 - COMPARISON BETWEEN PRESSURE TRANSDUCERS (AVL, 2008) (AVL, 2008) (AVL, 2002) (WŁODARCZYK, ET AL., 1998) (WŁODARCZYK, 2008) (INHER S.A, 2008)

The placement of a pressure transducer is also very important due to the flow patterns inside the cylinder of a diesel engine. But due to the fact that the only easily accessible way to insert a pressure transducer is by installing it in one of the glow plug holes, it has become the industry standard. Thus, glow plug type pressure transducers were used.

2.6.3 PRESSURE TRACE PHASING

It is important to have the pressure data and the shaft encoder data in proper phase for both heat release calculations and for the calculation of indicated power. Both the heat release calculations and the indicated power calculations are sensitive to phase shift, and a very small phase difference can alter results significantly. (Callahan, et al., 1985) It is not always possible to locate the engine's TDC position mechanically, and even if attempts are made to calibrate the shaft encoder relative to TDC, perfect phasing is not guaranteed. Dynamic phasing techniques can be used align the signals (Lancaster, et al., 1975).

To adjust the phase of a indicating set, the engine must be motored (driven by an electric motor, not firing). By plotting the cylinder pressure of a motored engine against the cylinder volume on a Log-Log graph, one can see the pressure curve running up and down itself. The line that forms should not (Lancaster, et al., 1975):

- Cross over itself,
- Have a broadening of the spike near the tip, or
- Form a curvature near the tip.

Hence, the spike formed on the Log-Log graph should be sharp and straight, as shown in Figure 11. By using the phasing used to obtain the correct Log-Log pressure spike, the rest of the indicating work on that setup can be properly phased.

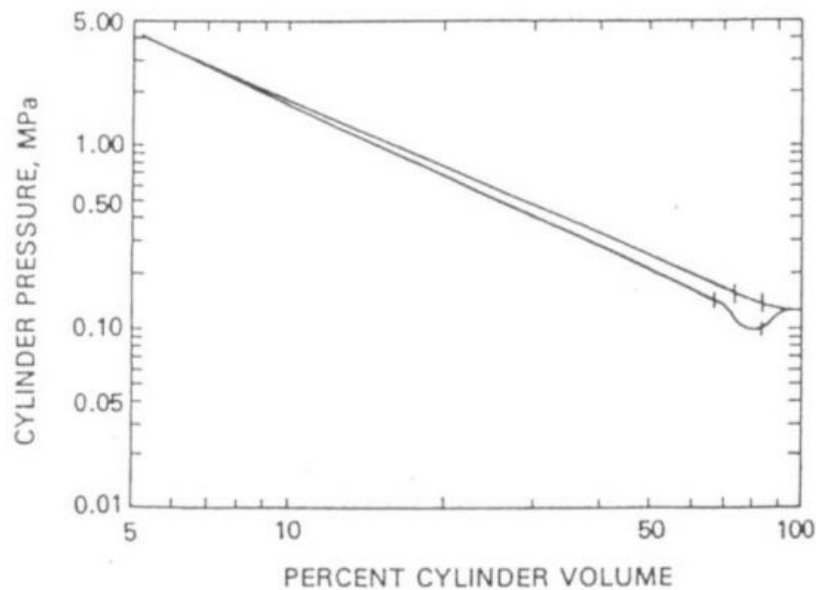


FIGURE 11 - DYNAMIC PHASING THROUGH THE USE OF A LOG P-LOG V GRAPH (CALLAHAN, ET AL., 1985)

2.6.4 INDICATING SUMMARY

In this section cylinder pressure indicating, or simply “indicating” was discussed. It was established that there are three ways in which the pressure and crank angle data could be used to compare the performance of diesel in an engine:

- Calculate indicated work done
- Calculate the approximate apparent heat release rate
- Comparing ignition delay
- Pressure trace phasing

Furthermore the shaft encoder technology and pressure transducers used for indicating was discussed. The use of an alternative pressure transducer was validated in the light of budget restrictions and the high cost of industry standard piezo-electric sensors. Its performance was compared, and the conclusion was made that an Optrand sensor was an appropriate sensor to use in this project.

2.7 LITERATURE REVIEW SUMMARY

In this chapter, a literature review was done in order to shed some light on the research question and project at hand. The following aspects were discussed:

- Details on the 1.9L TDI engine that is used in this project
- Various aspects of diesel fuel, including production, fuel properties and fuel standards
- Biodiesel production, properties, standards and biodiesel compatibility with regular engines.
- Testing procedures
- Diesel combustion in the engine’s combustion chamber.
- In-cylinder pressure indicating.

3 REDESIGN OF EXPERIMENTAL TEST CELL

For this project, the setup used by Palmer (2008) had to be reconfigured to accommodate a new engine. In this chapter, the new test setup will be discussed, starting with the old setup, then the physical connection of the new engine to its support systems and then the engine control and monitoring systems.

3.1 PREVIOUS SETUP (PALMER, 2008)

As mentioned in section 1, this project follows on a project completed by Palmer (2008). The objective of his project was to develop an autonomous and reconfigurable test cell to accommodate a newer engine in future work, like the project at hand. By the end of the project an entirely autonomous test cell was developed and tested and was ready for further development for bio-fuels testing. The test cell layout at the end of Palmer's thesis is shown in Figure 12 and the completed test bed is shown in Figure 13.

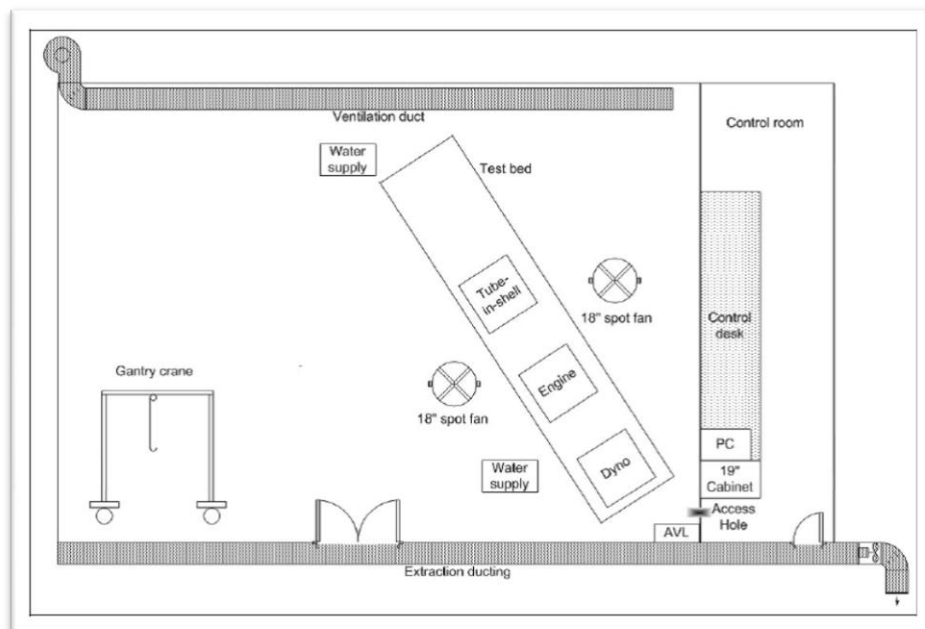


FIGURE 12 - TEST CELL LAYOUT (PALMER, 2008)



FIGURE 13 - COMPLETED TEST BED AT THE END OF PALMER'S PROJECT (PALMER, 2008)

The engine used in the first phase was a 2-litre Toyota 2C turbo diesel engine. The reason for using the Toyota engine was to validate the working of the test bed with a simple engine before using engines that are more complex.

The hardware that was included in the initial test cell was as follows:

- Test stand
- Large capacity tube and shell heat exchanger
- Schenck Dynobar 360 (waterbrake dynamometer) with load cell and controller
- AVL 7030 mass fuel balance
- Two spot fans for air circulation
- Ventilation ducts (built into the room)
- Cold water supply for cooling
- Allen Bradley Micrologix 1200 PLC along with all the necessary software, 4 channel analogue input module, a two input and two output analogue module and three thermocouple modules.
- Two computers
- Vaisala HMD60 Relative humidity sensor
- Vaisala barometer
- K-type thermocouples
- Honeywell three-way mixing valve and temperature controller.

The entire system had been integrated using Rockwell Automation's ladder logic software and ETA or 'Engine Test Automation' software to create a user-friendly SCADA interface to perform automated tests.

The decision was made to use as much as possible of the test cell layout as it was at the end of Palmer's project to minimize cost. For more information on the old test setup and detail on some of the equipment, refer to resource (Palmer, 2008).

3.2 NEW ENGINE AND PERIPHERAL COMPONENTS

As mentioned in section 1, VWSA sponsored two 1.9 litre TDI engines to the Stellenbosch University to be used in the BTF. The engines that they sponsored were of the BKC variant, which is a European variant of the 1.9L TDI engine found in the Golf. The problem was that the engine was not locally supported, and most of the associated parts for the engine needed to be imported. One of the engines was couriered back to VWSA B-plant to fit the engine with the necessary parts to run it. The engineers at product development at VWSA decided that the best route was to sponsor a locally supported engine. VWSA sponsored a third engine, a 1.9L TDI of the local ATD variant, along with all the associated parts that was needed to set up the engine.

The 1.9L TDI engine is described in detail in section 2.1.1.

3.3 ENGINE MOUNTING

Before installation of the engine began, the entire test rig was disassembled (shown in Figure 14). In order to accurately align the engine with the dynamometer a special CAD model of the engine and the test bed was created. All the test bed elements were measured up accurately and each element was constrained to its movable axis in the CAD assembly model. The engine's mounting interfaces were also measured up and an accurate CAD model was created of the engine interfaces. The engine model was used to space the test bed elements and to serve as a basis for the design of custom mounting brackets. By using the dimensions off the CAD model, it was possible to accurately align the engine with minimal adjustments. The CAD model along with the mounting brackets is shown in Figure 15.



FIGURE 14 - STRIPPED DOWN TEST BED BEFORE ENGINE INSTALLATION

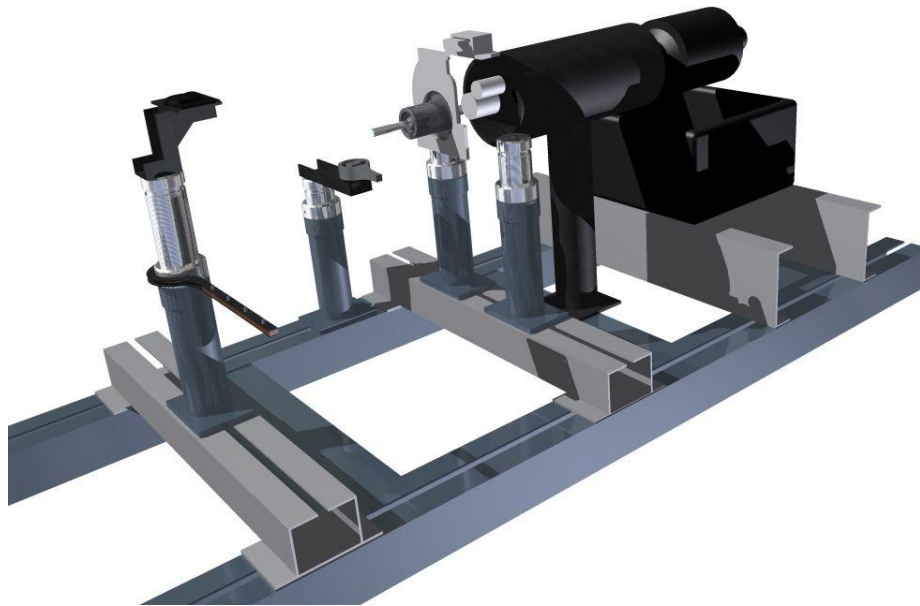


FIGURE 15 - CAD MODEL FOR ACCURATE MOUNTING OF THE ENGINE

The engine was mounted using the standard front engine mounting (near the #1 cylinder), the standard torque arm (bolted to the sump) and using the bell housing along with an adaptor plate that was supplied by VWSA. The adaptor plate bolts onto the open end of the bell housing and has a bracket at the top for a standard engine mounting, also supplied by VWSA. Thus, the engine hangs on the two engine mountings and is restrained by the torque arm.

The engine is designed to run with its pistons at a 13.5° angle CCW to the vertical if observed from the #1 cylinder to ensure proper flow of lubricants through the engine. The engine's running angle was checked after it was mounted by taking off the motor head and measuring its angle with a digital level on the flat face of the block. The same was done to ensure that the engine was installed horizontally along the length of the motor. Both angles were measured and found to be correct. A set of pictures of the setup is included in Appendix G, where the engine mountings are visible.

3.4 DRIVE SHAFT AND COUPLING

For the new experimental setup, the connection point for the motor was the clutch spline. VWSA test engineers recommended that the original clutch spline from a VW Polo gearbox (which was supplied with the engine) should be modified to transmit power from the engine to the cardan shaft rather than to make a new spline. The shaft that they supplied is shown in Appendix H. A power transmission assembly was designed (shown in Figure 16) roughly based on a similar design used by VW. The gearbox spline was casehardened and was too hard for conventional machining techniques, thus the shaft had to be precision ground.

After the mounting of the engine was complete, the need for a torsional damper was realised. The rubber damping-element from a BMW 530d propshaft was used and a set of adaptors was designed to incorporate the damper into the drive train. The CV joint was shortened to allow all the rotating parts to fit under the safety cover.

The ability for the transmission assembly to take the load of the 1.9L TDI engine is justified by the following:

- Splined shaft – The shaft was designed for the specific engine, therefore ensuring sufficient strength.
- First CV joint adaptor – It is made of similar material (EN36a) as the gearbox shaft and it is thicker than the shaft in all places. The spline is hardened and wire cut.
- CV-joint – The same CV joint was used in the previous research project (Palmer, 2008), and the new engine's performance falls into the same selection bracket in the Löbro CV joint catalogue used for the selection of that CV joint.
- Rubber damper – The rubber damper is designed to operate with a much larger engine (3L turbo diesel out of a 5 series BMW) and will be able to transmit the power without any foreseeable problem.
- Damper adaptor plates – The adaptor plates have a much larger cross section than any other part of the drive train. It is made of bright mild steel.
- All the bolts used in the assembly are high tensile bolts and secured with LOCTITE™ adhesive.

To ensure that the engine and the transmission components were running true, a clock gauge was used to check for run-out and a digital level was used to see if the shafts were perfectly horizontal. The use of locating spigots ensured that all parts ran true on connecting interfaces. Minimal adjustments to the torque arm ensured that the whole setup was running true. The power transmission unit and the rear end mounting of the engine with the adaptor plates are shown in Figure 17.



FIGURE 16 - POWER TRANSMISSION UNIT

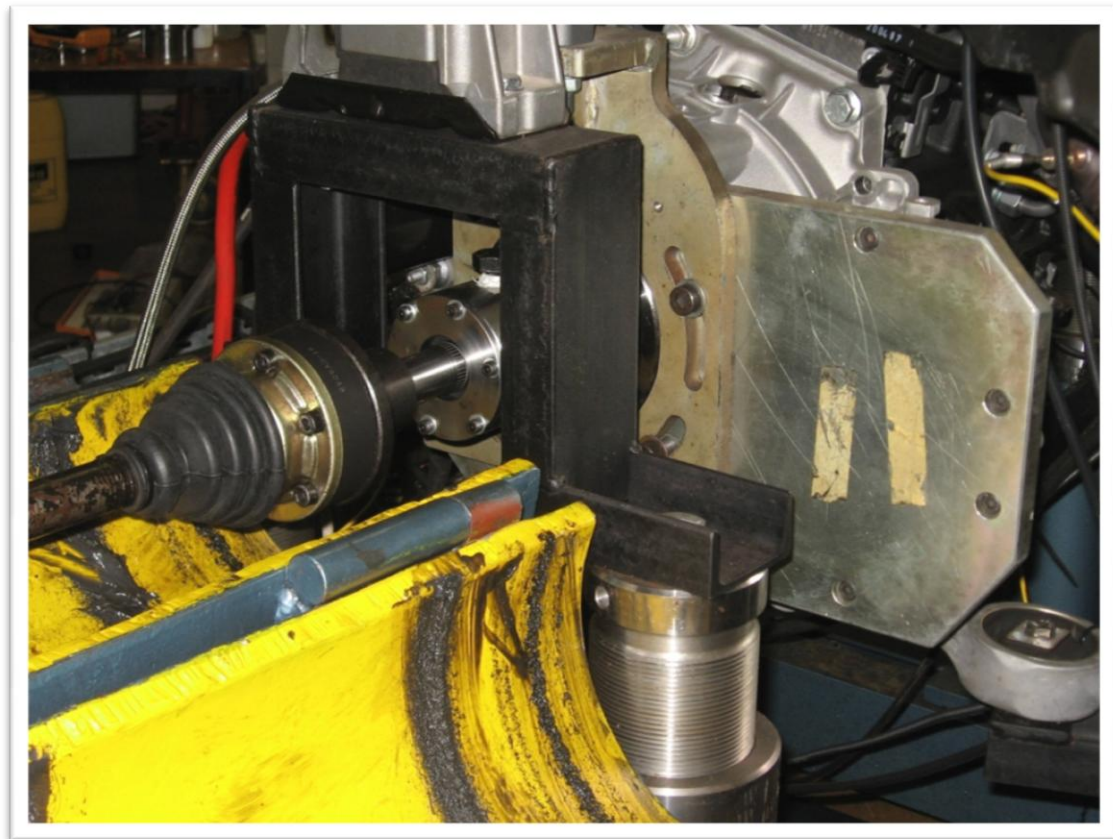


FIGURE 17 - REAR END MOUNTING AND POWER TRANSMISSION

3.5 COOLING AND WATER SUPPLY

In this section, the cooling of the engine, fuel and the dynamometer water supply will be discussed. The cooling of the engine, fuel and the dynamometer all make use of the cold water supply of the mechanical engineering building. This consists of an underground storage tank, rooftop storage tank, pumps, a small cooling tower and a network of pipes built into the building. For more information on the department's cooling infrastructure, please refer to Palmer (2008).

3.5.1 PRIMARY ENGINE COOLING

The VW ATD engine is water-cooled and has its own coolant pump, temperature control valve and a temperature transducer. To cool the engine, water has to be taken from the engine's hot water outlet, cooled, and returned to the engine's cold-water intake.

Initially the heat exchanger was set up with a counter current flow configuration, and with the cold water supply (shell side) wide open. A Honeywell three-way mixing valve is used to mix the cold-water stream from the heat exchanger outlet and the hot water stream from the engine outlet to regulate the coolant inlet temperature. The inlet and the outlet temperature of the engine coolant are measured using K-type thermocouples. All the piping used in the cooling system is 1¼-inch water hose.

To be able to control the coolant inlet temperature, a series of trial and error tests had to be done to determine some characteristics of the cooling system. The reason that calculations were not possible is due to the following unknown aspects of the cooling system:

- The capacity of the shell and tube heat exchanger.
- The flow rate of the cooling water through the shell.
- The flow rate of the coolant is unknown and will vary as the engine regulates the flow rate.

A Honeywell 6420A3007-3 valve actuator along with a Honeywell temperature controller was used to try to control the temperature of the inlet water supply. Initially a PID controller was implemented, but the overshoot in the transient conditions caused overheating of the engine. Another attempt using a bang-bang type control system (the same temperature control program used by Palmer (2008)), had an even worse effect on the temperature control. Palmer (2008) encountered the same problems in his project, but it was attributed to the slow-acting valve actuator used. This phenomenon raised questions about the compatibility of the heat exchanger, coolant temperature control system, the temperature control system of the engine and the nature of the cooling system in general. A series of experiments were done to find the problem.

Through testing, it was found that the engine's own temperature control keeps the coolant flow such that the outlet temperature of the coolant is maintained around a set point of 90°C to 95°C. However, if the inlet coolant temperature is too low, the engine throttles down the flow of the coolant. Thus, if the inlet temperature is too low, the coolant flow rate will be low. Thus, the response of the temperature control is slow.

As soon as the inlet temperature is at approximately 75°C, another effect kicks in. The engine opens its coolant regulator valve, and the coolant flow is now regulated by the speed of the engine (which governs the speed at which the coolant pump turns). The water that goes through the heat exchanger comes back at temperatures approaching room temperature, and is mixed with the hot water source (from the engine) at 90°C. This makes it a very difficult system to control with a feedback type controller, since very small adjustments in the position of the three-way valve causes a large change in the coolant supply temperature (the same problem experienced in the shower if the geyser temperature is set too high and a sticky tap is used to try and control it).

To remedy the temperature control problem, the shell and tube heat exchanger was set up in parallel flow configuration to decrease its cooling capacity and a ball valve was installed (coolant flow regulator valve) in the water supply line to the shell to throttle its water supply. The engine was then ran at full power, the three way mixing valve was opened fully (maximum cooling) and the coolant flow regulating valve was adjusted to make the engine inlet coolant temperature 65°C. By doing this, the cold stream was throttled to 65°C, and hot stream was 90°C at most operating conditions (may vary due to engine control).

During preliminary testing it was found that the most effective way to regulate the coolant inlet temperature was to adjust the position of the three-way valve using toggle switches from the control room. The temperature control was done this way during testing. A schematic of the engine-cooling pipe is shown in Figure 18

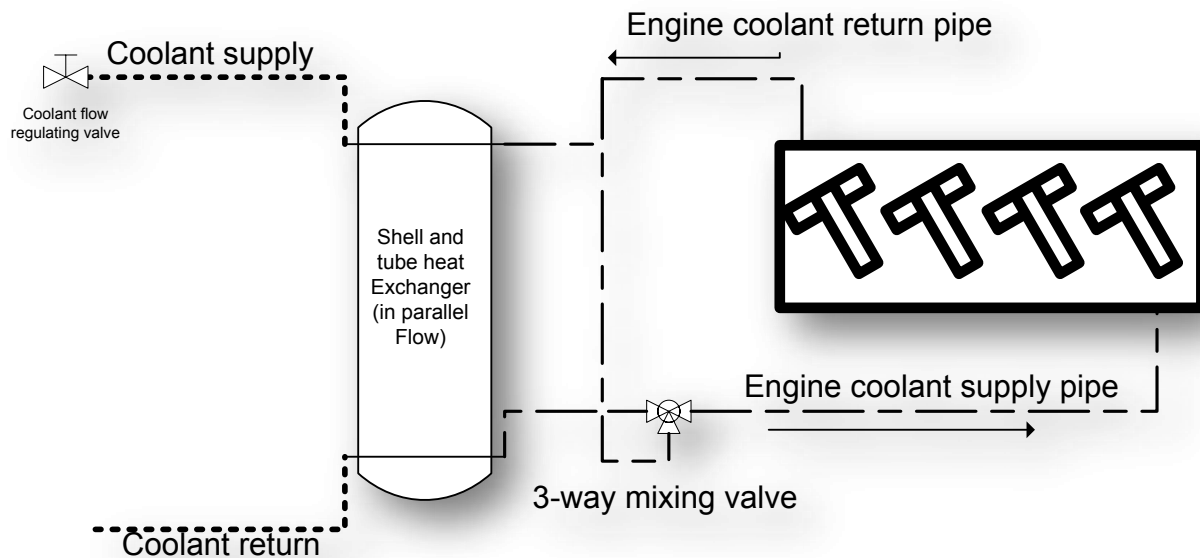


FIGURE 18 - ENGINE COOLING PIPE FLOW DIAGRAM

3.5.2 FUEL COOLING

During testing the engine returns hot fuel to the fuel supply vessel (in this case it is the AVL mass fuel balance) at temperatures in excess of 100°C. The reason for the hot fuel return is the injector bypass that takes place after compression (see section 2.1.3). The bypassed fuel is added to the rest of the fuel in the mass fuel balance's control vessel. Due to the small size of the control vessel, the supply fuel temperature leaving the vessel approaches that of the return fuel, which is too high (depending on engine, the supply fuel temperature should not exceed roughly 55 °C, based on the flash point of diesel). The problem with high temperature fuel is that the volatile components of the diesel will start forming vapour and may choke the injector nozzles. The vapour in the return line cause the mass fuel balance to oscillate as the fuel spurts out irregularly into the measuring vessel. Therefore, the fuel needs to be cooled before the fuel is returned to the mass fuel balance.

Normally in test cells there is a fuel conditioning unit that supplies cooled fuel to the engine and conditions the return fuel, but due to the fact that the test cell is still a work-in-progress, an intermediate solution had to be found. An old annulus type cooler was used to cool the return fuel. It consists of two copper pipes, a $\frac{3}{4}$ inch (OD) copper pipe and another 1 $\frac{1}{4}$ inch (OD) copper pipe brazed eccentrically around each other with appropriate fittings to allow water to be passed down the inner tube and diesel to be passed along the outer tube. The cooler is 1.2m long and is set up for counter current flow. A K-type thermocouple was installed to measure the temperature of the fuel that is returned to the mass fuel balance.

During preliminary testing, it was found that the fuel temperature was kept under 50°C. To see if the fuel affected the readings of the experimental setup temperature, a few tests were done with higher, lower and no water flow through the diesel cooler. Neither the power/torque curve nor the pressure profile was affected by the diesel temperature; however, the effects on the mass fuel balance were profound. See Section 4 for more information on the preliminary test runs and commissioning.

3.5.3 CHARGE AIR COOLING

The new VW engine installed on the test bed is equipped with a charge air cooler (also known as an intercooler), shown in Figure 19. The intercooler is usually located in a car's wheel well where there is a lot of airflow. Therefore, to cool the charge air, the intercooler needs to be supplied with a steady flow of cool ambient air through its radiator.

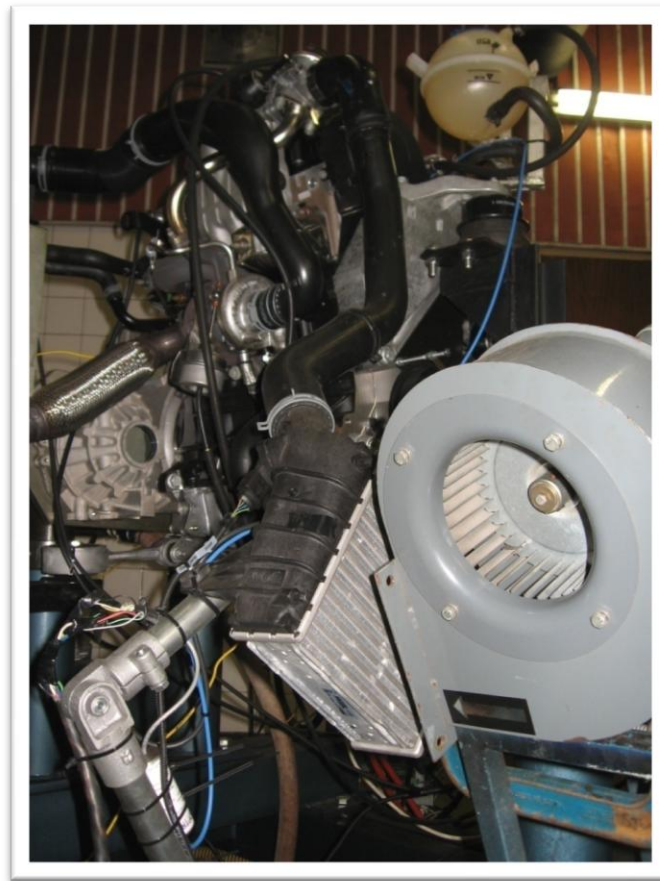


FIGURE 19 – INTERCOOLER WITH COOLING FAN (DUCTING REMOVED FOR DETAIL)

Rose+ Krieger scaffolding elements that are bolted to the test bed itself support the intercooler. A centrifugal fan was installed over the intercooler, which is supported by a steel frame clamped to the test bed.

3.5.4 FORCED CONVECTION OF THE ENGINE BLOCK

In a car, there is a considerable amount of airflow under the bonnet of the car and especially under the sump of the engine. This also cools the engine to a certain extent. As stated by Palmer (2008), the ventilation system of the test cell does not allow enough air flow over the engine itself since the air inlet is halfway up the wall on the one side of the test cell, and the extraction duct is near the roof. Thus, any airflow caused by the test cell's own ventilation system will not flow over the engine. To remedy this, two spot fans were implemented to move hot air away from the sump and engine block.

3.5.5 DYNAMOMETER WATER SUPPLY

The Schenck D360 is a waterbrake dynamometer, and needs water to dissipate the energy of the engine. The water supply of the dynamometer is included in this subsection because it forms

part of the piping layout of the test cell. The water supply of the dynamometer has to have a maximum pressure of 0.6 bars and a 1.6 L/s minimum flow rate (Stellenbosh Automotive Engineering, 2006). To optimize the control of the dynamometer, the flow rate of the dynamometer had to be adjusted for the power range of the engine. This was done by Palmer (2008) when he set up the engine and dynamometer control system according to the method is prescribed in the Schenck installation manual (Schenck Pegasus GmbH, 2001). The optimal flow rate of the dynamometer is set by running the engine at full load and then closing the gate valve until the water outlet of the dynamometer is at 50°C. For the new engine, the dynamometer water supply settings were kept the same, and the engine was run at full load. The outlet temperature did not rise above 50°C, therefore the dynamometer water supply valve was kept at the same setting.

3.5.6 COOLING AND WATER SUPPLY SUMMARY

This section dealt with the cooling of the engine, charge air, fuel and the water supply of the dynamometer. The engine is cooled primarily using a closed loop cooling system that utilizes a shell and tube type heat exchanger in parallel flow and temperature control is done by using a three-way mixing valve with a Honeywell temperature controller and valve actuator. The test cell ventilation system and two spot fans, enable forced convection to occur around the engine block, providing secondary engine cooling

Fuel is cooled using a copper annulus type cooler configured for counter flow. The fuel return temperature is effectively kept between 40 and 50°C but exact control of the fuel supply temperature is still inadequate. The charge air is cooled using the engine's OEM supplied intercooler unit and is cooled using a centrifugal fan.

The dynamometer water supply is also included in this section because it is part of the coolant water supply loop of the test cell. The dynamometer's water supply rate had been set up in a way to allow optimal control of the dynamometer. In Figure 20 a diagram of the entire test cell's water supply network is shown.

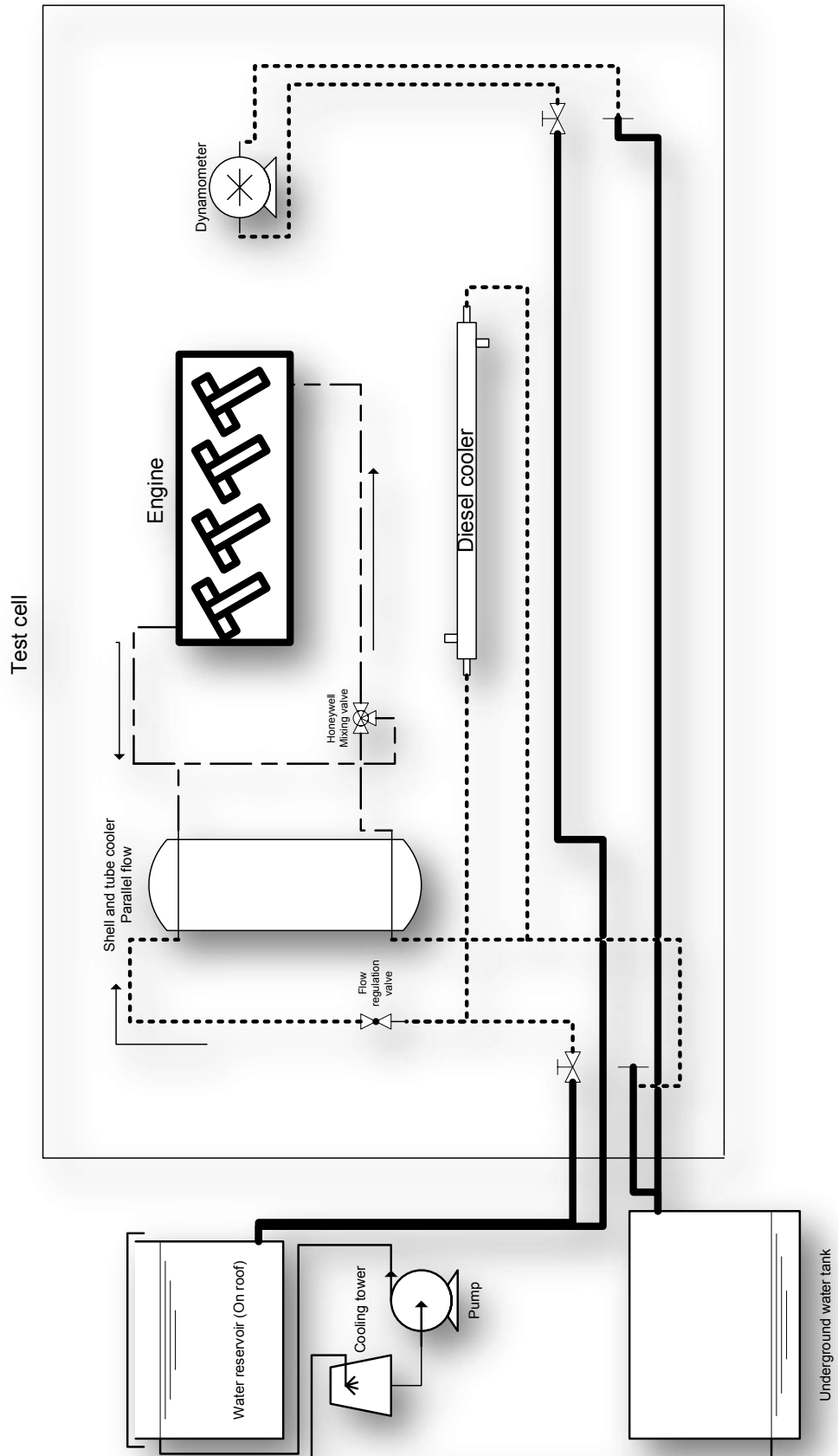


FIGURE 20 - WATER SUPPLY DIAGRAM

3.6 VENTILATION AND EXHAUST GAS EXTRACTION

To extract hot air and exhaust gasses from the test cell the test cell's built-in extraction and ventilation system is used. The extraction system consists of a fresh air duct and an extraction duct on either side of the test cell (the extraction duct is located on the door side of the test cell). The exhaust fumes are also extracted via the extraction duct, and the exhaust pipe of the engine is connected to the duct via a flexible steel hose that is bolted via a steel pipe to the extraction duct.

The original Polo exhaust system is used on the engine, including the catalytic converter and the silencer box. These components with proper mountings were supplied by VWSA along with the engine. The mid-section of the exhaust was omitted from the test setup, as there was no space for it. The first section of the exhaust system (the catalytic converter) is suspended on its own mountings, which is bolted onto a frame that is bolted to the test bed itself. The second section (the silencer) hangs with chains from the ceiling and the steel hose couples over the two exhaust pipes. Figure 21 shows the layout of the ventilation system and a photo of the exhaust system are shown in Figure 22.

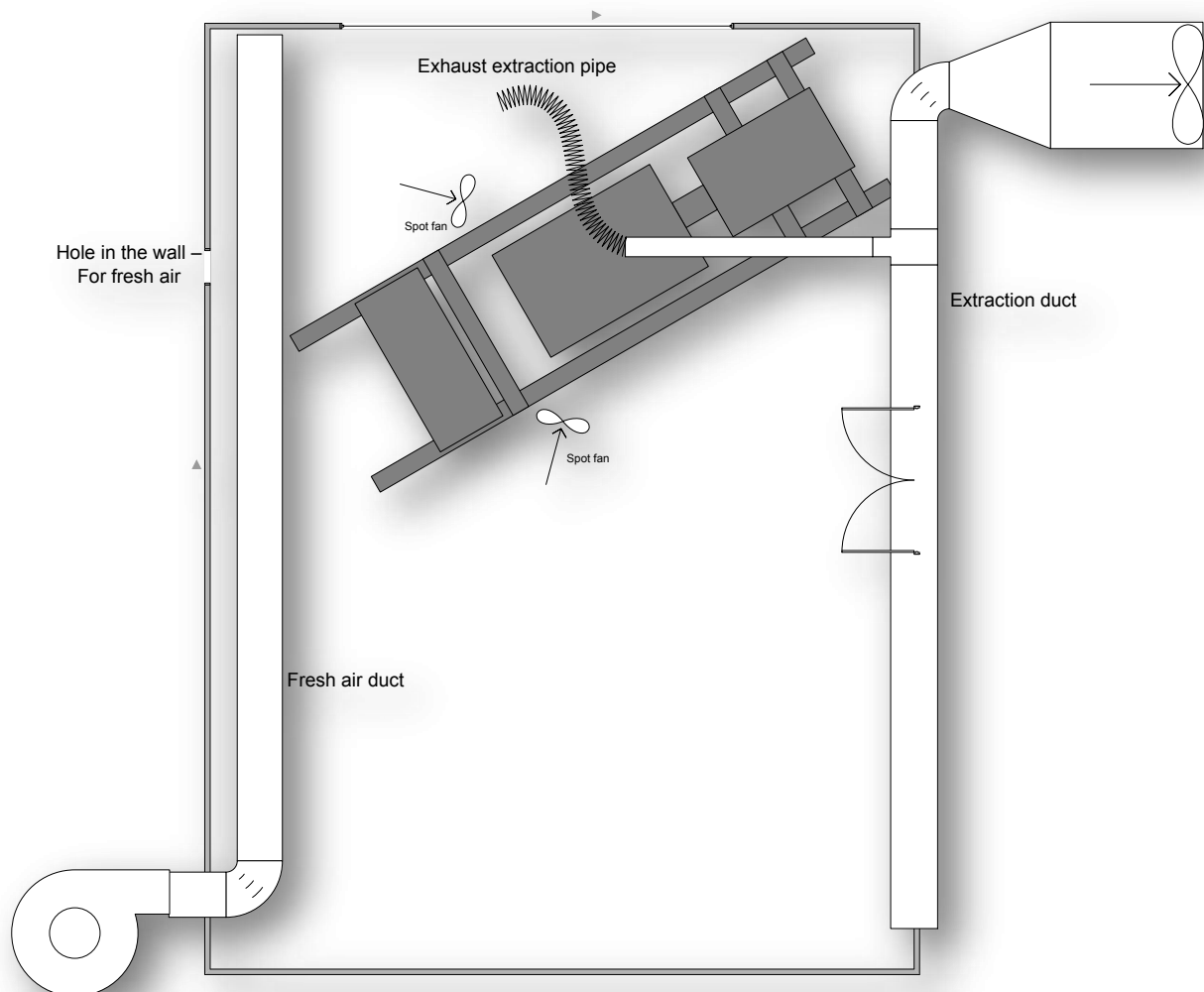


FIGURE 21 - VENTILATION SYSTEM



FIGURE 22 - EXHAUST SYSTEM

3.7 FUEL SUPPLY

Normally in a test cell, an entire fuel delivery and conditioning system would be available to deliver fuel to the engine. Because the test cells are still a work-in-progress, a temporary fuel delivery system is implemented. No endurance tests needed to be performed during this project, and only small batches of 15L of diesel at a time were needed for experiments. It was found during testing that 15L of diesel fuel was enough for warm-up, three power curves, and three cylinder pressure measurements.

The fuel to be tested is placed in a 15L jerry can, which is pumped up to the AVL mass fuel balance via a filter using a Bosch fuel pump. The fuel pump relay is wired in parallel with the mass fuel balance's refill valve, thus allowing the AVL to be refilled with no pressure head. The fuel flows from the AVL mass fuel balance through a fuel filter and a priming bulb towards the engine. The fuel return line is connected to the AVL via an annulus cooler and the return fuel is added to the AVL's measuring chamber. Standard 8mm fuel hose is used throughout. A sketch of the fuel delivery system is shown in Figure 23.

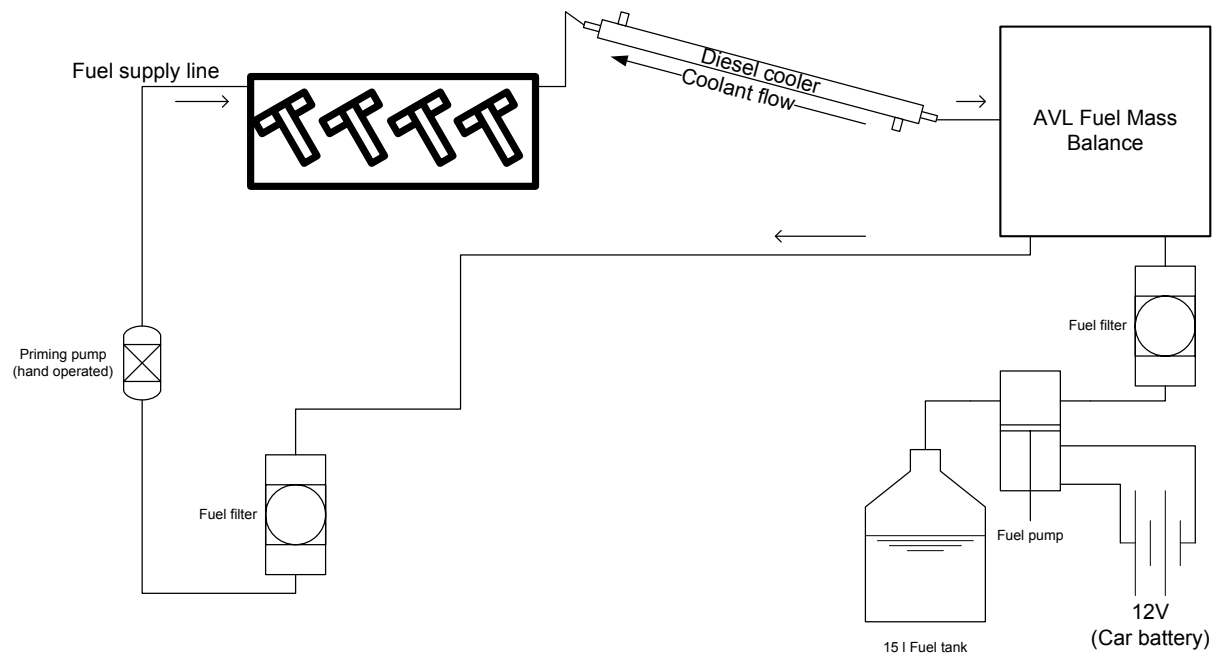


FIGURE 23 - FUEL DELIVERY DIAGRAM

3.8 VACUUM SYSTEM

The vacuum system built into a standard VW Polo is used to operate a large number of actuators throughout the car. Only three actuators are actually necessary to operate the engine, namely; exhaust gas recirculation valve, throttle vane, and turbo vain adjusting capsule.

Since the original vacuum control system is redundant, WWSA supplied an alternative, simpler vacuum control system along with the wiring loom. The control valves interface with the ECU and the vacuum pump supplies vacuum. The vacuum pump forms part of the preliminary fuel pump and is located on the back of the engine and driven by the camshaft. The layout of the vacuum system is shown in Figure 24.

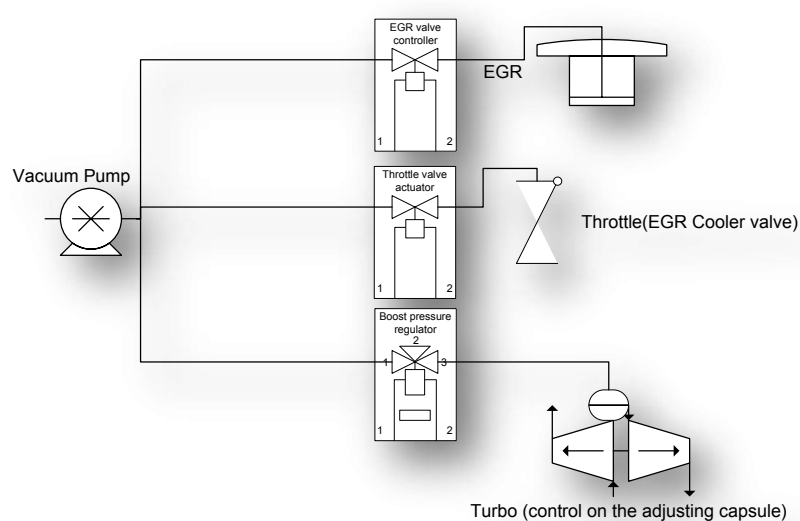


FIGURE 24 - VACUUM SYSTEM

3.9 ENGINE ELECTRIC AND ELECTRONIC SYSTEM

One of the reasons that Palmer (2008) used an older technology Toyota engine is because it had no engine electronics and advanced control systems. Thus, he could concentrate on the development of the autonomous test bench. The aim of the project at hand was to utilize the autonomous test bench built by Palmer (2008), and to integrate the new VW engine onto it. A few decisions were made that influenced the development of the engine control system and the way the engine's own control system and the test bed interfaced with the control system in the test cell. These were:

- That a proper VW engine test loom was to be used for testing (no other options available, discussed in section 3.9.1).
- That the original VW accelerator pedal was to be used to control the engine (common practice in engine testing).
- That no changes were to be made to the PLC's control software or to the ETA interface that Palmer (2008) created.
- That the original wiring of the test bed control systems were to be used.

This section is integral with section 3.10, thus common components to the systems dealt with will be mentioned. In this section the PLC terminals will only be indicated by the terminal names, but the PLC is discussed in section 3.10.1. The details of the connections of the engine to the PLC will be discussed in section 3.9.

3.9.1 LOOM AND ECU

At the initial stages of the project a decision had to be made concerning the use of an OEM wiring loom and ECU, or the use of an aftermarket or makeshift engine control system. VWSA agreed to sponsor a test loom, immobilizer and a custom test ECU along with the ATD engine. The test loom is a simplified version of the loom used in a regular car with only the necessary components on it to run the engine. Features such as glow plug relays, oil pressure sensors, oil temperature and a few other non-essential parts of the loom were removed, as they could be measured using test cell equipment (making data acquisition easier). The ECU also had been reprogrammed to accommodate the changes and not to go into limp mode after a problem occurred during testing. The immobilizer was also supplied along with the ignition key (cable tied to the ignition switch).

A detailed wiring diagram of both the electronic and electrical system combined is shown in Figure 27. The ECU that VW supplied is the same ECU used in the Polo TDI with the ATD engine (shown in Figure 25), namely a Bosch EDC (Electronic Diesel Controller). The ECU has two plugs. One plug has pins 1 to 81 (plug A) and attaches to the part of the loom that goes to the auxiliary parts of the engine. The other plug has pins 82 to 121 (plug B) on it and goes to the engine block itself. The plug layout and the wiring details of each pin are listed in Appendix I. The loom is shown in Figure 26.



FIGURE 25 - BOSCH EDC



FIGURE 26 – LOOM SPREAD OUT ON THE FLOOR

After the engine's mechanical installation was complete, all the sensors and actuators that came with the engine were installed and the loom was connected to the appropriate sensors. The entire loom including the vacuum system was fixed to an electrical backing plate that was bolted to the side of the test bed via Rose + Krieger scaffolding. The VAG-COM plug was installed to the CAN bus interface, and was connected to one of the computers via a 5m extension cable. The accelerator pedal was installed onto the pedal actuator. For more information on this, see section 3.10.1.

The ignition was wired to the PLC via two E-stop buttons, one inside the test cell and another inside the control room. The one E-stop also has a hard stop function built into it, which gives a

24V signal to the PLC (see wiring diagram in Figure 27). The ignition relay is switched through the PLC switch terminals *OUT1* and *DC1* using a 24V supply. The hard stop signal is picked up via the digital input *IN0/COM0*. All terminal allocations are the same as those devised in Palmer's (2008) project to allow the same PLC program to be used. For more information on the wiring of the electronic system, refer to the wiring diagram in Figure 27.

3.9.2 ELECTRIC SYSTEM

The new VW engine was supplied complete with an alternator and a starter motor. A 12V car battery is used to power the starter motor, and the alternator is wired up to charge the battery during testing. The starter motor is equipped with its own relay which needs a 12V supply to switch on the starter motor. The starter relay's 12V power supply is switched through another relay. The PLC switch terminals *OUT2* and *DC2* switch this relay, which is the same as the terminals used in Palmer's project. For more information on the wiring of the electric system, refer to the wiring diagram in Figure 27.

3.9.3 ENGINE ELECTRICAL AND ELECTRONIC SUMMARY

In this section the electric and electronic system associated with the engine was discussed. The loom was supplied by VWSA along with the engine, and it came complete with all the parts necessary to run the engine. The wiring of the loom is briefly overviewed to serve as a resource during faultfinding. The wiring of the electric system is also discussed briefly, along with the terminal wiring of the electric and electronic system to the PLC. The terminal allocation of the PLC was kept the same, making it possible to control the engine without altering the PLC program. A complete wiring diagram of the electronic and electric system is shown in Figure 27.

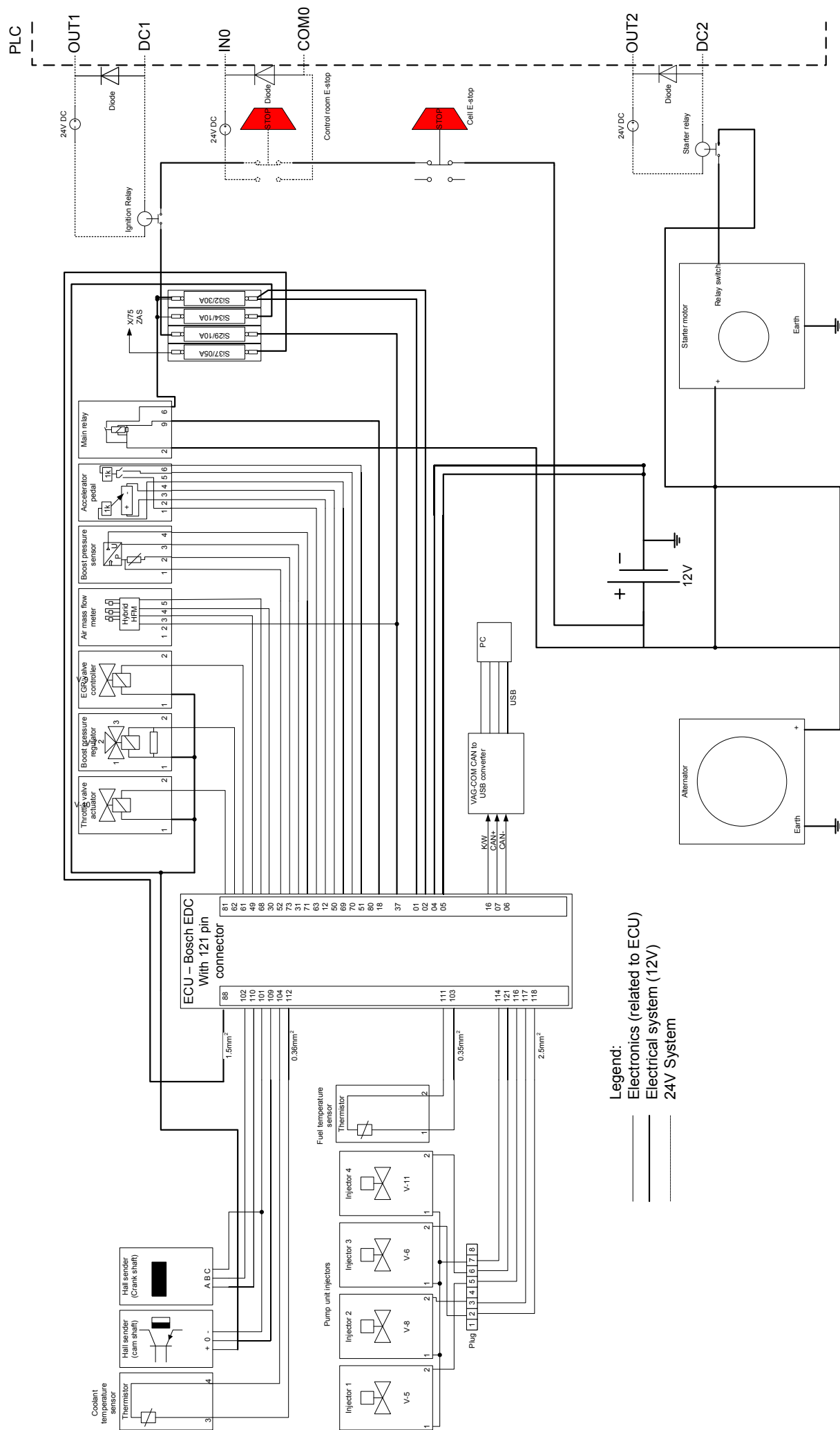


FIGURE 27 - ENGINE ELECTRIC AND ELECTRONIC SYSTEM

3.10 TEST CELL ELECTRONICS

Palmer (2008) set up the test cell control systems and electronics during his project. Therefore during this project, the control systems and electronics were modified to accommodate the requirements of the new engine. Initially, during the engine installation, it was decided to alter the original test bed electronics and software as little as possible. The annotation used in this thesis is consistent with Palmer's thesis, hence labels like "IN1+" refers to the pin on the PLC with the same label on the PLC. Standard electric notation is used throughout.

The PLC used is an Allen Bradley Micrologix 1200, and is used to sample all the analogue and digital signals coming from the test cell equipment and controls the test cell through its analogue and digital outputs. Along with the Micrologix 1200 PLC, five expansion modules are used:

- 4 channel analogue input module
- 2 input, 2 output analogue module
- 3 thermocouple modules

The PCL communicates to the PC using the serial port and RsLinx® software. The PLC is programmed using RsLogix®, a ladder logic programming package by Rockwell Automation®. For more information on the PLC, refer to Palmer (2008).

3.10.1 TEST CELL AND ENGINE CONTROL SYSTEMS

The engine setup as described in this chapter only requires the following inputs for control of the engine:

- starter relay,
- ignition relay, and
- accelerator pedal

The wiring of the starter and the ignition relays to the PLC is discussed in section 3.9. The accelerator pedal is fixed to the pedal actuator, and will be discussed in subsequent sections. The glow plug relay and wiring had been removed since the glow plugs are not used. Other aspects of the test cell that need control are the dynamometer and the coolant inlet temperature.

The dynamometer control was kept the same as with Palmer's (2008) project. The wiring of the dynamometer to the PLC is shown in Figure 28. The speed and the torque outputs of the D360 dynamometer are 0 to 10V signals and the control is done using a 0 to 10V signal.

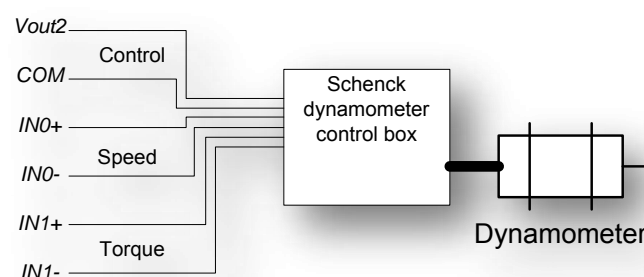


FIGURE 28 - DYNAMOMETER CONNECTION TO PLC

The same E-stop as was used by Palmer is used in the new setup and none of the wiring has been changed. Thus, the E-stop still gives a 24V signal between IN0 and COM0, which instructs the PLC to brake the engine (the PLC program was kept the same). In this way, the engine is stopped in the fastest way possible.

To adjust the accelerator pedal position, one of two methods could have been used. Either a pedal signal generator can be used instead of the pedal itself, or the pedal could be actuated mechanically using a stepper motor or a linear actuator. On further investigation, the latter option appeared to be cheaper. VWSA supplied a decommissioned throttle actuator from one of their old test cells. The throttle controller needed reconditioning and modification. It consists of a servo motor and a controller unit. The controller unit has a 0V position adjustment (for 0% pedal adjustment) and a 10V position adjustment (for 100% pedal adjustment). The pedal is connected to the same PLC terminals that drove the PWM generator (Vout1 and COM, shown in Figure 29), thus no alteration had to be made to the PLC program to accommodate the pedal actuator. The pedal actuator and control unit with the pedal is shown in Figure 30 and Figure 31 respectively. Calibration will be discussed in section 4.1.

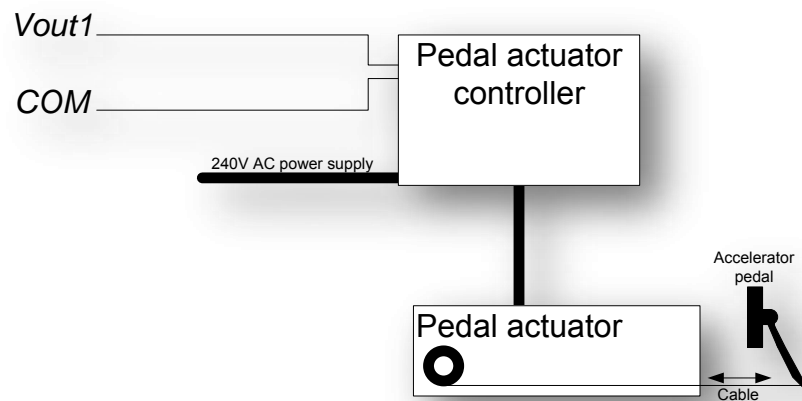


FIGURE 29 - WIRING OF THE PEDAL ACTUATOR



FIGURE 30 - THROTTLE ACTUATOR CONTROLLER

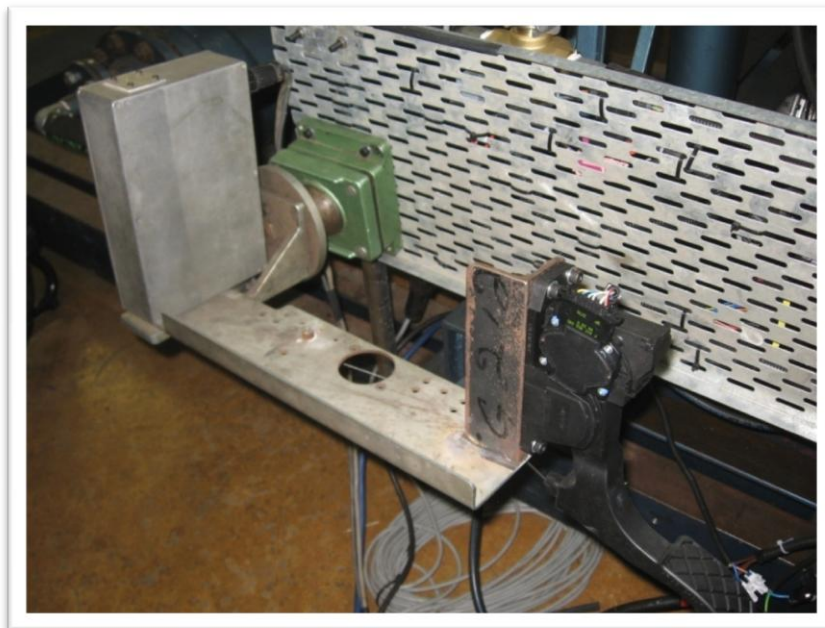


FIGURE 31 - THROTTLE ACTUATOR

As discussed in section 3.5.1, a Honeywell ML6420A (24V) valve actuator is used to control the coolant inlet temperature, and it was found that the best way to control the inlet water temperature was by hand. A set of manual switches is used to control the coolant temperature from the control room. Figure 32 shows the wiring of the valve actuator and Figure 33 shows how the valve actuator is wired to the test cell control switches.

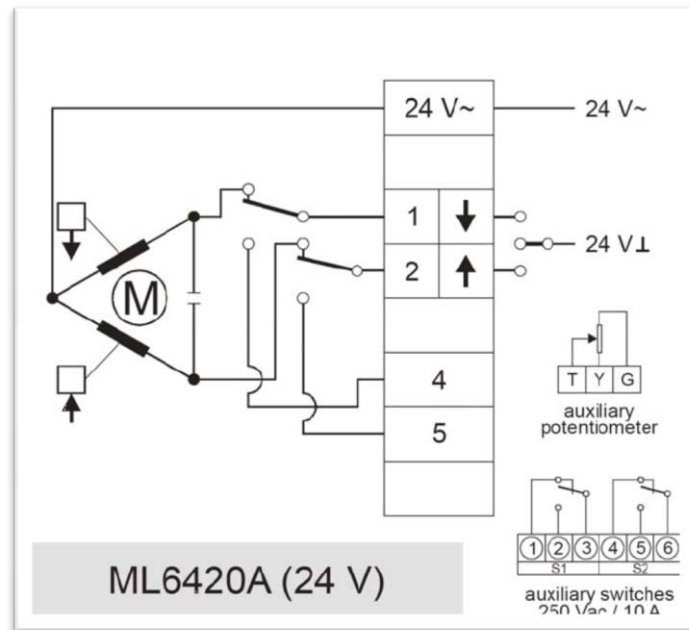


FIGURE 32 - ACTUATOR WIRING (HONEYWELL, 2008)

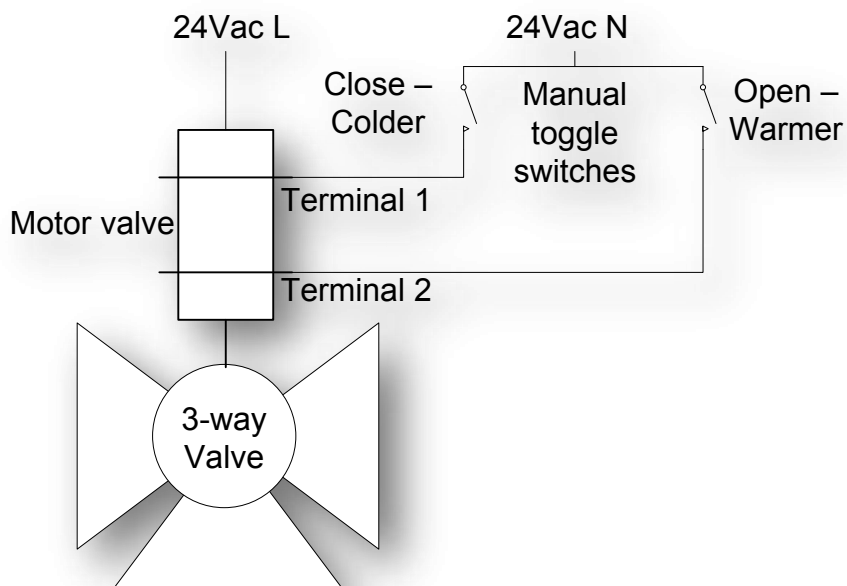


FIGURE 33 - VALVE ACTUATOR WIRING DIAGRAM

3.10.2 ENGINE AND TEST CELL MONITORING

There are a number of parameters that should be measured on the test rig, engine, ECU and in the test cell itself. These include:

- Engine
 - Air inlet temperature
 - Exhaust gas temperature
 - Coolant inlet temperature
 - Coolant outlet temperature
 - Oil temperature

- Oil pressure
- ECU
 - Fault signals
 - Engine operating parameters picked up by engine electronics
- Test rig
 - Fuel consumption
 - Engine speed
 - Engine torque
 - Fuel inlet temperature
- Test cell
 - Ambient temperature
 - Ambient barometric pressure
 - Relative humidity

All the temperatures are measured by 3mm K-type probe thermocouples due to their high temperature resistance and robustness. All the thermocouples are connected to the junction box installed by Palmer, which is wired to the PLC thermocouple expansion modules. The only difference is that the spare thermocouple is used to measure the inlet fuel temperature. The thermocouple layout is shown in Figure 34. Labels T1, T2 and T3 represent the thermocouple expansion units from left to right.

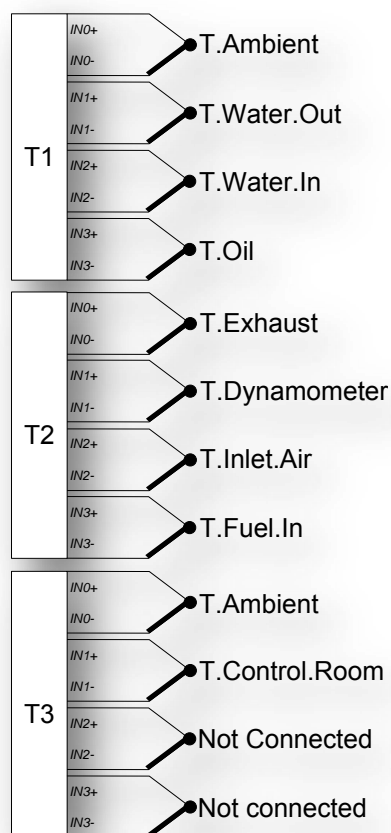


FIGURE 34 - THERMOCOUPLE WIRING

As discussed in section 2.1.4, the ECU monitors engine parameters and uses these signals as criteria in ECU algorithms to calculate the signal outputs to control the engine. Information, read and generated by the ECU, is stored in a memory register that can be accessed via the CAN bus. The CAN bus can be accessed via the diagnostics port in the loom, shown in Figure 27. Using a special hardware and software package called VAG-COM the CAN-bus can be used to:

- Read off, analyze and clear fault codes.
- Pair electronic components and immobilizers.
- Read off all and log engine-operating conditions.
- Read off and log all actuator commands in real time.
- Read off and log all calculated engine parameters.
- Display critical timing information in graphic form.

In the experimental setup at hand, VAG-COM is used to measure the following:

- Engine speed.
- Injected fuel quantity.
- Fuel consumption (only according to mapping).
- Engine mapping.
- Specified start of fuel injection.
- Specified injection duration.
- Synchronisation angle.
- Air intake pressure.
- Air intake temperature.
- Mass air intake.
- Mass air intake per stroke.
- EGR duty cycle.
- Coolant temperature.
- Fuel exit temperature.
- Fuel cooling state.

Most of these parameters can be read from the mapping on the ECU, but some are readouts of the sensors. The mapping plays an important role in seeing what the engine is doing in terms of control, enabling further investigation in combustion analysis. This will be discussed in detail in section 5.

The AVL 7030 fuel balance is a dynamic fuel balance that measures fuel consumption by mass. For more information on the working of the fuel balance, please refer to Palmer (2008). The setup of the fuel balance was not changed and the wiring was kept the same. Figure 35 shows how the AVL 7030 is wired to the 4-channel analogue input.

The oil pressure is measured using a Wika Ecotronic 0-10 bar pressure transducer. The pressure is measured right before the oil filter where the regular oil pressure sensor is installed in the VW engine. The stock oil pressure sensor was fitted with a $\frac{1}{8}$ " BSPF male fitting. A custom fitting was made to fit the socket and a 1m braided steel hose connects the engine oil system to the pressure sensor. The braided steel hose protects the pressure transducer heat and vibration. Figure 35 shows how the pressure transducer is wired to the PLC's 4-channel analogue input expansion module.

The barometric pressure, relative humidity and ambient temperature have to be measured to calculate a correction factor to compensate for differences in engine performance due to changes in atmospheric conditions. For more information on the ECE correction factor, refer to section 2.4. The barometric pressure is measured using a Vaisala PTB 110 barometric pressure transducer. The pressure transducer has a 0-5V output and is connected to the analogue input card as shown in Figure 35. The relative humidity is measured using a Vaisala HMD60 relative humidity sensor, which gives a 4-20mA output also connected to the 4-channel analogue expansion module.

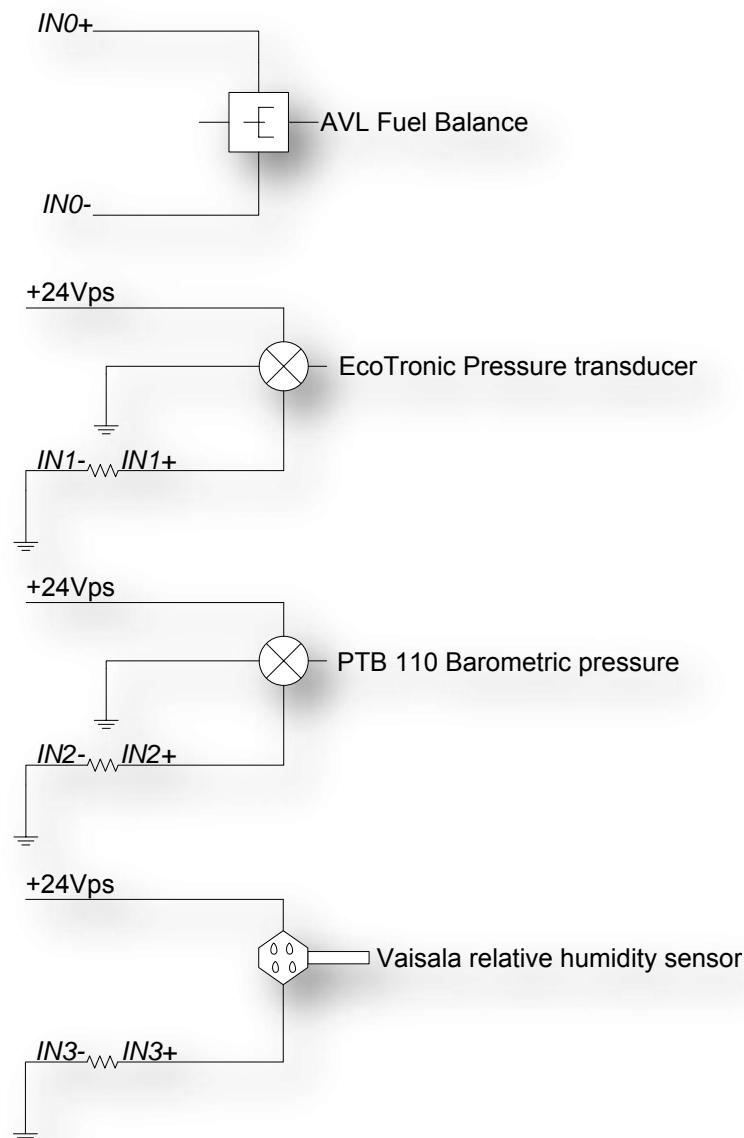


FIGURE 35 - 4 CHANNEL ANALOGUE INPUTS

Engine speed and torque is measured by instrumentation on the dynamometer. The dynamometer is fitted with a hall sensor picking up the engine speed (by sensing the teeth of a toothed wheel running past it) and the torque is measured using a load cell that is installed on the one side of the dynamometer. The calibration of the load cell is discussed in section 4.1. Both

the hall sensor and the load cell signals are picked up by the dynamometer control unit and are translated to a 0-10V signal that is passed through to the PLC. The connection of the dynamometer to the PLC was discussed in section 3.10.1.

3.10.3 TEST CELL ELECTRONICS SUMMARY

In this section, the test cell electronics was discussed under two classifications:

- Control electronics
- Measuring electronics

The test cell is controlled and monitored using an Allen Bradley Micrologix® 1200 series PLC with expansion modules. This forms the centre of the test cell's electronics. The PLC is controlled using a PC, using a SCADA package discussed in section 3.11.

3.11 CONTROL AND MONITORING SOFTWARE

To control and monitor the test cell the following software packages are used, namely ETA (Engine Test Automation), RSLinx® and RSLogix® 500. An additional package is used called VCDS, to interface with the VAG-COM diagnostics port to read off and alter ECU parameters. Two PCs are used for testing. The first PC with ETA is used to control the test cell and to record all the engine parameters measured by sensors wired to the PLC. The second PC is used either to log information extracted from the ECU or to store indicating data from the indicating equipment.

With the first PC, the PLC communicates with it via a serial port. RSLinx® is then used to communicate with the rest of the computer software that is needed to interface with the user. RSLogix® is used to program the PLC using ladder logic programming. The ladder logic program is discussed in section 3.11.2. ETA is a software package supplied by CAE (Cape Advanced Engineering) designed specifically to integrate a number of different components into one user-friendly environment for engine testing. ETA communicates with RSLinx® via DDE communication protocol. ETA handles the user interface, calibration, data logging, etc. For more information on ETA and the program used in this setup, refer to section 3.11.1.

The reason for the second PC is the fact that the high speed electronics used to log the indicated pressure in the cylinder is very memory intensive, and one PC cannot handle both the indicating and the engine control. The indicating hardware and software is discussed in section 3.12. VAG-COM and VCDS is discussed in section 3.11.3. A depiction of how hardware and software relate to each other is shown in Figure 36.

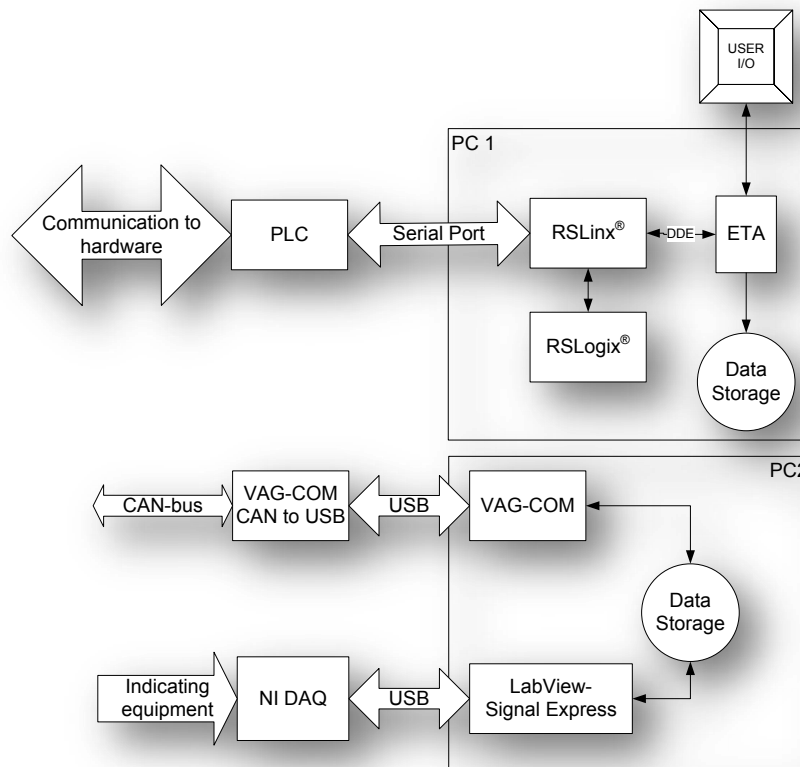


FIGURE 36 - CONTROL SOFTWARE

3.11.1 ENGINE TEST AUTOMATION (ETA)

ETA (Engine Test Automation) is a software package sold by CAE (Cape Advanced Engineering) and was designed specifically for engine testing. It enables a user to interface with numerous different components connected to a computer in one user interface, to control an engine test cell. ETA enables a user to:

- Do signal acquisition and conditioning.
- Calibrate sensors.
- Customize a user interface.
- Calculate virtual parameters.
- Set alarms for operating parameters.
- Log and analyze data.
- Create automated test cycles.

ETA communicates with the PLC using RSLinx® by utilizing DDE communication protocol. This means that the data are placed on the DDE client buffer registers in the form of raw data between zero and 32767. Thus, if a 0 to 10V signal is passed, 0V is passed as 0 and 10V as 32767 in whichever register it is placed. More information on the buffer addresses is given in section 3.11.2.

In ETA all the input and output channels can be assigned, scaled, virtual channels can be set up, and the display can be customized. The new ETA interface is an adaptation on the one that Palmer (2008) used, and a few changes were made in terms of scaling of values and calculation

of virtual channels. A screenshot of the interface is included in Appendix J. More information on calibration, scaling and correction factors is discussed in section 4.

3.11.2 PLC PROGRAM

Palmer (2008) programmed the PLC in RSLogix®, and due to the wiring scheme used, no large alterations to the PLC program had to be made. The only difference was that a new coolant temperature controller was implemented, which was later discarded when it was found that hand control of the temperature controller was more effective.

As in the previous setup, the MAIN program runs continually, calling two sub routines, IN and OUT. The IN ladder samples the channels on the PLC and passes the values to the N10: x buffer, which is read off by ETA. This is occupied as follows:

- Thermocouple expansion module 1 – N10:1 to N10:4
- Thermocouple expansion module 2 – N10:5 to N10:8
- Thermocouple expansion module 3 – N10:9 to N10:12
- 4 x Analogue input – N10:13 to N10:16
- 2A2D – N10:17 to N10:18
- Digital in – N10:99

Similarly, the OUT ladder reads off buffer values from N14: x (written by ETA) and write it to the appropriate registers in the PLC. The N14: x Buffer is occupied as follows:

- N14:1 – Torque setpoint
- N14:2 – Speed setpoint
- N14:6 – Throttle output
- N14:99 – Digital OUT

The coolant temperature controller has been deactivated in the new setup and the channels were left open, but the timer controlled grounding of the speed and torque setpoint pins were kept the same. Thus, the PLC program operates essentially the same than the old program. The ladder logic program is shown in Appendix J.

3.11.3 VAG-COM

As mentioned in section 3.10.2, VAG-COM is used to interrogate the ECU's data register for operating information and fault codes during testing. The VAG-COM hardware is a CAN to USB converter, and the VCDS software is used to perform tasks on the ECU via a computer. During a test, the following measuring blocks are measured in the specified order:

- 15
- 4
- 11
- 10
- 7
- 3

Each of these measuring blocks accesses a certain set of registers in the ECU and the result is the ability to read off the engine mapping as it is accessed and to read off engine sensors during operation.

VCDS is set up to log all the engine parameters during testing in a comma separated value (.csv) file that can be opened in Excel® for further analysis.

3.11.4 SOFTWARE SUMMARY

In this section, the software used in the test cell (except for indicating) was discussed. There are three primary packages used:

- RSLogix® – To program the PLC.
- ETA – For a user interface and data logging.
- VAG-COM – To interface with the ECU and to log operating parameters.

A secondary package, RSLinx® is used to facilitate communication between ETA and the PLC. All these packages were integrated to give the operator of the test cell the ability to control the engine autonomously and record all the critical engine parameters during test cycles.

3.12 INDICATING SETUP

As discussed in section 2.6, cylinder pressure indicating serves as a valuable diagnostic tool to analyze and compare how a fuel performs in a diesel engine. To perform cylinder pressure indicating the following hardware is needed:

- shaft encoder,
- pressure sensor, and
- high-speed data acquisition hardware.

As discussed in section 2.6.2, an Optrand sensor was selected as a pressure sensor. An AutoPSI-S pressure sensor was purchased in the PSIGlow-A format, which is a glow plug type pressure sensor.

The Optrand sensor requires a power supply of 9 to 18V and draws a maximum current of 85mA. The pressure transducer was installed into the number one cylinder via the glow plug hole. Figure 37 shows two PSIGlow-A sensors.



FIGURE 37 - PSIGLOW-A PRESSURE TRANSDUCERS

It was decided to use a Kübler 3671 singleturn absolute shaft encoder (shown in Figure 38). The specifications of the encoder are shown in Table 13. The shaft encoder was installed on the engine's crankshaft pulley using a custom-made steel adaptor. A small steel plate bolted to the engine is used to keep the shaft encoder at the same angle relative to the engine after calibration. A picture of the setup is shown in Figure 39.



FIGURE 38 - KÜBLER TYPE 3671 SHAFT ENCODER (KÜBLER, 2009)

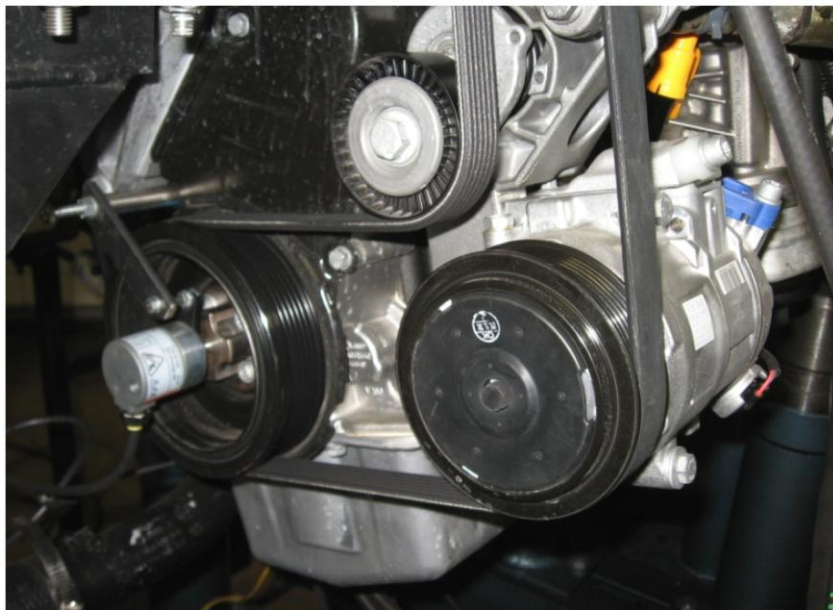


FIGURE 39 - SHAFT ENCODER SETUP

A National Instruments USB-9201 data acquisition card was used to record the pressure and the crank angle during tests. The NI 9201 is a high speed analogue data acquisition card.

Both the pressure transducer and the shaft encoder are powered by a voltage source set at 18V. The power supply earths and the signal output commons of both sensors are all connected to both the voltage source earth and the *COM* of the data acquisition card to prevent a ground loop. The signal wire of the shaft encoder is connected to *A10* and the signal from the pressure transducer is connected to *A11*. The wiring schematic is shown in Figure 40. The specifications of the components of the indicating set are presented in Appendix K.

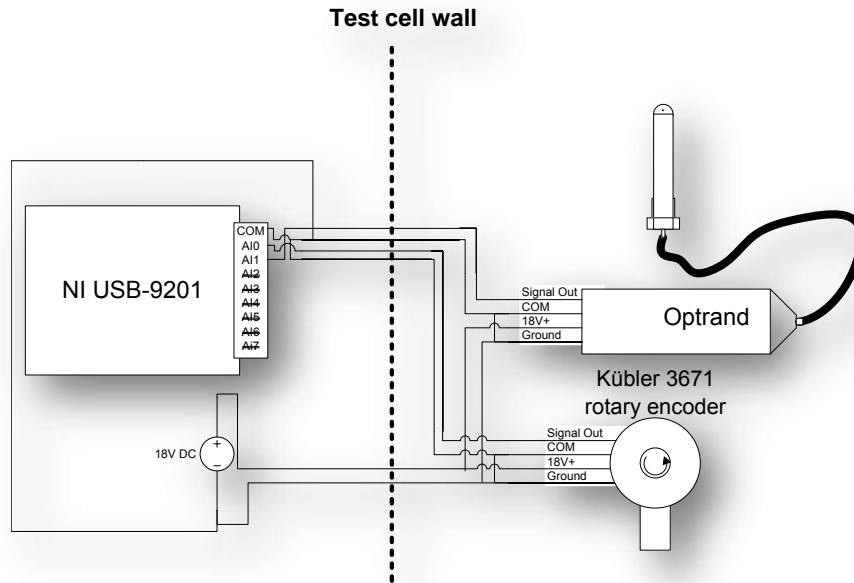


FIGURE 40 - INDICATING SET WIRING.

The data is captured, processed, displayed and stored using National Instrument's LabView SignalExpress. As discussed in section 4, the settings for the data acquisition were obtained through a test program to determine the measuring system's characteristics. The recording settings were as follows:

- Data acquisition
 - Continuous sampling
 - Sampling speed: 24kS/s (per channel)
 - Signal scaling ON:
 - AI0: Linear – 0-10V to 0-360°
 - AI1: Scaled by function to kPa
- Filter:
 - Butterworth
 - Low pass
 - Second order
 - 1.5kHz cutoff
- Power spectrum: On
- Log: Filtered data

These settings gave the best results, as discussed in section 4.

3.13 EXPERIMENTAL TEST CELL SETUP SUMMARY

This chapter dealt with the experimental setup that was created to compare the effect of bio-fuels compared on a modern 1.9L TDI engine with pump unit injection with normal mineral diesel. The following aspects were discussed:

- Mechanical installation
 - Mounting
 - Drive shaft connection

- Engine cooling and water supply
- Ventilation and exhaust gas handling
- Fuel supply
- Vacuum system
- Engine electric and electronic system
- Test cell electronics
- Software
- Indicating equipment

All the topics were discussed in sufficient detail so that the setup can be reproduced from this section (with some references to Palmer's thesis). The next phase of the project, following engine set-up, was preliminary testing and commissioning in which the set-up fine-tuned so as to achieve repeatable engine performance measurements. This is discussed in the next section. The completed test setup is shown in Figure 41.

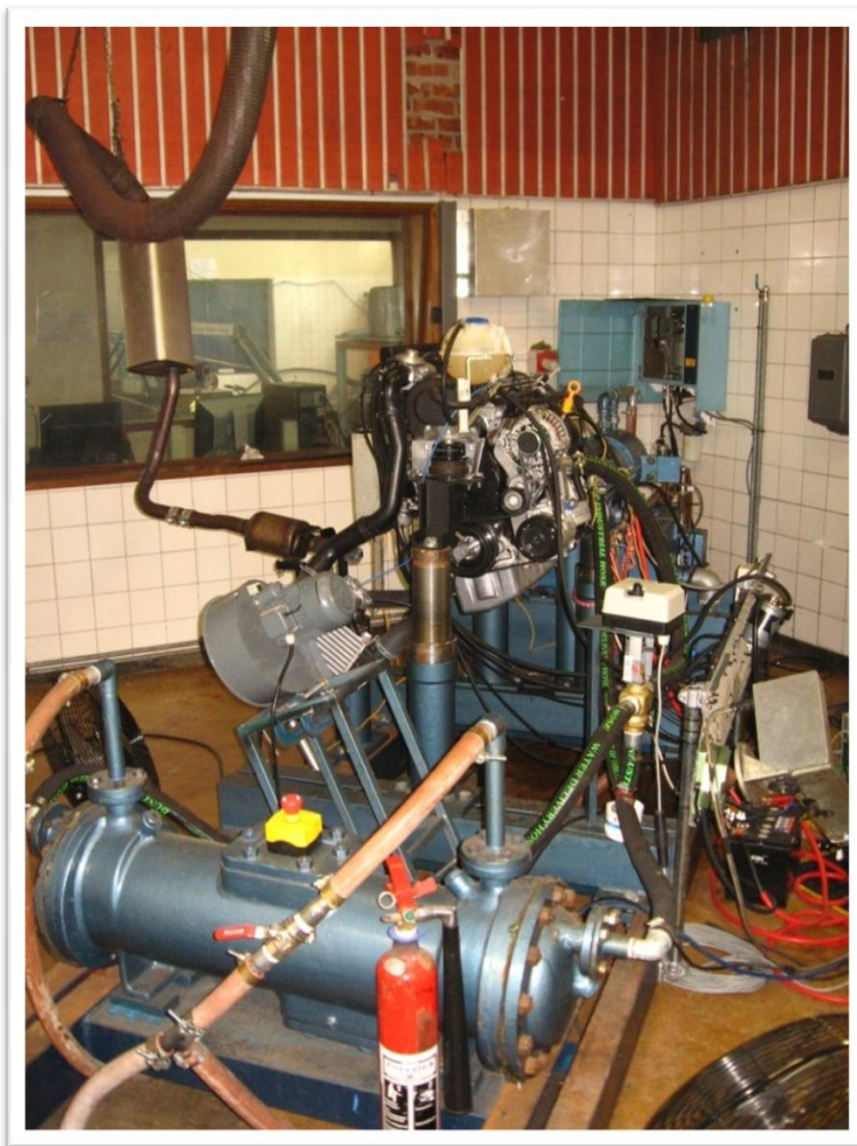


FIGURE 41 - COMPLETED TEST SETUP

4 SYSTEM COMMISSIONING AND REPEATABILITY ANALYSIS

To ensure the accuracy of testing, all the sensors had to be calibrated and the repeatability of the readings had to be evaluated before the test setup could be commissioned for research. This chapter deals with the calibration and preliminary tests that preceded commissioning.

4.1 SENSOR CALIBRATION

Before the test rig was evaluated, all the sensors were either calibrated or their calibration was checked. The sensors that were used in the old test rig were checked and verified. The sensors that were not moved, altered or changed in essential application were taken as calibrated and the calibration curve in ETA was kept the same. Table 2 summarizes the calibration of all the sensors that had been reused.

The calibration of the load cell (for torque measurement) was repeated to ensure that the calibration curve made in ETA was still valid. The torque arm was used just as prescribed in the Schenk manual (Schenk Pegasus GmbH, 2001) for calibration. An initial calibration was done; loading the load cell gradually with weights and unloading it, checking for hysteresis, linearity and accuracy of the load cell. The load cell's initial calibration was still found to be valid. Before and after each testing session the torque arms were used to check the readings of the load cell. No inconsistencies were found throughout preliminary and final testing phases.

The thermocouples were assumed to work correctly, as their readings were not critical to the research done during this project.

The calibration of the AVL 7030 was re-evaluated as prescribed in the user manual (AVL, 1984). According to the calibration checks, the AVL 7030 mass flow meter's readings were accurate and correlated with the previous calibration done by Palmer. However, it was found that the readings of the fuel balance fluctuated during testing. The reason for this problem is indirectly attributed to the engine's high injection pressure; causing high temperatures in the return fuel line (in excess of 100°C). The high fuel temperature in the return line causes the formation of vapour. This causes irregular fuel flow as bubbles are formed inside the return line. Attempts to remove these fluctuations by cooling the fuel to a temperature below the fuel's flash point, failed because the return line propagates these fluctuations in flow, even if the vapour is condensed in the fuel cooler.

An interesting observation could be made regarding the nature of the problem by comparing the fluctuation of the fuel consumption reading for the engine running on bio-diesel versus that of normal diesel. Greater fluctuations were observed using ULSD than in the case of biodiesel. This phenomenon can be attributed to the lower flash point of the ULSD compared to that of the biodiesel (55°C to 120°C (Bioservices cc, 2009))

Sensor	Implemented to measure:	Calibrated	Calibration method	Person responsible for initial calibration	Alterations made to sensor or installation changed in nature	Re-checked	Reason to doubt readings	Measurement accuracy critical	Problem
Load cell	Engine torque	Yes	Torque arm (Palmer, 2008)	Palmer (2008)	No	Yes (Johan Kotze)	No: Re-calibrated between tests always consistent	Yes	No
Dynamometer speed pickup	Engine speed	No	N/A	N/A	No	No	No: Physical design of sensor is very reliable and no check is required	Yes	No
Vaisala Relative humidity sensor	Test cell relative humidity (to calculate ECE correction factor)	Yes	OEM Calibration certificate H15-07400098	OEM	No	No	No: The sensor and calibration curve is unaltered form first setup	Yes	No
Vaisala PTB 110 Barometric pressure sensor	Test cell Barometric pressure (to calculate ECE correction factor)	Yes	OEM Calibration certificate H15-07490001	OEM	No	No	No: The sensor and calibration curve is unaltered form first setup	Yes	No
Wika Ecotronic pressure Transducer	Oil pressure	Yes	OEM Calibration certificate 08012004	OEM	No	No	No: The sensor and calibration curve is unaltered form first setup	No	No
AVL 7030 Fuel mass balance	Engine fuel consumption	Yes	Calibration done according to user manual	Palmer (2008)	No	Yes (Johan Kotze)	Engine fuel return line pulsates, causing readings to fluctuate	Yes	Yes
Wika K-type thermocouple	Assorted temperatures	Not the thermocouples but the measuring blocks	No	Palmer (2008)	No	No	No: The sensor and calibration curve is unaltered form first setup	No	No

TABLE 2 - CALIBRATION STATE OF RE-USED SENSORS

4.2 ENGINE AND TEST RIG CONTROL CALIBRATION, TUNING IN AND ECU DIAGNOSTICS

Before the engine could be tested, the following systems had to be tuned or checked:

- throttle controller,
- ECU diagnostics, and
- dynamometer control

The throttle controller was calibrated using the adjustment screws on the front of the servo controller. The throttle control in ETA was set to 0% and the zero screw was turned so that the throttle controller's cable was tight but the pedal was not moved. Then the throttle control was set to 100% and the span screw was turned until the pedal was completely pulled in. Since only power curves will be run, the intermediate accuracy of the actuator was not of such importance, but it was verified using VAG-COM by checking the accelerator pedal register while altering the throttle control in ETA. Values between the requested accelerator position and the accelerator position picked up by the ECU correlated well.

To check if the ECU was functioning normally, VAG-COM was used to pull off the ECU's fault codes and status. The results are shown in Appendix L and indicate that the ECU is ready to run the engine.

A PID controller controls the Dynamometer. The settings of the PID controller can be adjusted using the screws inside the controller box. Initially the PID controller was set to factory default settings, but during later testing, it was observed that the controller did not settle on a setpoint and kept the speed of the engine oscillating around the requested speed setpoint. On further inspection, it was also discovered that the belt that connected the servo to the butterfly valve (that regulates the water level in the dynamometer) was perished. This was replaced and the PID controller was re-tuned. The new optimal settings were found to be (the resistor number inside the controller is indicated in brackets).

- Proportional (R461) – 3
- Integral (R463) – 4
- Differential (R453) – 2

The dynamometer was retuned according to the Schenck user manual. (Schenck Pegasus GmbH, 2001).

4.3 TRIAL RUNS AND REPEATABILITY TESTS

Before testing commenced, the test rig with the new engine was tested for reliability, safety and repeatability. All tests were carried out after the engine was allowed to run up to operating temperature at 2000rpm and 20% throttle. Initially the engine was run at partial load to see if all the bolts were secure and to check for abnormal vibrations throughout the speed range. No problems were found. Then the drive train was tested, running the engine at maximum torque for half an hour. There were numerous problems with the drive train, these included spline failure (manufacturing problem), vibration (originating from a climbing torsional damper) and the loss of a CV-Joint (bad installation). All these problems were solved and testing commenced.

As discussed in section 3.5.1, there were a few problems with the cooling system, which were solved. The engine was then run for an hour at various speeds and power levels, and the test rig was considered safe and reliable and testing could commence.

A set of two power curves was performed on ULSD to evaluate the repeatability of the test setup. It was found that the repeatability of the tests were not completely up to standard and inconsistencies of up to 3% occurred between these initial power runs under similar conditions. The power curves are shown in Figure 42 and the difference in readings are shown in Figure 43. Even though the error does not seem to be great, the problem is that the difference in performance of biodiesel is expected to be in the order of 5%. Thus, the inconsistency is too great to allow for comparative studies between biodiesel and ULSD.

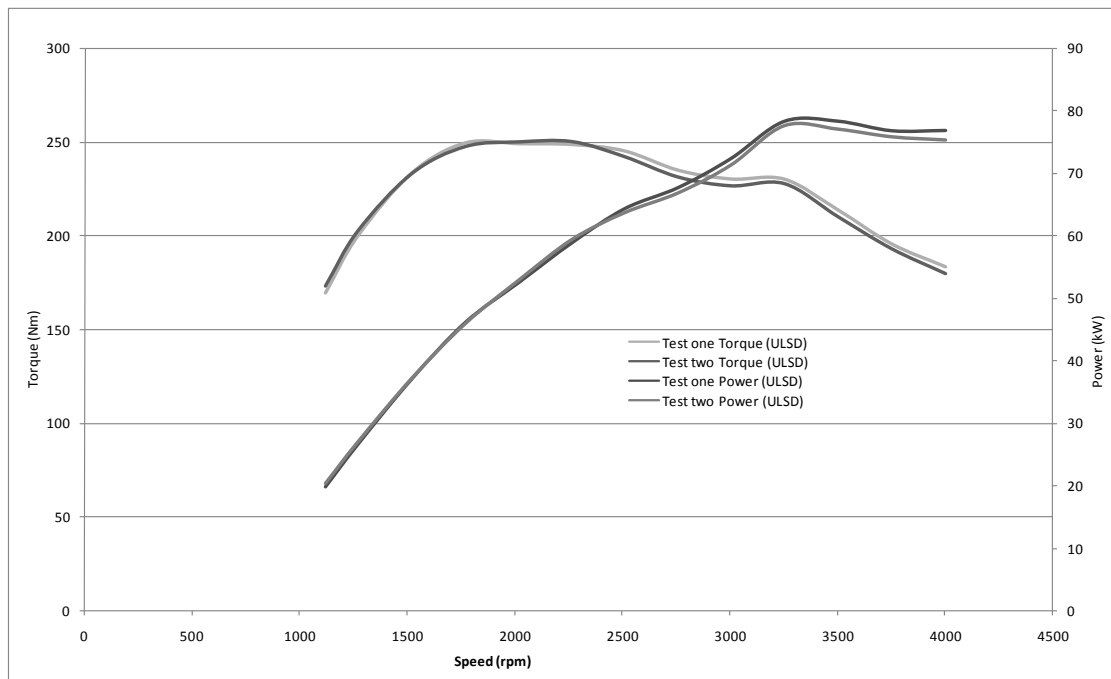


FIGURE 42 - INITIAL REPEATABILITY TESTS

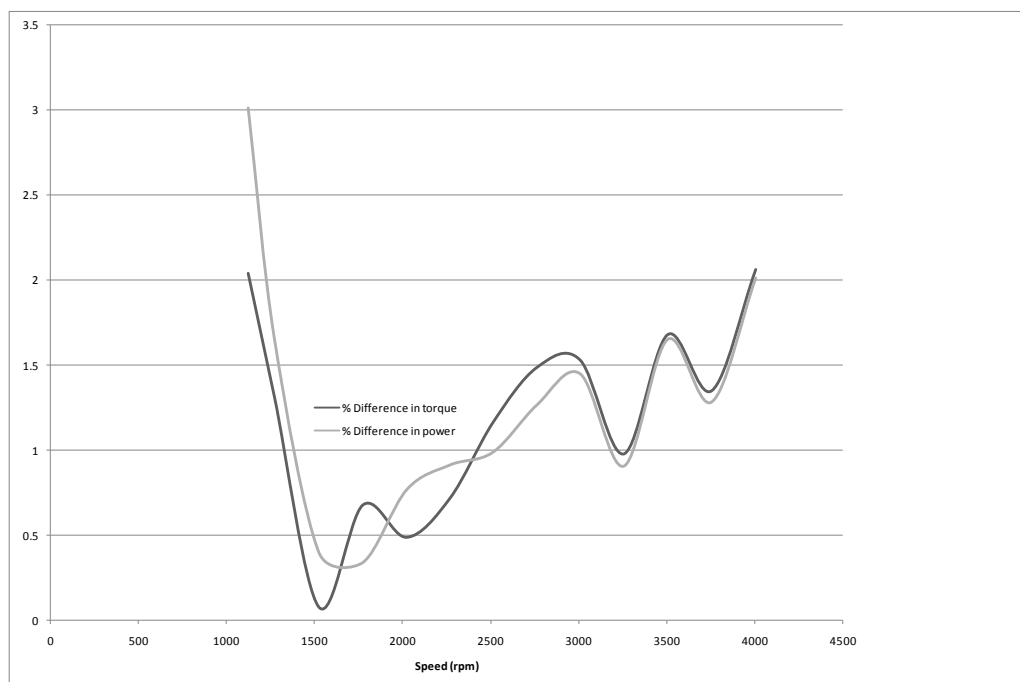


FIGURE 43 - % DIFFERENCE BETWEEN THE FIRST TWO POWER CURVES

After much testing and manipulation of data the problem was found to be that the ECE correction factor was calculated using the temperature at the wall of the test cell. The problem with this was that there was a temperature difference of up to 10°C between the air at the wall and the air that is sucked in at the clean air intake. By altering the thermocouple used in the ECE correction factor to the one located in the clean air system, the accuracy of the test setup was increased dramatically.

During further trials, the accuracy of the test setup was validated. Three of the power curves are shown in Figure 44. All three power curves were done on different days with different weather conditions. The values of the average errors between the power curves are shown in Figure 45. It can be seen from these graphs that the test is highly repeatable and that the experimental setup can be used in comparative studies.

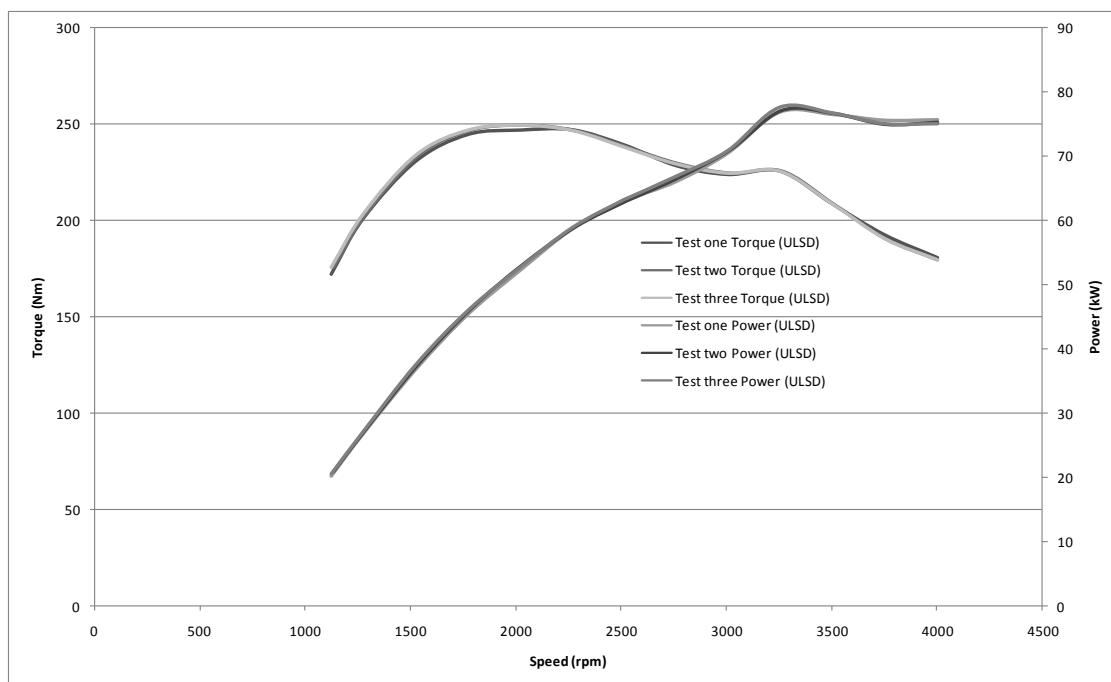


FIGURE 44 - REPEATABILITY AFTER MODIFIED ECE CORRECTION FACTOR

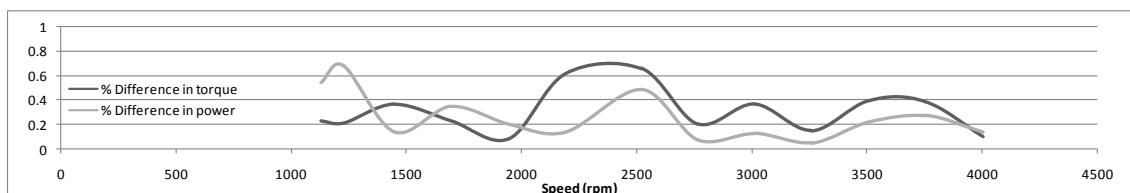


FIGURE 45 - % DIFFERENCE BETWEEN RUNS AFTER ECE CORRECTION FACTOR MODIFICATION

4.4 INDICATING, DATA FILTERING AND ANALYSIS

The indicating equipment enables a user to read off both the crank angle and the in-cylinder pressure of the first cylinder of the engine. Knowing the accuracy of the sensors enables one to know to which extent the data can be used to analyze and judge the performance of a fuel in an engine. This section deals with the integrity of the indicating set employed in this project.

4.4.1 ACCURACY OF THE INDICATING SENSORS

The indicating sensors are the Optrand PSIGlow sensor and the Kübler 7030 single turn magnetic shaft encoder. The calibration certificate of the Optrand sensor was supplied by Optrand. Optrand calibrates their sensors statically and dynamically before shipment. Static calibration was done using a method described in the user manual. The Dynamic calibration was done by running the PSIGlow sensor alongside a Kistler 6121 piezoelectric transducer in an internal combustion engine. The data is then used to calibrate the Optrand sensor (Włodarczyk, et al., 1998). The Optrand sensors have been proven to have a total error (taking thermal shock, hysteresis, and nonlinearity in account) of between $\pm 0.4\%$ and $\pm 1\%$ (Włodarczyk, et al., 1998).

The sensitivity of the sensor is indicated as 1.47mV/psi on the calibration certificate. Thus by converting the output signal (between 0.5V and 5V) using the following equation, the pressure is given in kPa.

$$P = \left(\frac{(V_{out} - 0.5) \times 1000}{1.47} \right) \times 6.894 \quad [4.1]$$

The conversion factor from psi to kPa is taken to be 6.894. This conversion is programmed into SignalExpress®, and the pressure is stored in kPa.

The rotary encoder has a specified linearity better than 1° on a 360° measurement range and the repeat accuracy is better than 0.1° on a 360° measuring range. The measuring resolution is 12bit. To calibrate the sensor to TDC of the first cylinder, the engine was first locked into TDC as prescribed by the Haynes owner's workshop manual for VW the Polo (Jex, 2007). Then the shaft encoder was installed into position on the adaptor on the end of the crank pulley along with the restraining plate (keeping the encoder aligned). Using a multi-meter, the hub of the shaft encoder was adjusted until the meter read 5.000V, before it was clamped down over the shaft of the adaptor. The reason TDC was assigned to 5V was due to the Butterworth filter's unit step response (see section 4.4.2). This prevents the noise in the shaft angle measurement from interfering with the pressure curve by having the noise in a plane between pressure pulses.

4.4.2 DATA FILTERING

Figure 46 shows a sample of the unfiltered data recorded from the indicating set. It can be noted that the graph is not continuous since the voltage of the shaft encoder only ranges between 0 and 10V. As mentioned earlier, it is unfavourable to have the break in the graph on the pressure curve for calculation purposes. To counteract the break in the pressure curve, the engine's 0° mark is calibrated to 5V so that the breaks fall in a valley between pressure spikes. The data is then manipulated mathematically to allow TDC and BDC to coincide with angles that are multiples of 180° .

During the first tests, noise was noticed on the signal, clearly visible in Figure 46, and a filter had to be implemented.

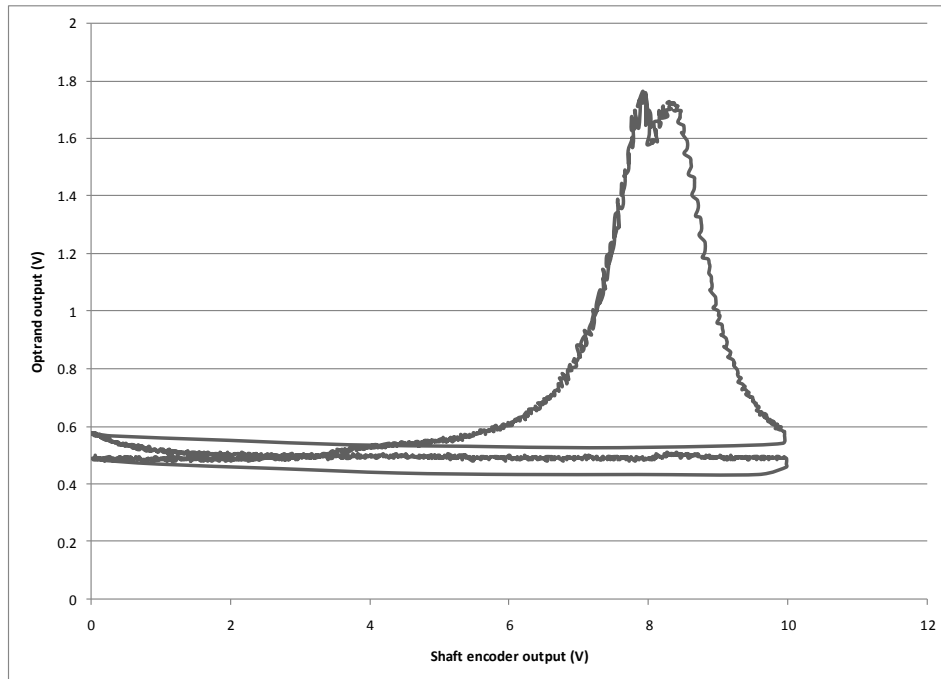


FIGURE 46 - UNFILTERED DATA SERIES

Before a filter could be applied to the signal, the nature of the noise had to be determined. To determine what the frequency of the noise is, a power spectrum analysis block was added to the data analysis software. From the power spectrum (shown in Appendix M) it was clear that the frequencies of the noise were at integer multiples of the engine speed, thus it is safe to assume that the origin of the noise is mainly due to the vibration of the engine. The solution was found by applying a low pass filter to the signal before the data was saved to the hard drive. The Butterworth filter was selected because it has no gain ripple in its frequency response and has a “flat” passband. The drawback of the Butterworth filter is that it has a very slow cut off gradient, which means that the filter needs to be designed with a smaller passband to allow the noise to be cancelled completely. If a first order filter was to be used, either some of the noise would be present or some of the vital information would be lost. A remedy to this is to use a higher order filter, allowing a sharper cut-off rate, widening the passband, and still cutting off the noise. This comes at a sacrifice; the higher order filters have a bad step response (a bit of an overshoot and a longer settling time), which gives bad data for the shaft encoder signal at the 0 to 10V transition point.

The selection of the filter setup was done by filtering the same set of data using different filter configurations (keeping in mind the filter’s negative step response and the noise cancellation). The following setups were used:

- 1st order with 0.5 kHz cut-off
- 1st order with 1 kHz cut-off
- 1st order with 1.5 kHz cut-off
- 1st order with 2 kHz cut-off
- 2nd order with 0.5 kHz cut-off
- 2nd order with 1 kHz cut-off
- 2nd order with 1.5 kHz cut-off
- 2nd order with 2 kHz cut-off

- 3rd order with 0.5 kHz cut-off
- 3rd order with 1 kHz cut-off
- 3rd order with 1.5 kHz cut-off
- 3rd order with 2 kHz cut-off

On inspection, the best results were found using the second order low pass Butterworth filter with a cut off frequency of 1.5 kHz. The filtered data is presented in Figure 47, which represents the filtered version of the data shown in Figure 46.

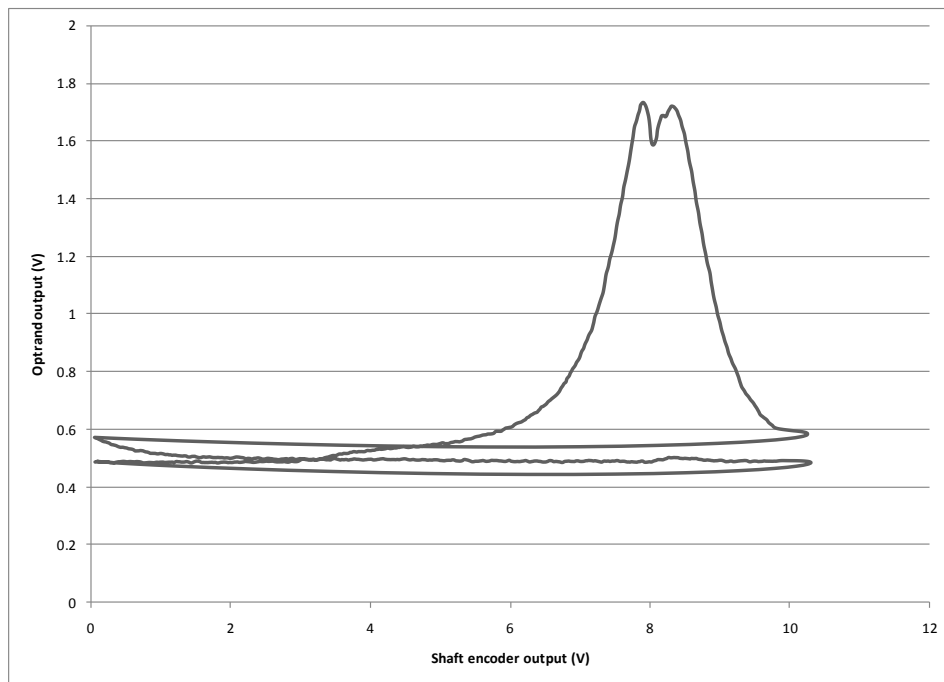


FIGURE 47 - FILTERED DATA SET

4.4.3 REPEATABILITY

To demonstrate the repeatability of the indicating system, a set of four complete engine cycles are plotted over each other in Figure 48. The data was taken from four time intervals as the engine was running at 1500 rpm with 30% throttle. It can be observed that all four pressure curves run perfectly on each other. This would suggest that the engine's pressure curve through a stroke is very repeatable under similar conditions.

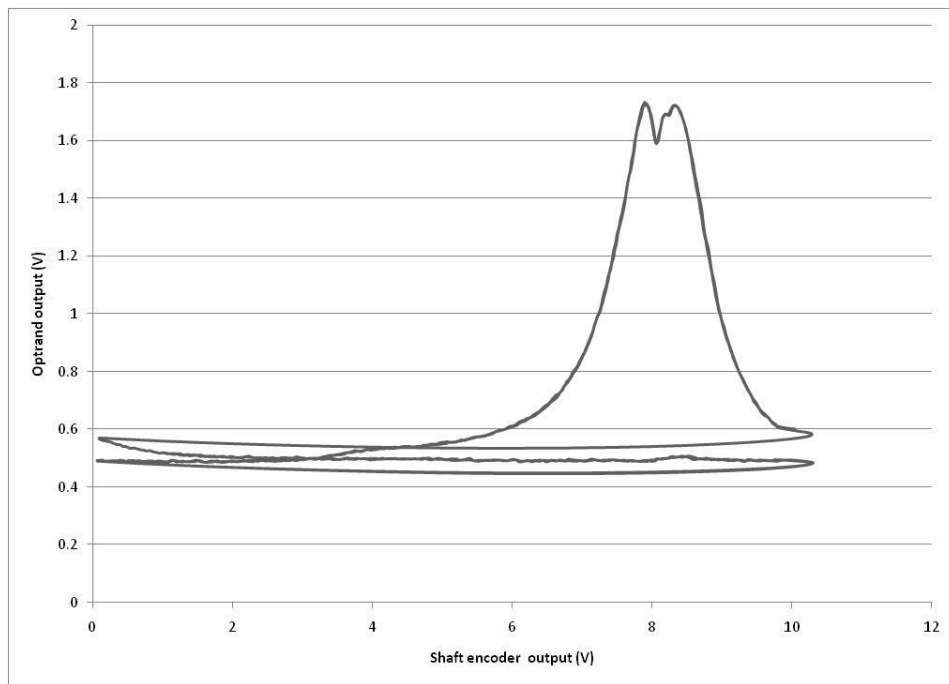


FIGURE 48 - REPEATABILITY DEMONSTRATION

4.5 SYSTEM COMMISSIONING AND REPEATABILITY ANALYSIS SUMMARY

This section discussed the process of commissioning the experimental setup created in this project. All the sensors in the test cell were calibrated and it was found that all the sensors worked properly except for the AVL mass fuel balance. The problem with the AVL mass fuel balance is due to an irresolvable incompatibility between the AVL 7030 mass fuel balance and the VW 1.9L TDI (ATD)'s fuel injection system.

Through testing, the experimental test cell proved to be reliable. Through the alteration of some parameters in the ECE correction factor the tests proved highly repeatable through trials.

The indicating set was successfully implemented and with a second order low-pass Butterworth filter, a clean signal of the pressure trace in the first cylinder of the engine could be measured.

5 FUELS TESTING

The chemical nature of biodiesel is in no way comparable to the chemical composition of regular mineral diesel, and naturally the question has to be asked; “How does the performance of the biodiesel compare to the performance of the normal diesel?” This is the same basic research question that was answered by Palmer (2008), using an older technology diesel engine. It was found that even a lower grade biodiesel performs well with an unmodified engine.

The question that needs to be answered in this project is whether a modern engine with high-pressure injection technology (more specifically pump unit injectors) is suited to run on biodiesel and how the performance figures of the engine differs to that of the engine running on ULSD. This is important due to the recent rise in popularity of cars running on diesel and the prospect of running cars on biodiesel that could significantly affect the carbon footprint of the average road user.

A secondary project goal was to evaluate a cost effective alternative to the traditional indicating set. Combustion analysis in an engine will give more insight on the behaviour of biodiesel in an engine. This section discusses the tests that were done on the new experimental setup based around the 1.9L TDI engine that was sponsored by VWSA.

5.1 TESTED FUEL SAMPLES

For the sake of consistency with Palmer’s (2008) thesis, it was decided to test ultra low sulphur diesel (ULSD) and biodiesel as well as the blends (the blend number indicates the mixing ratio, for example; B5 means 5% biodiesel and 95% ULSD):

- B5
- B10
- B15
- B50

To be able to do all the tests with the same diesel batch, the biodiesel and the ULSD were purchased in bulk, and a 210 Litre container of each was purchased for testing. A sample of each batch of diesel was sent away for testing to serve as a reference on the fuel quality used in these tests. The results of the biodiesel and normal diesel tests are shown in Table 3 and Table 4 respectively.

ANALYSIS	SPECIFICATION SANS 1935:2004	RESULT
APPEARANCE		CLEAR
DENSITY @ 15 deg C kg/l	0.860-0.900	0.8904 (PASS)
VISCOSITY @ 40 deg C	3.5-5.0	7.88 (FAIL)
FLASH POINT deg C	120 MIN	PASS @ 120deg c
WATER CONTENT%	0.05 MAX	0.13 (FAIL)
ACID VALUE mg KOH/g	0.5 MAX	0.44 (PASS)
FREE GLYCEROL%	0.02 MAX	0.05 (FAIL)
TOTAL GLYCEROL%	0.25 MAX	1.16 (FAIL)
CETANE INDEX	55 TYPICAL	49
IODINE VALUE		96.1
SULPHATED ASH	0.002 max	0.002
HEATING VALUE		39.360 MJ/kg

TABLE 3 - BIODIESEL TEST RESULTS

ANALYSIS	SPECIFICATION SABS 342	DIESEL SAMPLE
APPEARANCE	CLEAR	CLEAR
COLOUR		YELLOW
DENSITY kg/l @ 20 deg C	0.800 MIN	0.8206
VISCOSITY @ 40 deg C	2.2-5.3	3.49
FLASH POINT deg C	55 MIN	PASS
WATER ppm	500 MAX	45ppm
SEDIMENT	NEGATIVE	NEGATIVE
CETANE INDEX	55 TYPICAL	56
IODINE VALUE		105.8
SULPHATED ASH	0.002 max	0.001
HEATING VALUE		45.888 MJ/kg

DISTILLATION RANGE	SPECIFICATION	RESULT
IBP deg C		184
	10%	208
	20%	221
	30%	250
	40%	267
	50%	288
	60%	300
	70%	319
	80%	330
	90% 362 MAX	344
FBP deg C		384

TABLE 4 - ULSD TEST RESULTS

It can be seen from the tables that the biodiesel fails the SANS1935:2004 standard and the ULSD passes the SABS 342 standard.

The calorific value of the two fuel samples was measured using an IKA C200 calorimeter. The calorific value of biodiesel (39.360 MJ/kg) is 14.22% lower than the ULSD at (45.88MJ/kg). The cetane index of the biodiesel is below specification as well. Biodiesel is quoted in literature to have higher cetane indexes than that of normal diesel, but at 49, it is below average. The cetane index of the ULSD is at 56, which is better than expected.

Thus, looking at the fuel properties, the expectation is that the engine's maximum power output will be lower when run on the biodiesel due to the lower calorific content of the biodiesel. A slightly longer ignition delay can also be expected from biodiesel based on its lower cetane index.

5.2 TEST PROGRAM

The first set of tests that were done was the power curves with different fuels. Before a day of testing could commence, the calibration of the load cell was checked by loading the torque arm. The engine was run up to temperature using ULSD, and the testing commenced. A test cycle consisted out of the following steps:

1. Change fuel (ULSD, B5, B10, B15, B50 and pure biodiesel)
2. Bleed fuel lines
3. Run engine up to temperature at 2500 rpm and 40% throttle
4. Switch on VAG-COM to log ECU behaviour

5. Initiate test cycle 1: Power curve
6. Initiate test cycle 2: Power curve
7. Pressure indicating done at;
 - a. 3250 rpm at 100% throttle
 - b. 1750 rpm at 100% throttle
 - c. 1750 rpm at 45% throttle
8. Initiate test cycle 3: Power curve
9. Shut off engine and mix next batch of fuel

These steps were repeated for each fuel mix. The reason for doing three power curves per fuel was to check for non-linearity and abnormal behaviour of the engine during any stage of testing. If any one of the three power curves differed from the other two, another power curve was run. During testing, a few problems were experienced with the test setup. These problems were corrected and all the samples were re-tested. All the power curves done on the test bed were consistent, and only two bad test cycles occurred during the testing of B5 and B50. The bad tests were due to a pinched vacuum line. These outliers showed a notable decrease in power during peak torque conditions and a lowering of pressure boost from the turbocharger. The vacuum line was re-routed and the problem was solved.

5.3 TEST RESULTS

To compare the performance of the biodiesel to that of regular diesel, power curves were performed with the engine running on the respective fuel samples. Figure 49 shows all the power and torque curves of the fuel samples tested on one graph. It can be seen from the graph that there is no significant difference between the performances of the engine running on ULSD, B5, B10 and B15. There is a clear power loss when pure biodiesel is used in the engine, and as expected, the performance of B50 appears to be half way between that of ULSD and biodiesel.

To show the effect of the biodiesel and blends more clearly, the percentage of performance loss of the engine is shown in Figure 50. The slight power increase for the blends in the mid engine speed range region might be due to the improved lubricity of the biodiesel, improving the fuel pump and injector performance, but the subject need further investigation. The graph shows that the engine is most affected at high power conditions where more fuel is used, and that the loss in performance is only about 4.2 % at 4000 rpm (lower than the expected 14.22 % based on calorific content).

To illustrate the difference of the engine running on ULSD versus biodiesel better, only the two power/torque curves are plotted against each other in Figure 51. The maximum power of the engine running on ULSD is 78.75 kW at 3250 rpm while it is 75.98 kW at 3250 rpm for biodiesel. The torque figures also look similar, where the maximum torque of the engine running on ULSD is 253.8 Nm at 2000 rpm and it is 249.7 Nm at 2000 rpm for biodiesel.

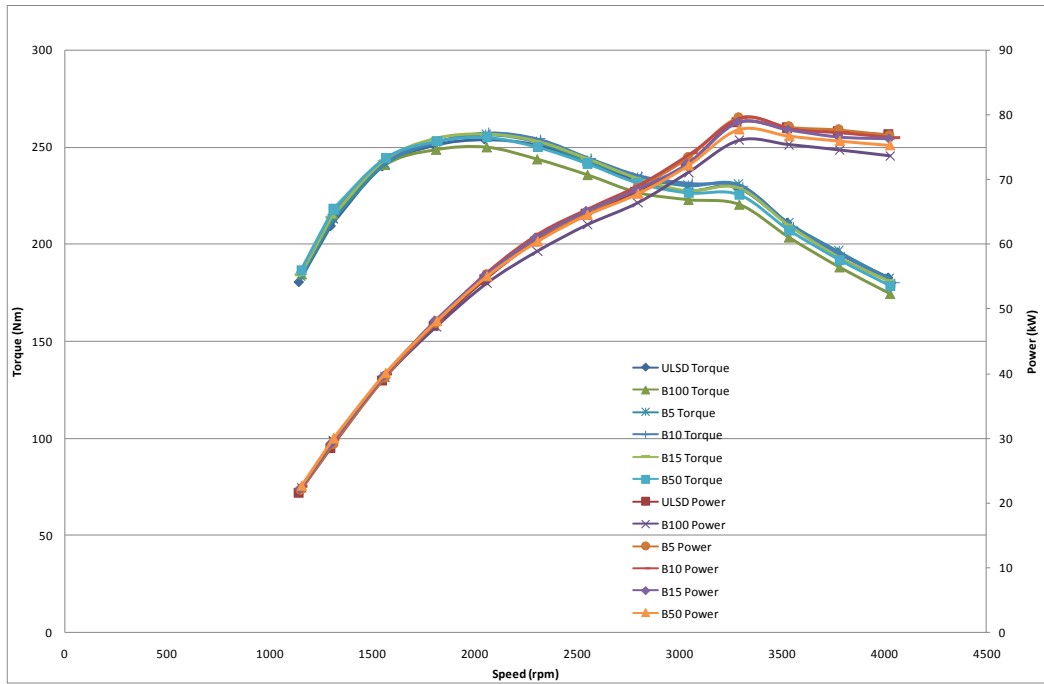


FIGURE 49 - POWER /TORQUE CURVES OF THE ENGINE RUNNING ON ULSD, BIODIESEL AND BLENDS

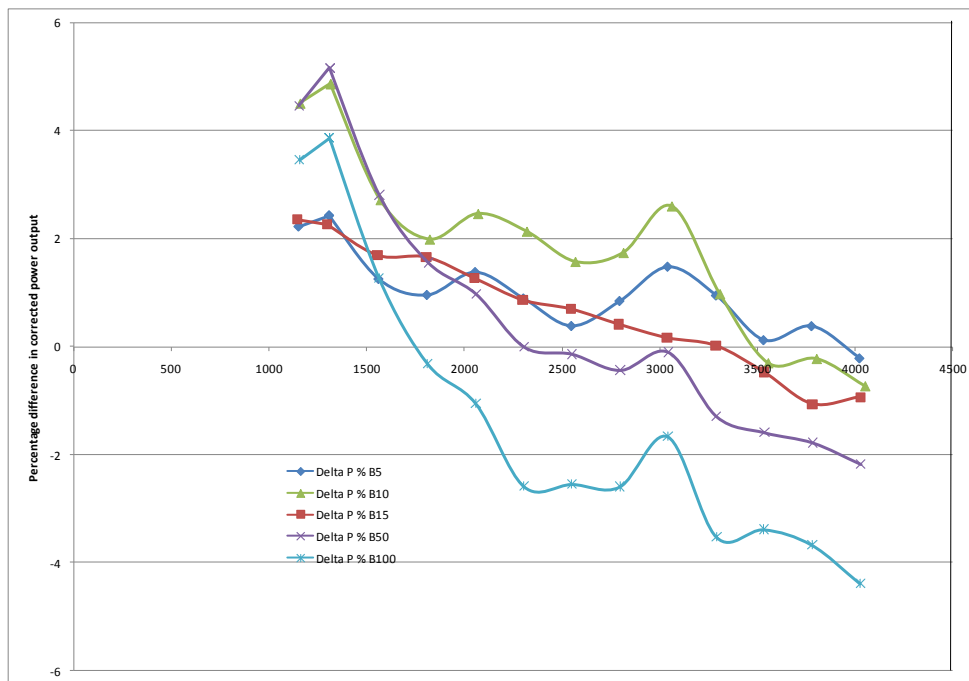


FIGURE 50 - PERCENTAGE DIFFERENCE IN CORRECTED POWER BETWEEN BIODIESEL AND BLENDS COMPARED TO ULSD

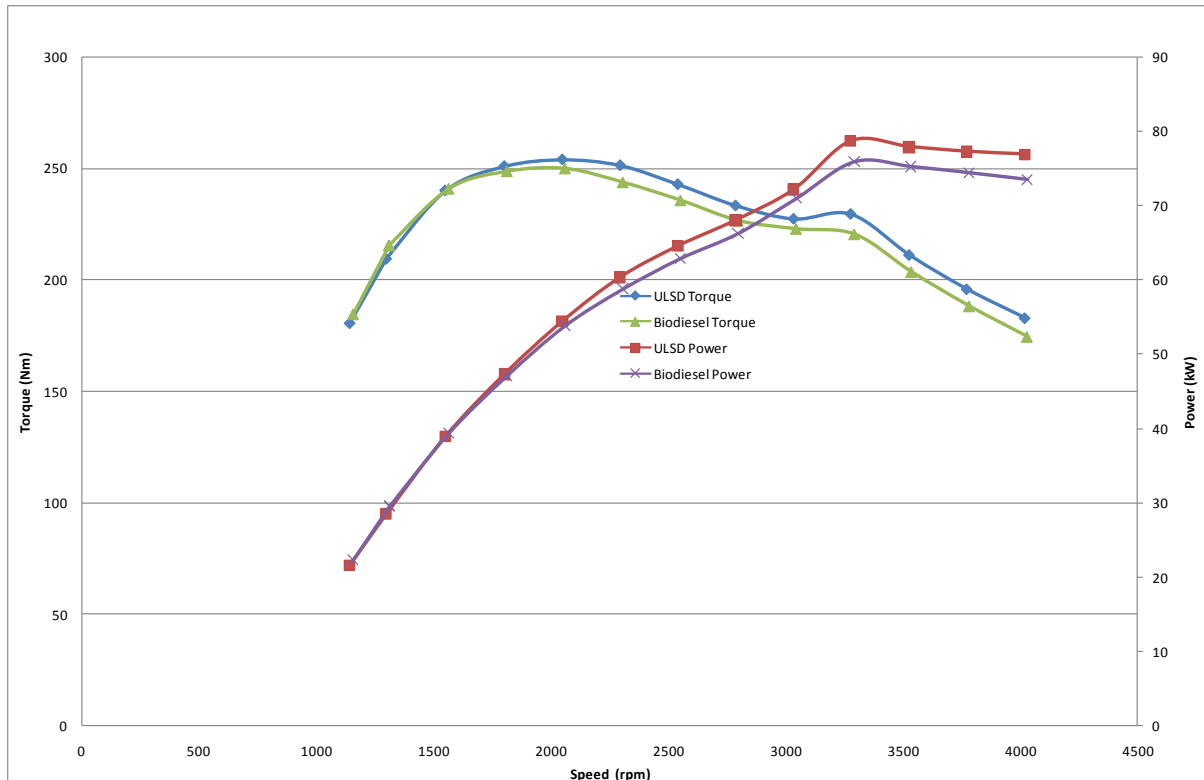


FIGURE 51 - POWER /TORQUE CURVES OF THE ENGINE RUNNING ON ULSD AND BIODIESEL

Even though the biodiesel used is of a very poor quality, it does not seem to affect the engine performance in the short term, except for a power loss that could be attributed to three factors:

- Lower calorific value: (Energy input, the main contributing factor)
- Ignition quality: (Ignition delay)
- Viscosity (Injector performance)

What is even more notable is the fact that the engine only lost 3.53% in maximum power output (and 4.2 at top speed), while the calorific value of the biodiesel was tested at 14.22%

The engine operating parameters were consistent throughout all tests and a slight decrease in oil and exhaust temperatures are observed. The long-term effects of biodiesel on the engine were not tested, and need further investigation.

5.4 FUEL CONSUMPTION MEASUREMENT

Fuel consumption measurement of an engine is a very important parameter in engine testing because it is necessary to calculate specific fuel consumption, efficiency and air/fuel ratios. These are important factors when it comes to engine testing (Heywood, 1988).

It was seen from the fuel consumption readings that the data is scattered and only a faint trend in fuel consumption was visible. Initially it was thought that the problem was with the AVL mass fuel balance, but after re-calibration, necessary checkups and maintenance procedures, it was realized that the mass fuel balance was not at fault. On further inspection, the problem was found to be the engine itself.

Notably the fuel consumption readings of ULSD is more scattered than that of biodiesel, and the trend is supported by the blends. This indicates that the problem is more prominent with the more volatile ULSD (flashpoint of 55°C) than with the biodiesel (flashpoint of 120°C) which gives a clue of the problem at hand.

The problem originates with the high fuel return temperature of the engine due to the high pressure that the diesel is exposed to just before it is returned to the AVL mass fuel balance. In the pump unit injector system the fuel is compressed to a pressure as high as 2050 bar, and then the fuel is either injected into the cylinder or it is shunted to the fuel return line. This causes the fuel in the return line to have temperatures in the order of 100°C, which is 45°C above the flashpoint of ULSD. The high temperature causes the more volatile fractions of the diesel to vaporise in the fuel return line. Vapour formation in the fuel line causes the fuel to be added to the measuring chamber in an erratic fashion. This causes the mass fuel balance to oscillate, skewing the readings. The AVL user manual prescribes that the solution to this problem is to cool the fuel to below its flashpoint, which was done, but had no effect on the readings of the AVL mass fuel balance. The application of a damper also had little effect on the problem. Regrettably, the problem remains unsolved, and all resources and equipment at the disposal of the BTF were used to try to correct the problem.

5.5 PRESSURE INDICATING

The pressure indicating experiments had two goals:

- To validate the working of the implemented pressure indicating setup.
- To see if the lower ignition quality of the Biodiesel affects the engine's combustion process.

This section discusses the indicating work done and observations based on the results obtained. Pressure indicating measurements were taken at the following conditions for the engine running on both biodiesel and ULSD:

- 100% Throttle / 3250 rpm (full power) running on ULSD
- 100% Throttle / 1750 rpm (maximum torque) running on ULSD
- 100% Throttle / 3250 rpm (full power) running on biodiesel
- 100% Throttle / 1750 rpm (maximum torque) running on biodiesel

5.5.1 PHASING

All attempts were made to calibrate the shaft encoder mechanically, to ensure that the pressure signal and the shaft encoder signal are in phase. The engine's crankshaft was locked with the #1 piston at TDC. The shaft encoder was installed, and using a multi-meter, the encoder was fixed to the shaft in a position correlating with a reading of 5.00V. Later it was found that the clamping mechanism of the encoder had the tendency to become loose during testing. The encoder was recalibrated (5V to TDC), and bonded to the crankshaft with an epoxy-based adhesive.

Motoring of the engine was not possible because the dynamometer is of the waterbrake type. Thus, the engine was cranked using its starter motor. This is far from ideal, since the starter motor could only rotate the engine at low speed, and the blow-by³ affected the pressure trace.

³ Blow-by is the leakage of gas past the pistons.

This can be observed from Figure 52 on the descending part of the pressure trace (a steeper less gradual pressure curve than on the ascending part). This causes the LogP-LogV graph in Figure 53 to be curved (and not straight, as in Figure 11). Nevertheless, the motoring curve could be used to improve the phasing between the pressure and the crank angle signals. Using the LogP-LogV graph in Figure 53, the phase difference was determined. The phase correction was an 11.8° advance of the pressure trace.

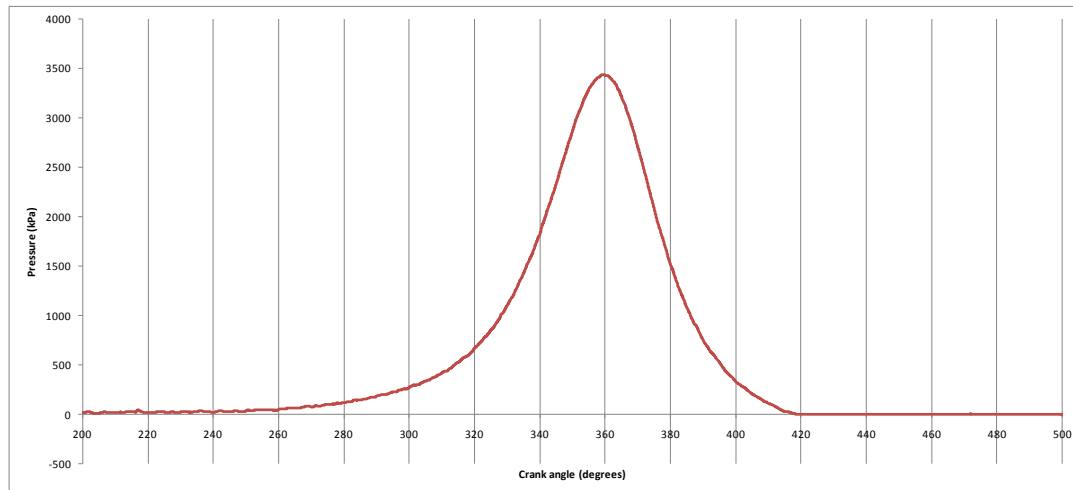


FIGURE 52 - "MOTORING" PRESSURE VS. CRANK ANGLE

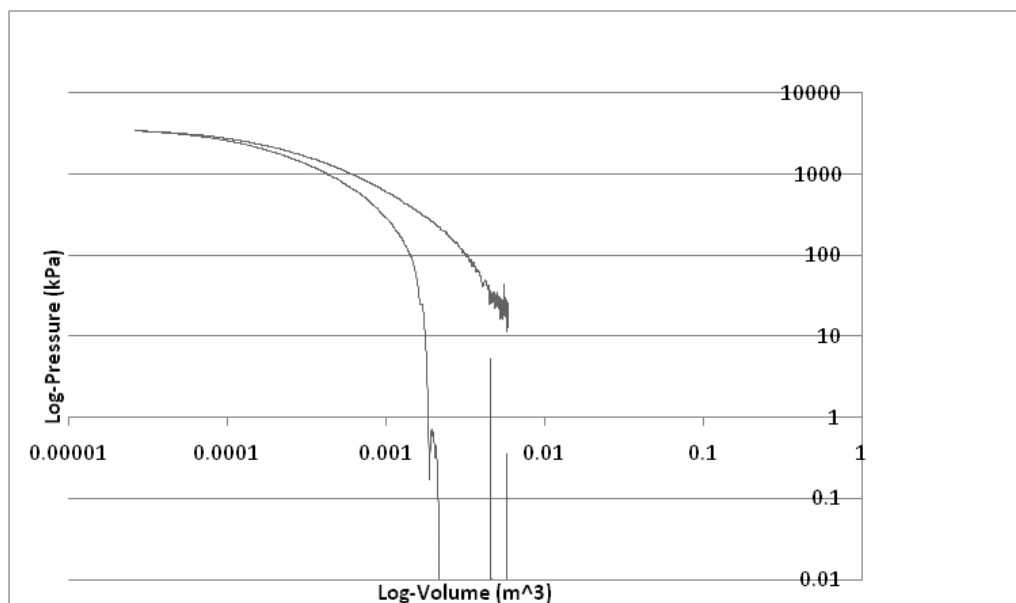


FIGURE 53 - LOGP-LOGV FOR PHASING

5.5.2 INDICATED WORK CALCULATION

The data obtained from the indicating set yielded the pressure vs. volume profiles shown in Figure 54 and Figure 55. The curves in Figure 54 were measured while the engine was running at 100% throttle and 1750 rpm (maximum torque) and Figure 55 shows the pressure/volume curves of the engine running at 100% throttle and 3250 rpm (full-power)

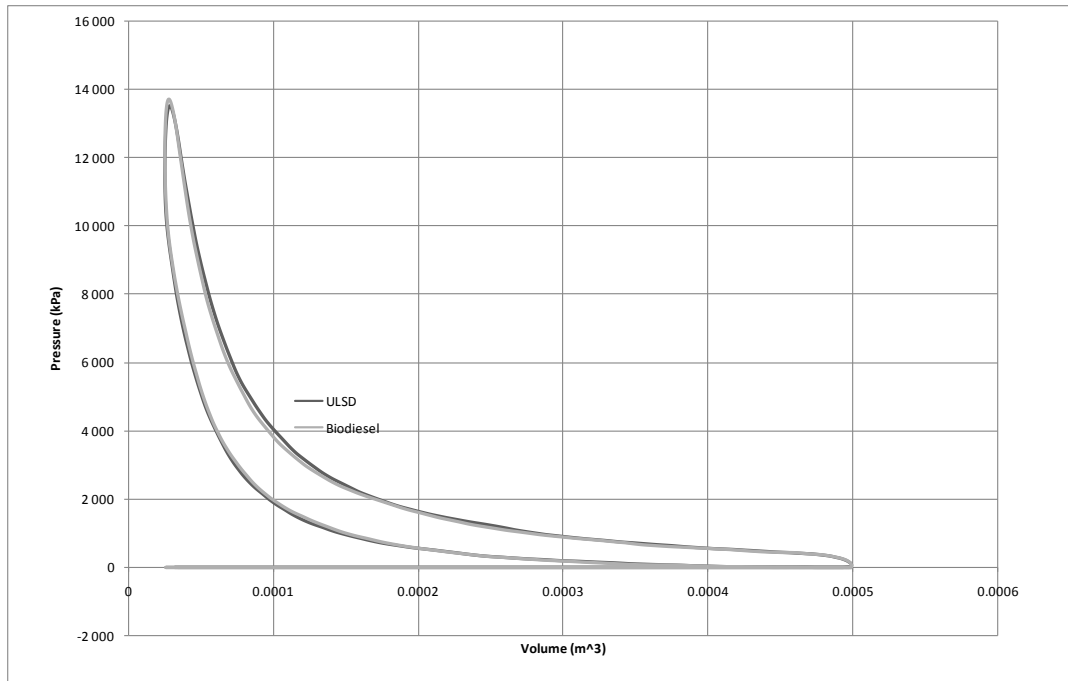


FIGURE 54 - PRESSURE VS. VOLUME GRAPHS (100% THROTTLE / 1750 RPM)

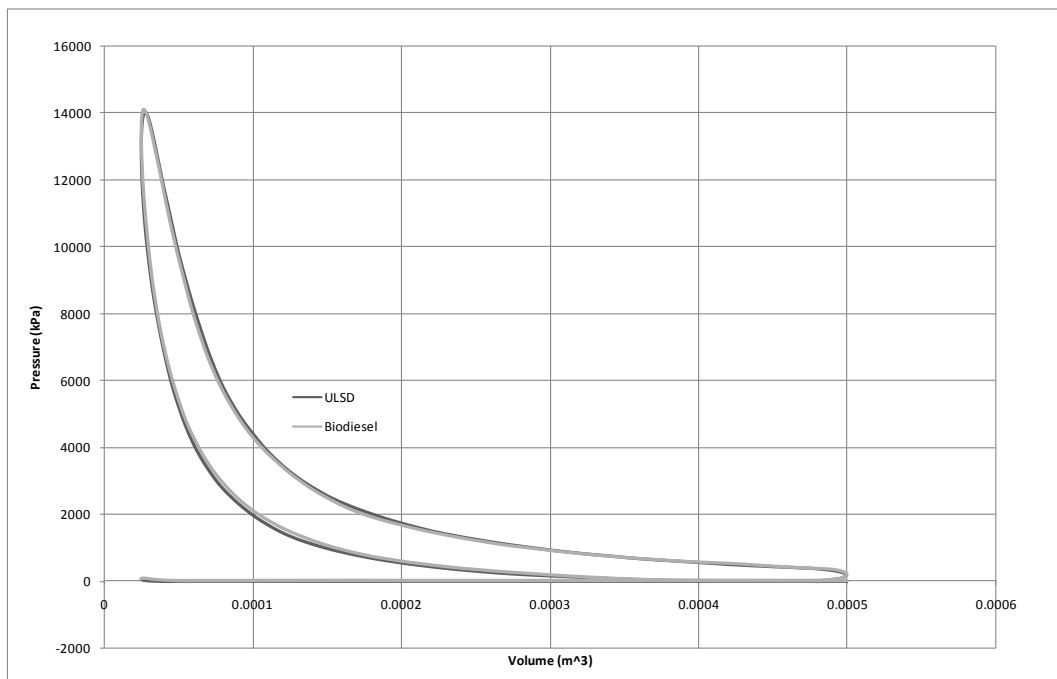


FIGURE 55 - PRESSURE VS. VOLUME GRAPHS (100% THROTTLE / 3250 RPM)

By integrating the compression and power stroke using equations 2.5 and 2.6, it is possible to calculate the net indicated power supplied to the engine. A shortcoming of the current indicating set is the fact that the shaft encoder is analogue, and the pressure and shaft position readings are measured at discrete increments of time instead of crank angle. To integrate the pressure and volume data, numerical integration need to be performed. Only trapezium integration (Equation 5.1) could be used since other numerical integration techniques, such as Simpson's rule, can only be done on data that has discrete increments of the independent variable (which is the crank angle in this case).

Trapezium integration:
$$I_i = \frac{\Delta V(P_i + P_{i+1})}{2} \quad 5.1$$

Where P denotes pressure and V denotes volume.

The results of the indicated power and mechanical efficiency are shown in Table 5. In Table 5 the indicated power is displayed next to the measured power output of the engine at given conditions. The mechanical efficiency of the engine is shown in the last column. It should be noted that this value is highly sensitive to phasing errors (Callahan, et al., 1985). Taking into consideration the phasing issues of the experimental setup, these values for mechanical efficiency should not be used to form a basis of any argument. In this case, it is simply a demonstration of the consistency of the indicated power measurement. For the same reason, the percentage difference between the engine performances is shown running on either fuel.

Indicated power	Indicated power (kW)	Measured power (kW)	% difference between indicated power values	% difference between measured power values	Mechanical efficiency (%)
Biodiesel 100% throttle / 3250 rpm	95.44	75.97	3.68	3.53	74.37
ULSD 100% throttle / 3250 rpm	99.09	78.75			74.18
Biodiesel 100% throttle / 1750 rpm	58.87	47.12	0.61	0.42	75.07
ULSD 100% throttle / 1750 rpm	59.23	47.32			74.83

TABLE 5 - INDICATED POWER

From Table 5 it can be deduced that the indicating set delivers consistent data, but that the lack of motoring capability in the BTF makes absolute measurements of indicated power and mechanical efficiency of the engine impossible.

On a comparative basis, it can be observed that the percentage power loss measured during dynamometer testing and indicating is very close. Thus, it is safe to assume that the loss of power observed during the testing of biodiesel is accounted for in the indicated power measurement. Variation of the comparative figures presented in Table 5 can be attributed to:

- the inaccuracy of trapezium integration, and
- the irregular increments at which the crank angle is measured.

The irregular measurement of crank angle actually limits the pressure indicating analysis more severely. Due to various aspects of the physical experimental setup and the nature of the sensors, noise will always be present in the pressure indicating signals. One of the best ways to filter noise is to average indicating data between multiple power strokes (Callahan, et al., 1985), and with irregular crank angle measurement, this is not possible. The effects of noise are even more pronounced in the heat release analysis, where first derivatives of the pressure and volume signals are taken.

5.5.3 HEAT RELEASE ANALYSIS

By applying equation 2.10 to the indicating data, a heat release curve is produced. The heat release curve during the compression and power stroke of the engine is plotted for the same sets of data displayed in Figure 54 and Figure 55, and is presented in Figure 56 and Figure 57.

From Figure 56 and Figure 57, the following observations can be made between the biodiesel and ULSD heat releases for both the 1750 rpm and 3250 rpm tests:

- Only a slight difference in ignition delay is observable for biodiesel in both the 1720 rpm and 3250 rpm tests.
- Hence, it is normal to see that there is no significantly difference in the rise of heat release rate during the premixed burning period (since the amount of vaporised diesel is roughly the same by the end of the ignition delay).
- Diffusion burning and after burning periods falls roughly into the same “time” slots in both the 1750 rpm and 3250 rpm cases.
- The deduction can be made that the cetane index of the biodiesel does not affect the combustion process.
- The peak heat release rate for ULSD is generally higher than in the case of biodiesel. This is expected, since biodiesel has a lower heating value.

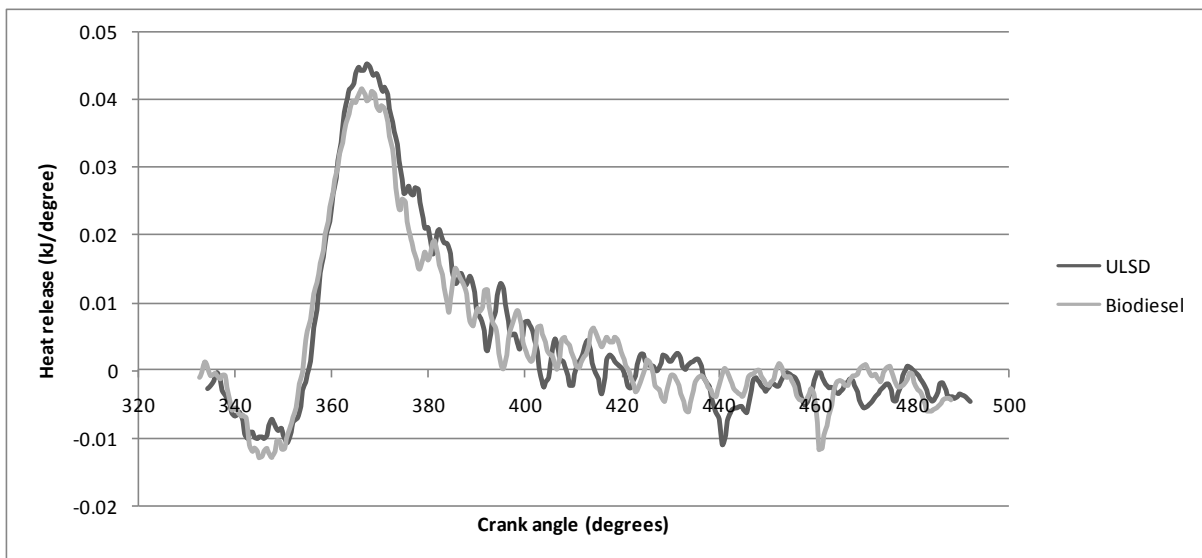


FIGURE 56 - HEAT RELEASE (100% THROTTLE/ 1750 RPM - MAXIMUM TORQUE)

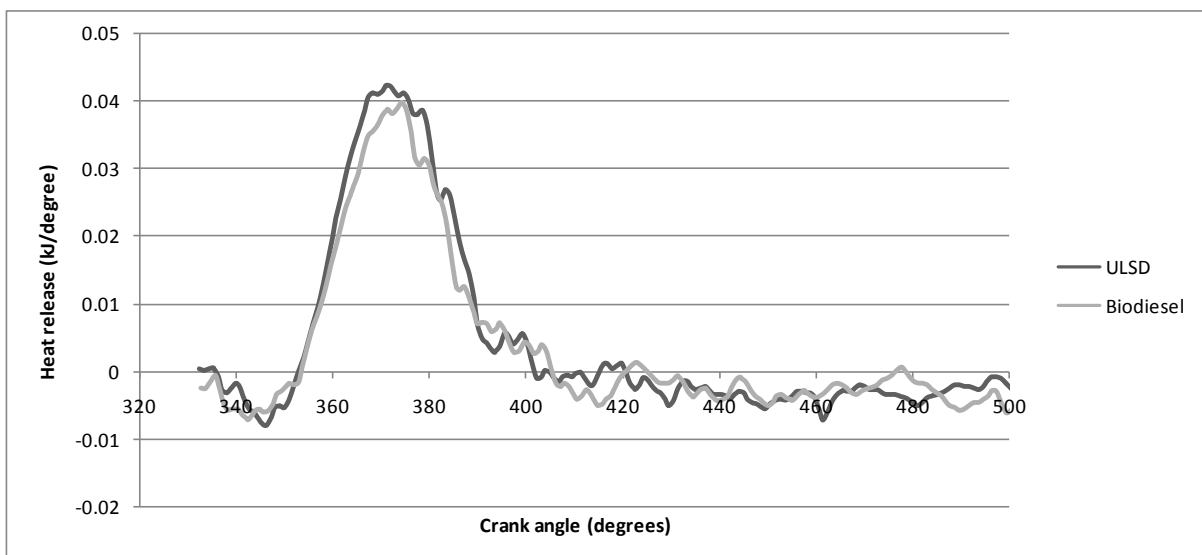


FIGURE 57 - HEAT RELEASE (100% THROTTLE / 3250 RPM - MAXIMUM POWER)

5.6 SUMMARY

A novel, low-cost indicating set was improvised, and it was used to obtain the indicated power and heat release of the test engine running on ULSD and biodiesel. The tests were done at peak torque conditions (100% throttle and 1750 rpm) and at peak power conditions (100% throttle and 3250 rpm). The following observations can be made concerning the performance of biodiesel in the test engine (compared to ULSD):

- The lower cetane value of the biodiesel do not significantly affect the ignition delay period of the engine.
- It is evident from both the indicated power and the heat release curves that the lower heating value of the biodiesel lowers the engine's performance.

The following observations and recommendations can be made regarding the indicating set:

- The analogue shaft encoder and data acquisition hardware makes it extremely hard to trigger pressure and shaft position readings at set angular increments of the shaft encoder. This makes it hard to filter out noise by averaging, and other filtering methods need to be used.
- A low pass Butterworth filter is used to filter the signal. While this is adequate for display and numerical integration, remnant first and second order noise adversely affects the calculation of heat release. It was possible to do a simplified heat release, but the noise in the data made it difficult to do further analysis, since it yielded incomprehensible data or unacceptable errors.
- The lack of motoring capability in the BTF does not enable operators to correct the phase between the encoder signal and the pressure trace.
- The Optrand pressure transducer works exceptionally well. Given its low cost, low maintenance and simplicity, it can be recommended for future use.
- The appropriate hardware to calibrate the Optrand sensors needs to be acquired.
- The use of a FPGA (field programmable gate array) type data acquisition system is recommended for future research. This is due to its ability to process indicating data at high speed and in real time. One such system is the National Instruments Compact Rio system, and further investigation is suggested.
- It is recommended that a DC dynamometer be used for future indicating work at the BTF to obtain a set of hot motoring curves across the full speed range of the engine.

6 CONCLUSIONS AND RECOMMENDATIONS

After the test cell was upgraded and the engine installed, it was commissioned and biodiesel was tested in a comparative study. Results from the new test setup proved to be highly repeatable and is suitable for fuel performance research. The performance of Fatty Acid Methyl Esters (FAME) biodiesel was tested and compared to Ultra Low Sulphur Diesel (ULSD).

In a chemical analysis the ULSD proved to be of a good standard, while that of the biodiesel failed the SANS 1935:2004 standard. More notably the biodiesel had a cetane index of 49, where the ULSD was at 56. The energy content of the biodiesel also rated 14.22% lower, at 39.36 MJ/kg where ULSD was at 45.88 MJ/kg. However, during testing it was found that the engine's performance was only decreased by a maximum value of 4.2%. It is suspected that the higher viscosity and improved lubricity of biodiesel improves the performance of the pump unit injectors, which cause more fuel to be injected into the combustion chamber. If this were the case, it would suggest that pump unit injection technology is well suited for biodiesel applications. Fuel consumption measurement is one tool that will shed light on this observation.

The fuel consumption measurement equipment of the BTF was affected by the nature of the test engine's pump unit injector system, and no accurate fuel consumption measurements could be done. Various approaches were used to correct the issue, but the problem remains unsolved. Thus, no investigation could be done on the performance of the injection system and fuel efficiency of the engine.

In-cylinder pressure indicating work is a powerful tool in combustion analysis. Traditional piezo-electric indicating sets are expensive, and a more cost effective alternative was sought. An optical pressure transducer was purchased along with a magnetic type analogue shaft encoder and high-speed data acquisition hardware. This formed a cost effective indicating set. The indicating exercise in this project served a dual purpose, namely: to investigate the performance of this particular indicating setup and to investigate the effect that the lower cetane index of biodiesel has on the combustion process of the engine.

The result of the indicating work showed that the combustion process of biodiesel is very similar to that of ULSD, even though the peak heat release rate of the biodiesel is lower. There was no significant difference in ignition delay found during heat release analysis, which would suggest that the engine is not affected significantly by the lower ignition quality of biodiesel.

The optical pressure transducer proved to work well, and it is recommended for future indicating work if a cost effective alternative is sought. However, the performance of the shaft encoder and data acquisition system proved to be substandard. Another aspect of the indicating setup that proved to be a problem is the lack of motoring capabilities. Motoring the engine is needed to correct the pressure and encoder signal phase, which is vital in absolute heat release and indicated power analysis. Recommendations for future indicating setups include:

- Incremental shaft encoder with one sample per degree resolution, digital output and a trigger output. A "through shaft" clamping mechanism is also recommended because of encoder calibration.
- The use of a DC dynamometer.
- The use of a National Instruments Compact Rio FPGA type data acquisition system (or similar).

A recommendation for future work on the BTF is to develop engine-testing software that integrates pressure indicating and the engine testing software packages into one work environment. This should preferably be done using a single FPGA type platform to improve system performance.

Other recommendations are:

- The installation of a fuel conditioning unit into the BTF.
- The installation of another fuel consumption measurement device or modifications to the current mass fuel balance in order to measure fuel consumption accurately.
- Research on the performance of biodiesel in pump unit injectors.
- Future work on emissions testing (the appropriate hardware is however required).

7 BIBLIOGRAPHY

- AVL. 2002.** *Engine indicating user handbook*. [PDF] Graz : AVL, 2002.
- AVL. 2008.** AVL-Glow Plug Sensor. AVL. [Online] 2008. [Cited: October 29, 2008.] www.avl.com.
- AVL. 2008.** *High pressure indicating set*. [Document] Graz : AVL, 2008.
- . **1984.** *Operating Manual: Dynamic Fuel Consumption Measuring equipment 730*. Graz : AVL, 1984.
- Bauer, H. 1999.** *Automotive electrics and electronics*. Stuttgart : SAE, 1999. 0768005086.
- Bioservices cc. 2009.** *Stellenbosch Diesel*. Randburg: Bioservices cc, 2009. Test Results.
- . **2009.** *Stellenbosch Biodiesel*. Randburg: Bioservices cc, 2009. Test results.
- Callahan, J.T., Yost, M.D. and Thomas, W.R. 1985.** *Acquisition and Interpretation of Diesel Engine Heat release Data*. San Antonio, TX : SAE, 1985. 0148-7191-85-1021.
- Demirbas, A. 2006.** *Biodiesel production via non-catalytic SFC method and biodiesel fuel characteristics*. Turkey : Karadeniz Technical university, 2006, 2006.
- Dieselnets. 2009.** Appendix: Biodiesel composition and properties of components. [Online] March 1, 2009. [Cited: November 2, 2009.] http://www.dieselnets.com.ez.sun.ac.za/tech/fuel_biodiesel_app.html.
- . **2007.** Diesel net: Emission Standards. [Online] July 2007. [Cited: August 5, 2009.] <http://www.dieselnets.com.ez.sun.ac.za/standards/eu/ld.php>.
- . **2009.** Fuel Regulations. [Online] August 2, 2009. [Cited: November 2, 2009.] <http://www.dieselnets.com.ez.sun.ac.za/standards/fuels.html>.
- Figliola, R.S. and Beasley, D.E. 2006.** *Theory and design for mechanical measurements*. Clemson : Wiley, 2006. 978-0-471-44593-7.
- Heisler, H. 1995.** *Advanced engine technology*. London : Arnold, 1995. 0340568224.
- Heywood, J.B. 1988.** *Internal combustion engine fundamentals*. New York : McGraw-Hill, Inc., 1988. 007028637.
- Honeywell. 2008.** ML6420A (24V) User manual. 2008.
- Hsu, B.D. 2002.** *Practical diesel-engine combustion analysis*. Warrendale : SAE International, 2002.
- INHER S.A. 2008.** QJ1121. [Document] Johannesburg : INHER S.A, 2008.
- Jääskeläinen, H. 2009.** Biodiesel standards and properties. [Online] January 1, 2009. [Cited: November 2, 2009.] http://www.dieselnets.com.ez.sun.ac.za/tech/fuel_biodiesel_std.html.

- . **2009.** Compatibility of biodiesel with petroleum diesel engines. [Online] March 1, 2009. [Cited: November 2, 2009.] http://www.dieselnets.com.ez.sun.ac.za/tech/fuel_biodiesel_comp.html#dilution.
- Jex, R M. 2007.** *VW Polo owners' workshop manual*. Somerset: Haynes Publishing, 2007.
- Kubler. 2009.** *3671_en*. [Document - Manual] s.l.: Kubler, 2009.
- Lancaster, D.R., Krieger, R.B. and Lienesch, J.H. 1975.** Measurement and analysis of engine pressure data. s.l.: SAE Paper, 1975. 750026.
- National Instruments. 2009.** *NI USB-9201*. [Document - Manual] Johannesburg : NI, 2009.
- Optrand. 2008.** *Quotation - University of Stellenbosch*. [Document] Plymouth : Optrand, 2008.
- Owen, K. and Coley, T. 1990.** *Automotive fuels handbook*. Warrendale: SAE, 1990. ISBN 1-56091-064-X.
- Palmer, D. 2008.** *The development of a bio fuels engine testing facility*. 2008: University of Stellenbosch, 2008.
- Schenck Pegasus GmbH. 2001.** *Hydraulic dynamometer Type D*. Darmstadt: Schenck, 2001.
- Stellenbosch Automotive Engineering. 2006.** *Schenck installation manual*. Atlantis: CAE, 2006.
- Swanepoel, R. 2008.** *Renewable energy systems*. Stellenbosch : CRSES, 2008.
- Van Gerpen, J. 2005.** *Biodiesel production and fuel quality*. Idaho: University of Idaho, 2005.
- VWAG. 1998.** *1.9 Litre TDI trainer info*. Wolfsburg: s.n., September 18, 1998.
- . **1998.** *Self-study programme 209*. Wolfsburg: s.n., December 1, 1998.
- Włodarczyk, M.T., et al. 1998.** *Embedded fibre-optic combustion-pressure sensors automotive engines*. Plymouth: Fisita, 1998.
- Włodarczyk, R. 2008.** *Quote - J Kotze 18 sep 08*. [PDF] Trou, USA: Optrand, 2008.

APPENDIX A: BIODIESEL COMPOSITION

These tables summarise the composition of some of the common fatty oils used to produce biodiesel. The designation Ca:b is used to describe the length of the fatty acid chains in carbon atoms. b Designates the number of unsaturated carbon – carbon bonds. (Dieselnet, 2009)

		Rapeseed (high erucic)	Rapeseed (low erucic)	Soybean	Sunflower	Coconut oil	Palm kernel oil	Palm oil (Africa)	Palm oil (Indonesia)	Beef tallow	Chicken fat	Fish oil
Saturated fatty acids	< C10:0					~13	~7					trace
	C12:0	trace	trace		trace	41-46	41-45	trace	trace-0.5	trace		trace
	C14:0	trace	trace	<0.5	trace-0.1	18-21	15-17	1-2	~1	2-4	~1	6-9
	C16:0	2-4	3-6	8-12	5.5-8	9-12	7-10	41-46	41-47	23-29	20-24	11-20
	C18:0	1-2	1-2.5	3-5	2.5-6.5	2-4	2-3	4-6.5	4-6	20-35	4-7	1-4
	C20:0	0.5-1	<1	<0.5	<0.5	trace	trace-0.3	~0.5	~0.5	<0.5		trace-1
	C22:0	0.5-2.0	trace-0.5	trace	0.5-1.0	trace	trace-0.5			trace		trace
	C24:0	0.5	trace-0.2		<0.5							trace-1
	C14:1					trace				~0.5		trace
	C16:1	~0.5	0.1-0.5	trace	<0.5	trace		<0.5	~0.5	2-4	~7	6-11
Unsaturated fatty acids	C18:1	11-24	52-66	18-25	14-34	5-9	10-18	37-42	37-41	26-45	38-44	12-15
	C18:2	10-22	17-25	49-57	55-73	0.5-3	1-3	8-12	~10	2-6	18-23	1-2
	C18:3	7-13	8-11	6-11	trace-0.4	trace	trace-0.5	trace-0.5	trace-0.5	~1	~1	0.5-1
	C20:1	~10	1.5-3.5	<0.5	<0.5	trace	trace-0.5	trace	trace	<0.5		1-16
	C20:x*		trace-0.1							trace		6-19
	C22:1	41-52	trace-2.5		trace-0.3							1-20
	C22:x*									~0.5	0.5-1	5-14
	C24:1		trace									trace-1
	Phosphatides	2.5		1.1-3.2	<1.5				0.05-0.1	<0.07		
	Tocopherols	0.07-0.08		0.09-0.12	0.07-0.1	0.003			0.02-0.12	0.001		
Other constituents	Sterols	0.5-1.1		0.2-0.4	0.25-0.45	0.05-0.1	0.08-0.12		0.04-0.08	0.08-0.14		~0.3
* x > 1 trace ≤ 0.05%												

TABLE 6 - COMPOSITION OF COMMON FATTY OILS, %(M/M) (DIESELNET, 2009)

CN average of reported cetane numbers, D613; **[CN]** reported CN range; **DCN** average of reported derived cetane number; **[DCN]** reported DCN range; **p** density, kg/dm³; **M** molecular mass, kg/kmol; **MP** melting point, °C; **BP** boiling point, °C; **v** kinematic viscosity @40°C, mm²/s; **η** average of reported dynamic viscosity @40°C, mPa·s; **[η]** reported dynamic viscosities; **ΔH** heat of combustion, kJ/mol; **Δh** heat of combustion, kJ/g;

Fatty Acid					Ester													
Des.	Common Name	Systematic Name	Formula	Name	Formula	CN	[CN]	DCN	[DCN]	ρ	M	MP	BP	v	η	[η]	ΔH	Δh
C6:0	Caproic	Hexanoic	C ₆ H ₁₂ O ₂	methyl caproate	C ₇ H ₁₄ O ₂	18		24			130.2							
C8:0	Caprylic	Octanoic	C ₈ H ₁₆ O ₂	methyl caprylate	C ₉ H ₁₈ O ₂	34				0.8775 (20°C)	158.2	-40	193	1.19	1.00	0.99,1.01	5494	34.7
C10:0	Capric	Decanoic	C ₁₀ H ₂₀ O ₂	methyl caprate	C ₁₁ H ₂₂ O ₂	48	47.2, 47.9			0.8730 (20°C)	186.3	-18	224	1.72	1.44	1.40,1.47	6832	36.7
C12:0	Lauric	Dodecanoic	C ₁₂ H ₂₄ O ₂	methyl laurate	C ₁₃ H ₂₆ O ₂	61	60.8, 61.2, 61.4	54		0.8702 (20°C)	214.3	5.2	262	2.43	1.97	1.95,1.98	8138	38.0
C14:0	Myristic	Tetradecanoic	C ₁₄ H ₂₈ O ₂	methyl myristate	C ₁₅ H ₃₀ O ₂	70	66.2, 73.5			0.8671 (20°C)	242.4	19	295	3.23	2.75	2.69,2.81	9446	39.0
C16:0	Palmitic	Hexadecanoic	C ₁₆ H ₃₂ O ₂	methyl palmitate	C ₁₇ H ₃₄ O ₂	74	74.3, 74.5	88	85.6, 91, 85.9	0.8520 (37.8°C)	270.5	30	417	4.38	3.68	3.60,3.76	10669	39.5
C18:0	Stearic	Octadecanoic	C ₁₈ H ₃₆ O ₂	methyl stearate	C ₁₉ H ₃₈ O ₂	81	75.6, 86.9	101		0.8498 (40°C)	298.5	39.1	443	5.51	4.81	4.74,4.88	11962	40.1
C16:1	Palmitoleic	cis-9-Hexadecenoic	C ₁₆ H ₃₀ O ₂	methyl palmitoleate	C ₁₇ H ₃₂ O ₂			51			268.4			3.67			10548	39.3
C18:1	Oleic	cis-9-Octadecenoic	C ₁₈ H ₃₄ O ₂	methyl oleate	C ₁₉ H ₃₆ O ₂	54	52.5, 56	65	55, 59.3, 80	0.8739 (20°C)	296.5	-19.9	349	4.51	3.80	3.73,3.87	11887	40.1
C18:1	Elaidic	trans-9-Octadecenoic	C ₁₈ H ₃₄ O ₂	methyl elaidate	C ₁₉ H ₃₆ O ₂						296.5			5.86				
C18:1	Vaccenic	trans-11-Octadecenoic	C ₁₈ H ₃₄ O ₂	methyl vaccenate	C ₁₉ H ₃₆ O ₂						296.5			5.41				
C22:1	Erucic	cis-13-Docosenoic	C ₂₂ H ₄₂ O ₂	methyl erucate	C ₂₃ H ₄₄ O ₂						352.6	-1.2		7.21	6.09	5.91,6.27		
C22:1	Brassicidic	trans-13-Docosenoic	C ₂₂ H ₄₂ O ₂	methyl brassidate	C ₂₃ H ₄₄ O ₂						352.6							
C18:2	Linoleic	cis,cis-9,12-Octadecadienoic	C ₁₈ H ₃₂ O ₂	methyl linoleate	C ₁₉ H ₃₄ O ₂	43	41.7, 42.6, 45.9	40	38.2, 42.2	0.8886 (10°C)	294.5	-35	366	3.64	3.11	3.05,3.17		
C18:3	cis-Eleostearic	trans,cis,trans-9,11,13-Octadecatrienoic	C ₁₈ H ₃₀ O ₂	methyl cis-eleostearate	C ₁₉ H ₃₂ O ₂						292.5							
C18:3	trans-Eleostearic	trans,trans,trans-9,11,13-Octadecatrienoic	C ₁₈ H ₃₀ O ₂	methyl trans-eleostearate	C ₁₉ H ₃₂ O ₂						292.5							
C18:3	Linolenic	cis,cis,cis-9,11,13-Octadecatrienoic	C ₁₈ H ₃₀ O ₂	methyl linolenate	C ₁₉ H ₃₂ O ₂	23				0.8950 (25°C)	292.5	-45.5		3.27	2.75	2.65,2.84		

TABLE 7 - PROPERTIES OF COMMON METHYL ESTERS (DIESELNET, 2009)

APPENDIX B: US AND EU BIODIESEL SPECIFICATIONS

Property	ASTM D975-08a		ASTM D6751-08		EN 590:2004		EN 14214:2003	
Flash point, min	No 1D 38 °C No 2D 52 °C	D93	93 °C	D93	55 °C	EN 22719	120 °C	prEN ISO 3679
Water & sediment, max	0.05% vol	D2709	0.050% vol	D2709				
Water, max					200 mg/kg	EN ISO 12937	500 mg/kg	EN ISO 12937
Total contamination, max					24 mg/kg	EN 12662	24 mg/kg	EN 12662
Distillation temperature (% vol recovered)	90%: 1D 288 °C max 2D 282-338 °C	D86	90%: 360 °C max	D1160	65%: 250 °C min 85%: 350 °C max	EN ISO 3405		
Kinematic viscosity	1D 1.3- 2.4 mm ² /s 2D 1.9- 4.1 mm ² /s	D445	1.9-6.0 mm ² /s	D445	2.0-4.5 mm ² /s	EN ISO 3104	3.5-5.0 mm ² /s	EN ISO 3104
						EN ISO 3675		EN ISO 3675
Density					820-845 kg/m ³	EN ISO 12185	860-900 kg/m ³	EN ISO 12185
Ester content	5% vol. max	EN 14078			5% vol. max FAME	EN 14078	96.5% min	EN 14103
Ash, max	0.01% wt	D482			0.01% wt	EN ISO 6245		
Sulfated Ash, max			0.020% mass	D874			0.02% mass	ISO 3987
Sulfur, max (by mass)	1D and 2D: S15 15 mg/kg S500 0.05% S5000 0.50%	D5453 D2622 D1292	Two grades: S15 15 ppm S500 0.05%	D5453	Two grades: 50 mg/kg 10 mg/kg	EN ISO 14596 EN ISO 8754 EN ISO 24269	10 mg/kg	prEN ISO 20846 prEN ISO 20884
Copper strip corrosion, max	No 3	D130	No 3	D130	class 1	EN ISO 2160	class 1	EN ISO 2160
Cetane number, min	40	D613	47	D613	51.0	EN ISO 5165	51.0	EN ISO 5165
Cetane index, min					46.0	EN ISO 4354		
One of ⁽³⁾ : - cetane index - aromaticity	40 min 35% vol max	D976-80 D1319						
PAH, max					11% wt	IP 391 EN 12916		
Operability, one of: - cloud point - LTFT/CFPP	Report	D2500 D4539 D6371						
Cloud point			Report	D2500	Location & season dependant	EN 23015		
CFPP					Location & season dependant	EN 116	Location & season dependant	EN 116
Carbon residue, max	1D: 0.15% wt 2D: 0.35% wt on 10% distillation residue	D524	0.050% wt based on 100% sample but reported using 10% residual calculation	D4530	0.30% wt	EN ISO 10370	0.30% wt on 10% distillation residue	EN ISO 10370
Acid number, max			0.50 mg KOH/g	D664			0.50 mg KOH/g	EN 14104
Oxidation stability			3 hrs min	EN 14112	25 g/m ³ max	EN ISO 12205	6.0 hrs min	EN 14112
Iodine value, max							120 ⁽¹⁾	EN 14111
Linolenic acid methyl ester, max							12.0% wt	EN 14103
Polyunsaturated methyl esters, max							1% wt	No method specified
Alcohol control			0.2% mass methanol max, or 130 °C flash point max	EN 14110 D93			0.20% wt methanol max	EN 14110
Monoglycerides, diglycerides & triglycerides, max							MG 0.8% wt DG 0.2% wt TG 0.2% wt	EN 14105
Group I metals (Na + K), max			5 mg/kg	EN 14538			5.0 mg/kg	EN 14108 EN 14109
Group II metals (Ca + Mg), max			5 mg/kg	EN 14538			5.0 mg/kg	EN 14538
Free glycerin, max			0.020% wt	D6584			0.02% wt	EN 14105 EN 14106
Total glycerin, max			0.240% wt	D6584			0.25% wt	EN 14105
Phosphorous, max			0.001% wt	D4951			10 mg/kg	EN 14107
Lubricity, max	520 µm	D6079			460 µm	ISO 12156-1		
Conductivity, min	25 pS/m	D2624 D4308						
Cold soak filterability, max			360 s, 200 s if fuel temperature ≤ 12 °C	D6751 Annex A1				

(1) Spain's Royal Decree 1700/2003 sets the maximum iodine value at 140 to facilitate the use of soybean oil as a feedstock.
(2) D129 is only applicable to S5000 grades.
(3) Limits only apply to S15 and S500 grades.

TABLE 8 - US AND EU BIODIESEL SPECIFICATIONS (JÄÄSKELÄINEN, 2009)

APPENDIX C: BIODIESEL COMPATIBILITY WITH ELASTOMER MATERIALS

Material	Effect of Biodiesel Relative to Diesel Fuel
Fluorosilicon	Hardness little change, swell +7%
Nitrile rubber	Hardness -20%, swell +18%, reduced tensile strength
Nylon 6/6	Decreased elongation, reduced tensile strength
High density polypropylene	Hardness -10%, swell +8 to 15%
Teflon	Little change
Viton 401-C	Little Change
Viton GFLT	Little change
Polyurethane	Hardness little change, swell +6%
Polyvinyl	Much worse
Tygon	Worse

TABLE 9 - BIODIESEL COMPATIBILITY WITH ELASTOMER MATERIALS (JÄÄSKELÄINEN, 2009)

APPENDIX D: POTENTIAL PROBLEMS IN FUEL INJECTION SYSTEMS USING BIODIESEL

Fuel Characteristic	Effect	Failure Mode
Fatty acid methyl esters (general)	Softening, swelling or hardening and cracking of some elastomers including nitrile rubbers (physical effect depends upon elastomer composition)	Fuel leakage
	Displacement of deposits from diesel operation	Filter plugging
Free methanol in FAME	Corrodes aluminum & zinc Low flash point	Corrosion of FIE
FAME process chemicals	Entry of potassium & sodium and water hardness (alkaline earth metals)	Filter plugging
	Entry of free fatty acids hastens the corrosion of non-ferrous metals, e.g. zinc	Corrosion of FIE
	Salt formation with organic acids (soaps)	Filter plugging
	Sedimentation	Sticking moving parts
Free water	Reversion (hydrolysis) of FAME to fatty acid and methanol	Filter plugging
	Corrosion	Corrosion of FIE
	Promotion of bacterial growth	Filter plugging
	Increase of electrical conductivity of fuel	
Free glycerin	Corrosion of non-ferrous metals Soaking of cellulose filters Sediment on moving parts and lacquering	Filter clogging Injector coking
Mono-, di- and triglyceride	Similar to glycerine	Injector coking
Free fatty acid†	Provides an electrolyte and hastens the corrosion of zinc Salts of organic acids Organic compounds formed	Corrosion of FIE Filter plugging Sediment on parts
Higher modulus of elasticity	Increase of injection pressure	Potential for reduced service life
High viscosity at low temperature	Generates excessive heat locally in rotary distributor pumps Higher stressed components	Fuel delivery problems Pump seizures Early life failures Poor nozzle spray atomization
Solid impurities/particles	Potential lubricity problems	Reduced service life Nozzle seat wear Blocked nozzles
Aging products		
Corrosive acids (formic & acetic)	Corrosion of all metal parts	Corrosion of FIE
Higher molecular organic acids	Similar to fatty acid	
Polymerization products	Deposits, especially precipitation from fuel mixes	Filter plugging Lacquer formation by soluble polymers in hot areas

† Concern over free fatty acids was expressed in the 2000 position statement but was not included in the updated statements issued in 2004 and 2007

TABLE 10 - POTENTIAL PROBLEMS WITH BIODIESEL - FUEL INJECTION EQUIPMENT (FIE) (JÄÄSKELÄINEN, 2009)

Characteristic	Consequences for FIE	Vehicle Consequences
Alkali metals (Na+K, Ca+Mg)	Sediment; pump & injector failure	Increased smoke No start
Aging Products (from insufficient oxidative stability)		
Insoluble polymers (sludge, gum)	Filter clogging Deposit formation inside FIE Seizure of moving parts Injector coking	Stalling No start Increased smoke
Soluble polymers	Resins formed inside FIE	Stalling No start
Aging acids	Corrosion of metal parts Soap formation with metal ions from wear or corrosion	Stalling No start Increased smoke
Peroxides	Hardening of elastomers	Fuel leakage

TABLE 11 - POTENTIAL BIODIESEL CONCERNS BY BOSCH (JÄÄSKELÄINEN, 2009)

APPENDIX E: GEOMETRICAL PROPERTIES OF A RECIPROCATING ENGINE

An engine's piston and crank action is more commonly known as the slider crank action in machine theory. Since the heart of all conventional reciprocating engines is based on the slider crank action, general machine theory dictates the movement of an engine's piston and the volumetric changes in the cylinder. Figure 58 shows the geometry of a cylinder, piston, connecting rod and crankshaft.

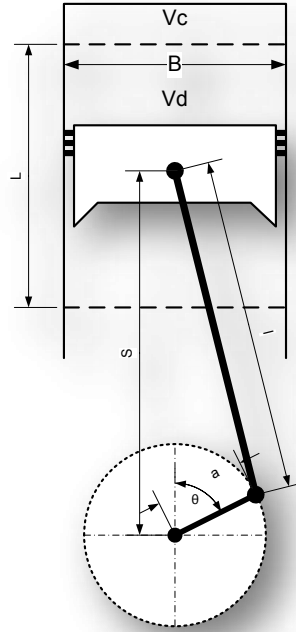


FIGURE 58 - GEOMETRY OF A SINGLE CYLINDER AND CRANK CONNECTION

In Figure 58 the legend and the values for these geometries for the ATD engine are:

- $B \rightarrow$ Bore = 79.5 mm
- $L \rightarrow$ Stroke = 95.5 mm
- $l \rightarrow$ Connecting rod length = 144 mm
- $a \rightarrow$ Crank radius = 47.75 mm
- $\theta \rightarrow$ Crank angle
- $S = a \cos \theta + \sqrt{(l^2 - a^2 \sin^2 \theta)}$
- $V_c \rightarrow$ Clearance volume = 0.00002633 m³
- $V_d \rightarrow$ Displaced volume = 0.00047405 m³

The cylinder volume at any crank position is (Heywood, 1988):

$$V = V_c + \frac{\pi B^2}{4} (l + a - s) \quad \text{E.1}$$

The ratio between the maximum cylinder volume and minimum cylinder volume is known as the compression ratio, designated r_c . The compression ratio of the ATD engine is 19:1.

With basic mathematical manipulation the surface area of the inside of the cylinder can be calculated as a function of crank angle (Heywood, 1988):

$$A = A_{ch} + A_p + \pi B(l + a - s) \quad \text{E.2}$$

Where A_{ch} is the surface area of the cylinder head and A_p is the piston crown surface area.

Mean piston speed is obtained from (Heywood, 1988):

$$\bar{S}_p = 2LN \quad \text{E.3}$$

Where N designates the rotational speed of the crankshaft.

The instantaneous speed of the piston can be calculated by (Heywood, 1988):

$$S_p = \frac{dS}{dt} \quad \text{E.4}$$

APPENDIX F: DERIVATION OF THE SIMPLIFIED HEAT RELEASE MODEL

The energy balance for the cylinder of a direct injection diesel engine can be written as (Heywood, 1988):

$$\frac{dQ}{dt} - p \frac{dV}{dt} + \dot{m}_f h_f = \frac{dU}{dt} \quad \text{F.1}$$

If U is taken to be sensible internal energy of the cylinder contents and h_f is the sensible enthalpy of the injected fuel, then $\frac{dQ}{dt}$ becomes the heat released during combustion (positive value) and the heat transfer from the system (negative value). And with:

$$U = U_s = U(T) - U(298K) \quad \text{F.2}$$

and
$$h_s = h_{s,f} = h_{s,f}(T) - h(298K) \quad \text{F.3}$$

and
$$h_{s,f} \approx 0 \quad \text{F.4}$$

Then:
$$\frac{dQ_n}{dt} = \frac{dQ_{ch}}{dt} - \frac{dQ_{ht}}{dt} = p \frac{dV}{dt} + \frac{dU_s}{dt} \quad \text{F.5}$$

Thus the apparent net heat-release rate, $\frac{dQ_n}{dt}$, is the difference between the gross heat-release rate, $\frac{dQ_{ch}}{dt}$, and the rate of heat transfer to the walls of the cylinder, $\frac{dQ_{ht}}{dt}$. And this is equal to the rate at which work is done on the piston, plus the rate of change of the internal energy of the cylinder contents.

If we model the contents of the cylinder as an ideal gas, then the equation becomes,

$$\frac{dQ_n}{dt} = p \frac{dV}{dt} + mc_v \frac{dT}{dt} \quad \text{F.6}$$

From the ideal gas law, and with R assumed to be constant (for simplicity), the following equation can be written;

$$\frac{dp}{p} + \frac{dV}{V} = \frac{dT}{T} \quad \text{F.7}$$

And using this to eliminate temperature from the previous equation, the final equation can be written as;

$$\frac{dQ_n}{dT} = \left(1 + \frac{c_v}{R}\right) p \frac{dV}{dT} + \frac{c_v}{R} V \frac{dp}{dT} \quad \text{F.8}$$

Or
$$\frac{dQ_n}{dt} = \frac{\gamma}{\gamma - 1} p \frac{dV}{dt} + \frac{1}{\gamma - 1} V \frac{dp}{dt} \quad \text{F.9}$$

Where
$$\gamma = \frac{c_p}{c_v} \quad \text{F.10}$$

APPENDIX G: PICTURES OF EXPERIMENTAL SETUP

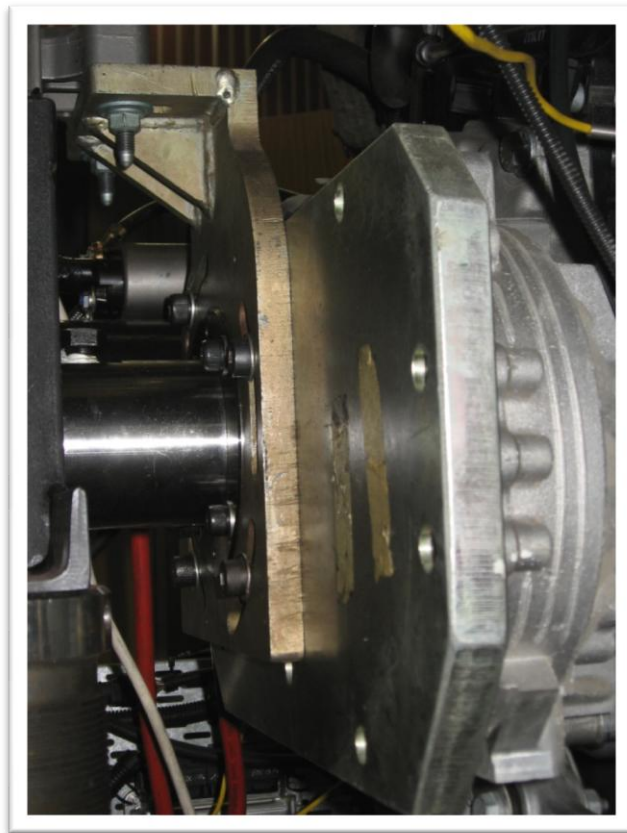


FIGURE 59 - BELL HOUSING ADAPTOR PLATE



FIGURE 60 - EXHAUST THERMOCOUPLE INSTALLATION

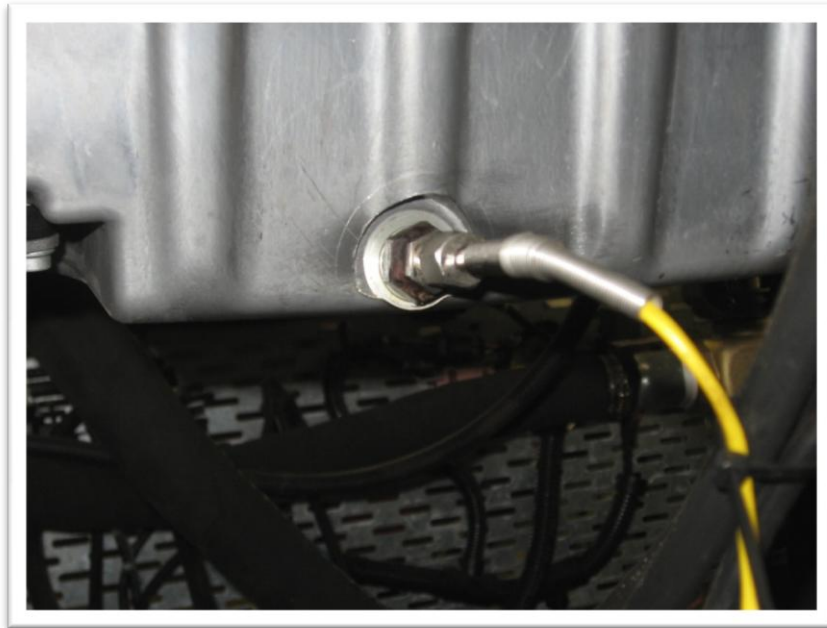


FIGURE 61 - OIL TEMPERATURE THERMOCOUPLE

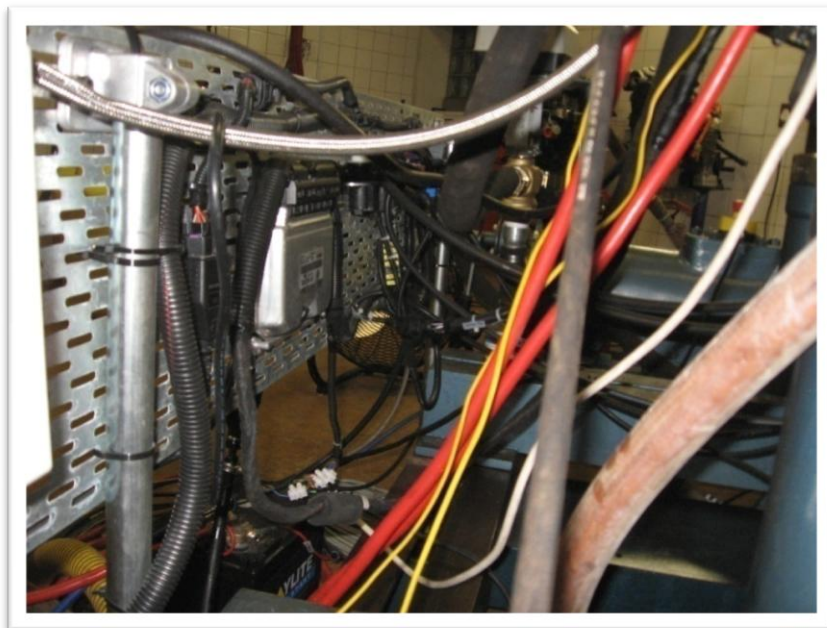


FIGURE 62 - ELECTRONICS BACKBOARD

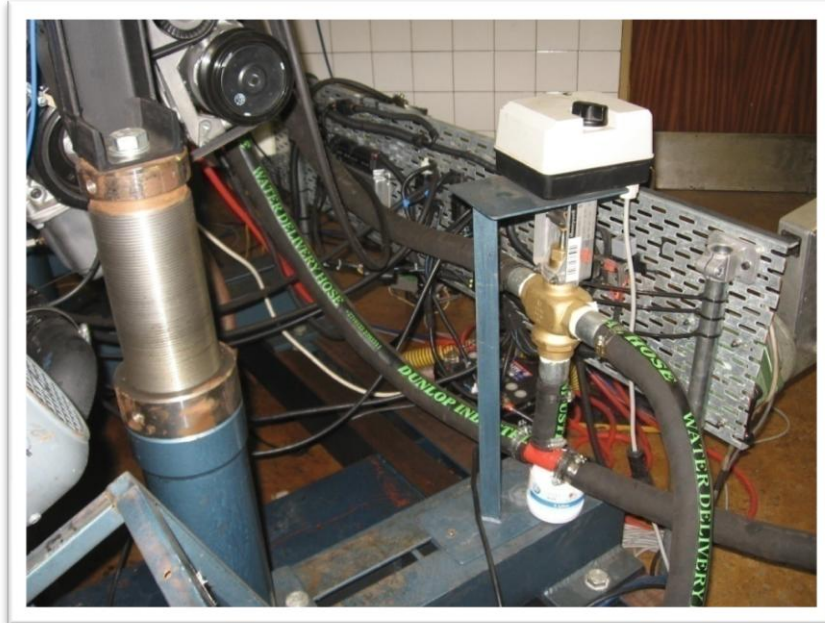


FIGURE 63 - ENGINE COOLANT TEMPERATURE CONTROL SYSTEM



FIGURE 64 - SHELL AND TUBE HEAT EXCHANGER



FIGURE 65 - CLEAN AIR SYSTEM

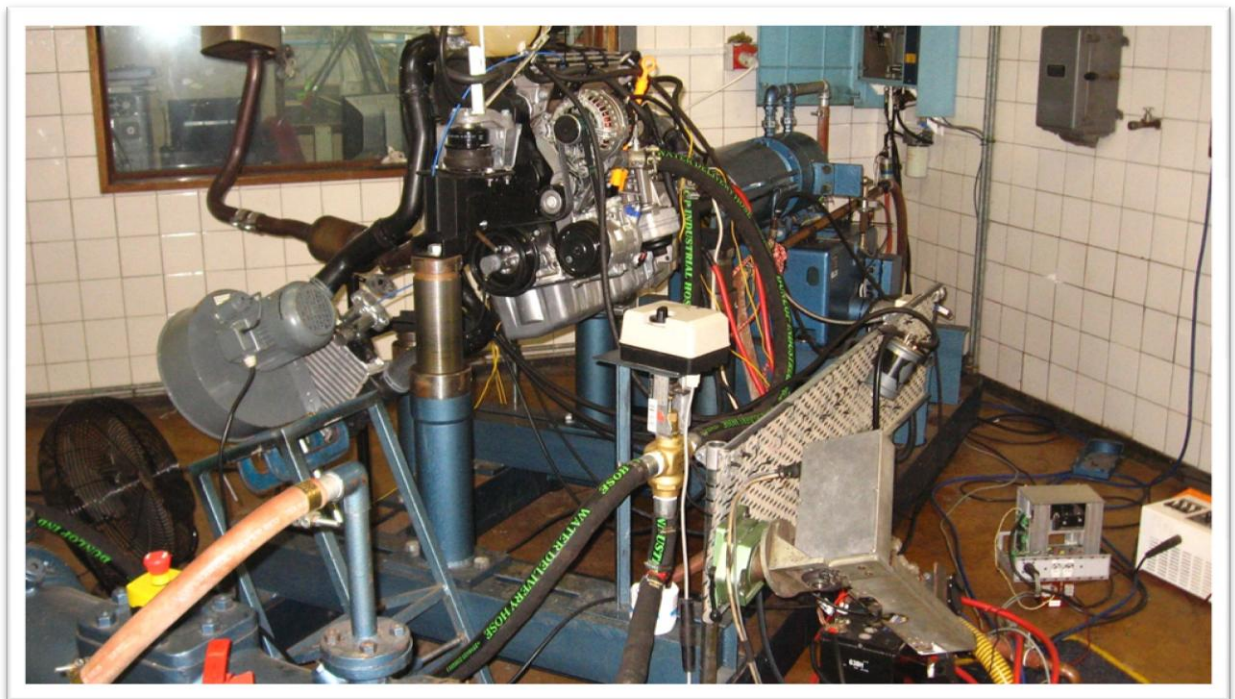


FIGURE 66 - COMPLETE TEST SETUP

APPENDIX H: DRIVE SHAFT



FIGURE 67 – SPLINED SHAFT FROM A POLO GEARBOX SUPPLIED BY VWSA



FIGURE 68 - SHAFT WITH GEARS GROUND OFF AND WITH BEARING LOCATORS MACHINED



FIGURE 69 - COMPLETE POWER TRANSMISSION

APPENDIX I: ECU PIN ASSIGNMENTS

In Figure 70, the pin layout of the ECU 121 pin plug are shown.

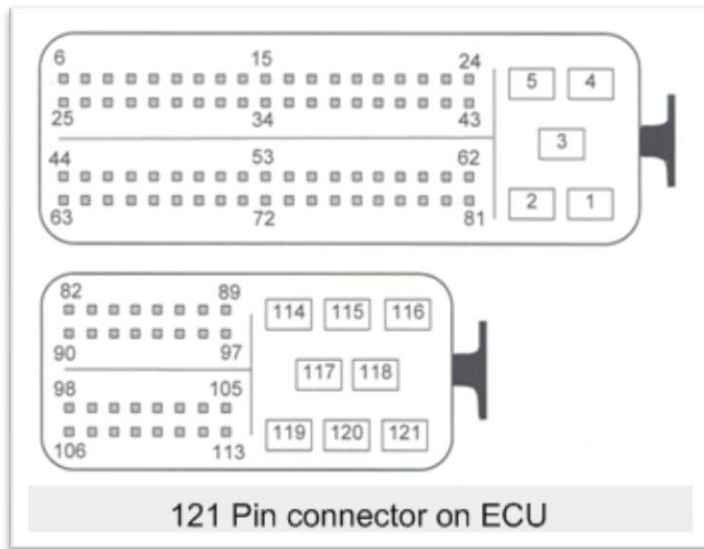


FIGURE 70 - DEPICTION OF THE ECU 121 PIN PLUG TO THE LOOM

The loom connects to the following sensors and actuators on the engine (pin numbers shown in brackets):

- Vacuum throttle valve actuator (81 – Plug A)
- Vacuum boost pressure regulator (62 – Plug A)
- Vacuum EGR Valve controller (61 – Plug A)
- Air mass Flow meter(49, 68, 30, 37 – Plug A)
- Boost pressure sensor (52, 73, 31, 71 – Plug A)
- Accelerator pedal (63, 12, 50, 69, 70, 51 – Plug A)
- Main relay (18 – Plug A)
- Ignition (37 – Plug A)
- 12V Power supply + (1, 2 – Plug A)
- 12V Power supply earth (4,5 – Plug A)
- CAN Pos (7 – Plug A)
- CAN Neg (6 – Plug A)
- CAN K/W (16 – Plug A)
- 12V Power supply + (88 – Plug B)
- Coolant temperature thermistor (104, 112 – Plug B)
- Hall sensor for cam shaft position (101,109 – Plug B)
- Hall sensor for Crank speed/position (102,110 – Plug B)
- Injector common (114 – Plug B)
- Injector 1 (121 – Plug B)
- Injector 2 (116 – Plug B)
- Injector 3 (117 – Plug B)
- Injector 4 (118 – Plug B)

APPENDIX J: TEST SOFTWARE

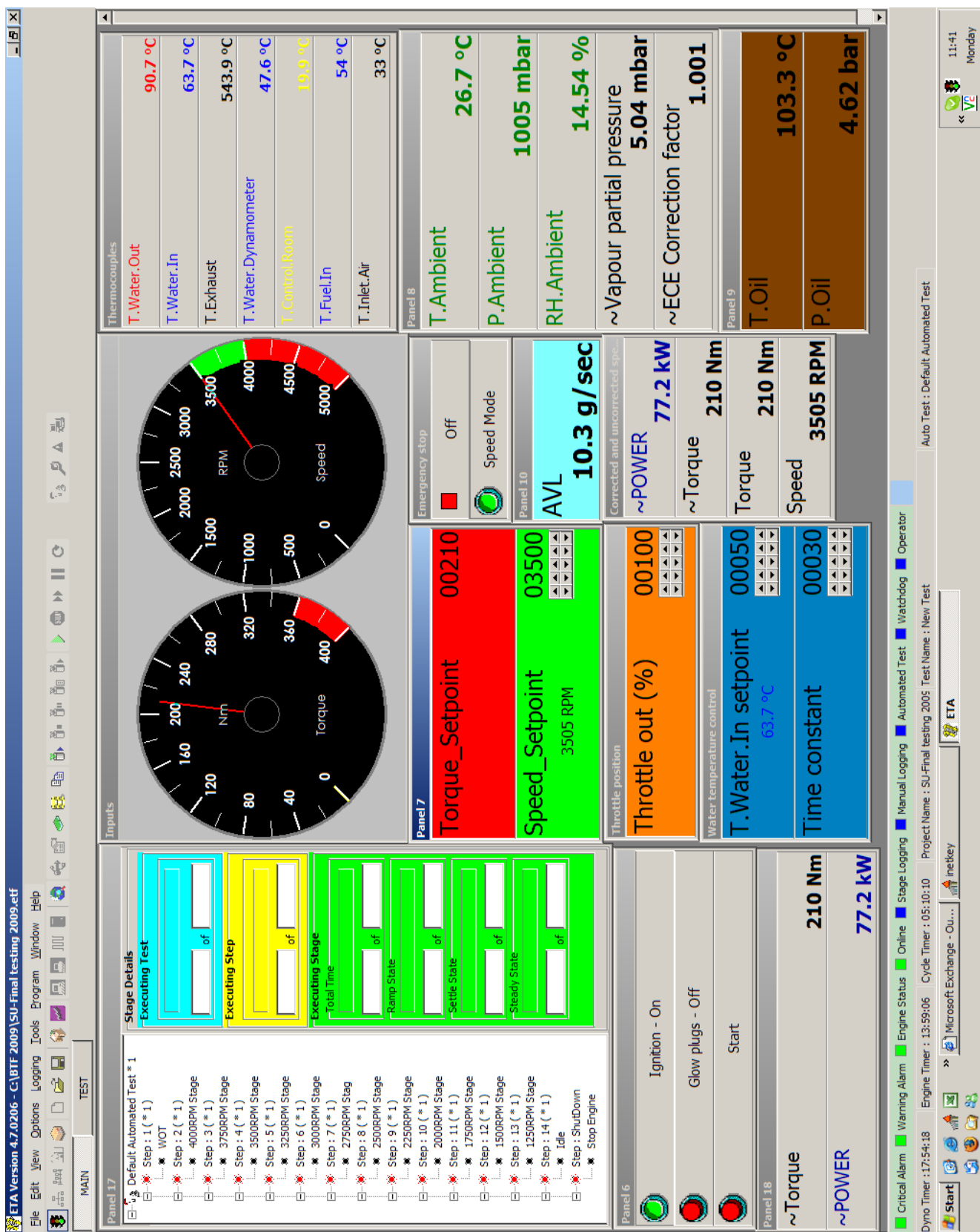


FIGURE 71 - ETA USER INTERFACE



FIGURE 72 - PLC LADDER LOGIC PROGRAM (PALMER, 2008)

LAD 3 - OUT --- Total Rungs in File = 11



LAD 3 - OUT --- Total Rungs in File = 11



APPENDIX K: PRESSURE INDICATING EQUIPMENT

The specifications of the indicating set is summarised in Table 12, Table 13 and Table 14.

Optrand	
Measuring range	0 to 200 bar
Lifetime	1.00E+09
Overload	400 bar
Sensitivity	1.42mV/psi
Natural frequency	>120 kHz
Nonlinearity	±1% FSO
Operating temperature	-40 to 300°C

TABLE 12 – OPTRAND AUTOPSI-S PRESSURE TRANSDUCER PROPERTIES

Kübler 3671	
Max speed	6000 min ⁻¹
Starting torque	<0.06 Nm
Radial load capacity on shaft	40 N
Axial load capacity on shaft	20 N
Mass	200 g
Working temperature range	-40 °C to +85 °C
Shock resistance	5000 m/s ²
Vibration resistance	300 m/s ² , 10 to 2000 Hz
Permanent shock resistance	1000 m/s ² , 2 ms
Vibration (broad-band random)	5 to 2500 Hz, 100 m/s ² RMS
Supply voltage	18...30 V DC
Current consumption	38 mA max
Reverse polarity protection	Yes
Resolution	12 Bit
Linearity	< 1 °
Repeat accuracy	< 0.01 °

TABLE 13 - SHAFT ENCODER SPECIFICATIONS (KUBLER, 2009)

NI USB-9201	
General	
Form Factor	USB
OS Support	Windows
Measurement type	Voltage
Isolation Type	Ch-Earth Ground Isolation
Analogue input	
Number of channels	8
Sample rate	500 kS/s
Resolution	12 bits
Simultaneous Sampling	No
Max Voltage Range	-10v to 10V
Range Accuracy	.053V
Min Voltage range	-10v to 10V
Range Accuracy	.053V
Number of ranges	1
On-Board memory	0

TABLE 14 - NI USB 9201 SPECIFICATIONS (NATIONAL INSTRUMENTS, 2009)

APPENDIX L: DEFAULT FAULT CODES FOR THE MODIFIED BOSCH EDC

Tuesday, 28, July, 2009, 09:43:27:41758
VCDS Version: Release 805.0
Data version: 20080625

Chassis Type: 6N - VW Polo
Scan: 01 02 03 08 15 17 19 25 41 45 46 55

Address 01: Engine Labels: 038-906-019-AXR.1b1
Part No: 038 906 019 DD
Component: 1,9l R4 EDC 0000FFE4S200
Coding: 00002
Shop #: WSC 01689

Part No: H77
Component: PST Nr. 23 VWZ1Z0Y0753256
H77 PST Nr. 23 VWZ1Z0Y0753256

7 Faults Found:
18020 - Engine Control Module Incorrectly Coded
 P1612 - 35-00 - -
16989 - Internal Control Module: ROM Error
 P0605 - 35-00 - -
18047 - Accelerator Position Sensor 1/2 (G79/G185): Implausible Signal
 P1639 - 35-00 - -
65280 - Development code 1
 35-00 - -
65280 - Development code 1
 35-00 - -
17932 - Fuel Pump Relay (J17): Open or Short to Ground
 P1524 - 35-10 - - - Intermittent
17978 - Engine Start Blocked by Immobilizer
 P1570 - 35-10 - - - Intermittent
Readiness: 0 0 X X X

Address 25: Immobilizer Labels: None
Part No: 6X0 953 257
Component: IMMO 0007
Coding: 00001
Shop #: WSC 01690

Part No: H77
Component: PST Nr. 23 VWZ1Z0Y0753256
H77 PST Nr. 23 VWZ1Z0Y0753256

2 Faults Found:
01314 - Engine Control Module
 65-10 - Unauthorized - Intermittent
01202 - Diagnostic Cable
 44-00 - Short Circuit

End -----

APPENDIX M: INDICATING POWER SPECTRUMS AND FILTER

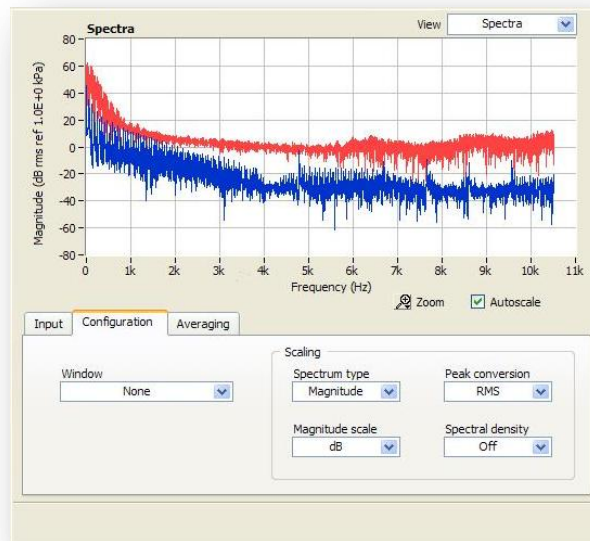


FIGURE 73 - POWER SPECTRUM OF NOISY INDICATING SIGNALS (SIGNALEXPRESS)

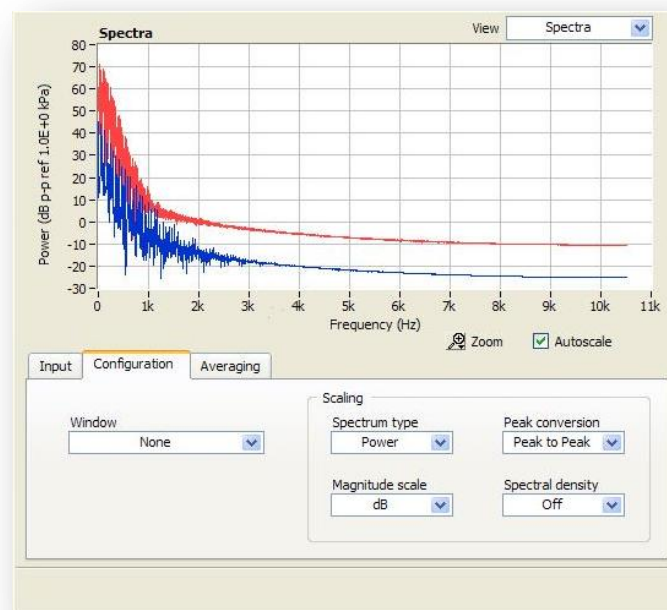


FIGURE 74 - POWER SPECTRUM OF INDICATING SIGNALS AFTER FILTERING (SIGNALEXPRESS)